Laser Thrombolysis: Basic Ablation Studies

Ujwal Setlur Sathyam

B.E., Mangalore University, India (1992)

M.S., Oregon Graduate Institute of Science & Technology (1994)

A dissertation submitted to the faculty of the
Oregon Graduate Institute of Science & Technology
in partial fulfillment of the
requirements for the degree
Doctor of Philosophy
in
Electrical Engineering

October 1996

The dissertation "Laser thrombolysis: basic ablation studies" by Ujwal Setlur Sathyam has been examined and approved by the following Examination Committee:

<div style="text-align:right">

_____

Scott A. Prahl
Assistant Professor
Thesis Research Advisor

_____

J. Fred Holmes
Professor and Department Head

_____

V. S. Rao Gudimetla
Assistant Professor

_____

Kenton W. Gregory
Director
Oregon Medical Laser Center

</div>

Dedication

In the memory of my grandmother, Padma Iyengar

Acknowledgements

My entry into the field of biomedical optics was serendipitous to say the least. In fact, I had been barely aware that it existed at all. My advisor Scott Prahl and I joined OGI around the same time; he was looking for students, while I was trying to decide what to do now that I had gotten myself into graduate school. At that time I had no clue that Scott was considered the guru of light propagation in tissue. I was just a green electronics engineer who knew next to nothing about optics and had had his last biology course in high school.

From Scott I learned the art of presenting data, mathematical handwaving, physics, optical alignment, and aikido. I have him to thank for my Macintosh fanaticism and scorn for all Microsoft software. It was not always a bed of roses. Scott's idea of bringing me and my fellow student Elaine up to speed was three-hour research meetings once or twice a week. However, Scott taught me the most valuable gift: how to learn. He also encouraged me to speak my mind, something that at times I take too far. Thank you, Scott, for keeping it interesting.

Alan Shearin has almost been a second advisor to me. Alan is a true engineer and the most practical person I have met. He is blessed with a genius for designing an experimental apparatus. Our experiments together constitute the bulk of this research. Thank you, Alan, for the hours you spent showing me how things worked instead of referring me to a manual.

Ken Gregory is the director of our laboratory and a cardiologist. His clinical experience was very valuable to the direction of this research. His attendance made our research meetings lively, and we enjoyed shattering each other's wishful musings. Thank you, Ken, for being so approachable and for the many international meetings we got to attend.

Elaine LaJoie was my first labmate, and I quickly discovered that she was a great person to chat with and irritate. She however had a sharp tongue of her own. Thank you, Elaine, for not pulling any punches. Thanks to my other fellow graduate students Priya, Neena, Javed, Shafqat, Radhika, Anurag, HanQun, Krishna, Sean, Badri, and John for sharing the experience; to Lisa Buckley for always being there to talk to; to Deb Bahlman-Tuke who is the most connected person I have ever met.

None of this could have been accomplished without the support from my family. They always had faith in my academic potential, even during some of the dark periods. I must also thank Veena for keeping me sane and listening to my ranting and raving these past few months. She was definitely the catalyst in finishing up this thesis.

Contents

List of Figures

Abstract

Laser Thrombolysis: Basic Ablation Studies

Ujwal Setlur Sathyam, Ph.D.
Oregon Graduate Institute of Science & Technology, 1996

Supervising Professor: Scott A. Prahl

Laser thrombolysis is a procedure that is being developed to treat cardiovascular disease and stroke by removing clots occluding arteries of the heart and the brain. This thesis presents studies of pulsed ablation phenomena that take place during during laser thrombolysis. The main goals were to optimize laser parameters for efficient ablation, and to investigate the ablation mechanism. Most of the studies described here used a gel-based clot model, and selected results were verified using porcine clot.

A parametric study was performed to identify the optimal wavelength, spot size, pulse energies, and repetition rate for maximum material removal. The minimum radiant exposures to achieve ablation at any wavelength were measured. The results suggest that most visible wavelengths were equally efficient at removing material at radiant exposures above threshold. Larger catheters are likely to ablate more efficiently. Ablation was initiated at surface temperatures just above $100°$C. A vapor bubble was formed during ablation. The vapor bubbles expanded and collapsed within $500\,\mu$s after the laser pulse. Less than 5% of the total pulse energy is coupled into the bubble energy. A large part of the delivered energy is unaccounted for and is likely released partly as acoustic transients from the vapor expansion and partly wasted as heat. When the ablation process was studied within the cylindrical confines of a tube, dilation of the vessel due to bubble expansion was observed at clinically relevant energies.

The thesis concludes by summarizing the relevance of the gel results to the implementation of

laser thrombolysis. It proposes optimal laser parameters for the design of a next generation laser system; a doubled Nd:YAG laser is suggested. It also suggests that the current laser and delivery systems may not be able to completely remove large clot burden that is sometimes encountered in heart attacks. However, laser thrombolysis may emerge as a favored treatment for strokes where the occlusion is generally smaller and rapid recanalization is of paramount importance. A final hypothesis is that laser thrombolysis should be done at radiant exposures close to threshold to minimize any damaging effects of the bubble dynamics on the vessel wall.

Chapter 1

Introduction

Cardiovascular disease occurs when arteries and veins become occluded with atherosclerotic plaque and clot cutting off blood supply to vital organs. This can lead to potentially fatal conditions such as heart attacks, strokes, and pulmonary embolism.

Laser thrombolysis is an interventional procedure that removes clot by delivering microsecond pulses via a fluid core catheter. The removal of the clot results in a restoration of blood flow while maintaining vascular integrity. Some of the main advantages of laser thrombolysis over conventional treatment of cardiovascular disease are higher efficacy rates and potential safety.

To cause injury to tissue with light, the tissue has to absorb the energy. The amount of energy absorbed by the tissue depends on the wavelength of the light. The absorption by thrombus is significantly higher than that by arterial tissue in the visible region of the electromagnetic spectrum. This allows lasers to selectively remove thrombus without injuring the vessel wall by using a wavelength in this region. Current investigations of laser thrombolysis use tunable pulsed-dye lasers operating in the visible region with pulse lengths of $1\text{--}2\,\mu$s. The absorption of light by the thrombus leads to the explosive vaporization of part of the clot and the formation of rapidly expanding and collapsing vapor bubbles (figure 1.1). The dynamics of the vapor bubbles generate pressure transients that disrupt the clot.

Laser thrombolysis was first used to treat acute myocardial infarctions caused by thrombosed native coronary arteries that supply the heart muscles. Preclinical and early clinical studies have demonstrated effective removal of thrombus and restoration of blood flow. Pulsed lasers have also been used to remove clots in occluded bypass grafts and femoral arteries. Recently, there has been considerable interest in using this technique to remove cerebral clots in the arteries of the brain. This can be an important step towards the treatment of stroke that can be caused by occlusions in the brain arteries.

1.1   Motivation

The use of lasers to remove tissue was suggested soon after the development of the first laser in 1960. Some of the clinical applications of lasers to ablate tissue are bone removal, cartilage smoothing, corneal reshaping, burn treatment, and laser angioplasty. Laser angioplasty targets the plaque that is usually present along with clot in diseased arteries. The use of optical fibers capable of delivering light to previously inaccessible places in the body has made the medical laser particularly attractive for many minimally invasive techniques.

The development of a safe and effective laser system for arterial recanalization is a complex task involving the selection of optimal laser parameters and delivery of the energy. Early enthusiasm for laser angioplasty and laser thrombolysis was tempered by unacceptable failure rates. Some of this was due to poor designs of laser and delivery systems and a lack of understanding of the ablation mechanism. The last ten years have seen progress in the design of the system and have rejuvenated the interest in laser-assisted recanalization techniques.

The broad goal of this research is to make laser thrombolysis a safe and rapid procedure, so that it may be accepted as a standard treatment modality for vascular disease. Both basic research into the physical ablation phenomena and clinical trials are required to achieve this. This thesis addresses some of the questions regarding the basic physical processes during laser thrombolysis. With a better understanding of the ablation process, it may be possible to specify optimal parameters for the design of the laser and delivery systems.

1.2   Vascular disease

Vascular disease is the major cause of death and disability in the United States. More health care dollars are spent on the treatment of various types of vascular disease than any others. One cause of vessel disease is the accumulation of plaque and thrombus (clot) in the arteries resulting in reduction and/or cessation of blood flow to vital organs. Another related cause is thromboembolism where a piece of a clot formed elsewhere breaks off and floats downstream blocking blood flow to a vital organ.

Coronary artery thrombosis resulting in myocardial infarction occurs in over 1.5 million people in the United States, and over 500,000 will die as a consequence [1, 2]. Thrombosis of coronary artery bypass grafts is the major cause of bypass graft closure at a rate of about 200,000 cases per year [3]. Thrombosis can also occur in cerebral arteries and lead to strokes. Over 80% of strokes

are ischemic in nature and are attributed to thrombosis and embolism [4]. Venous thrombosis can lead to pulmonary embolism where a piece of the clot detaches and embolizes downstream in the lung.

Normally, blood constituents do not interact with intact vascular endothelium that is a thin layer of cells lining the insides of vessels. However, the exposure of flowing blood to disrupted vasculature or to cardiovascular devices initiates complex mechanisms leading to thrombosis. There is rapid deposition of platelets, insoluble fibrin, leukocytes, and entrapped erythrocytes [5]. Clots can also form when the blood flow slows down as in most cases of venous thrombosis.

Not all clots are created equal. The etiology and characteristics of the thrombus, and therefore its preferred treatment modality depend on where it is formed. Vascular occlusions can occur almost anywhere in the vascular system including in the coronary arteries, bypass grafts, cerebrovasculature, and in the peripheral blood vessels. Arterial flow conditions give rise to platelet-rich "white" thrombi, and static venous flow yields "red" thrombi rich in fibrin and red blood cells.

The mainstay of thrombus management is a regimen of pharmacological therapy that includes thrombolytics to dissolve the clot and anticoagulants to prevent clotting. Streptokinase, urokinase, and tPA are examples of thrombolytics, and heparin is an anticoagulant. The use of these drugs has been shown to improve cardiac function [6, 7]. Alternate approaches to vascular recanalization are balloon angioplasty, rotoblader atherectomy, and aspiration devices [8, 9, 10, 11]. In balloon angioplasty a balloon is inflated inside the vessel to mechanically re-mold the lumen. When all else fails or if the thrombus burden is too large, bypass surgery may be performed.

1.2.1 Thrombosis of coronary arteries

Acute coronary thrombosis is common to the pathogenesis of myocardial infarction and of unstable angina. Fissuring or rupture of an atherosclerotic plaque plays a fundamental role in the formation of coronary artery thrombosis [12]. When the injury to the vessel is mild, the thrombogenic stimulus is relatively limited, and the resulting occlusion is transient as in unstable angina. The endothelium is denuded with thrombi adherent to the surface of the plaque. Deep vessel injury results in persistent thrombotic occlusion and myocardial infarction. Major plaque disruption exposes the lipid core to the lumen. Blood enters the core and thrombus forms within the plaque expanding its volume rapidly. The intraplaque component of the thrombus is very rich in platelets. The intraluminal part forms as the last stage of the occlusion and is rich in fibrin and red cells.

Thrombolytic therapy with pharmacological agents is paramount in myocardial infarction, but it is less effective in unstable angina [13]. The reduction in mortality associated with the use of thrombolytic agents is impressive [14, 7]. The most feared complication of thrombolytic therapy is intracranial hemorrhage since fatality rates in such cases can range from 44% to 75% [15]. Some patients have contra-indications to the drugs and cannot receive them due to bleeding disorders, recent strokes, etc. Also, the thrombus burden is usually not removed completely. Residual thrombus is very thrombogenic acting as substrate for additional clot formation. Re-occlusion of the artery is therefore a problem.

Percutaneous interventional techniques like balloon angioplasty and atherectomy were initially used as a secondary treatment to keep the vessel open after thrombolytic therapy. Angioplasty has now evolved as a primary intervention for patients who have shown contra-indications to thrombolytics. Acute results of balloon angioplasty are promising with a relatively low rate of abrupt vessel closure ($\sim$5%) [16]. Drawbacks, however, appear in the short-term follow-up phases where vessel closure rates of 30–50% within six months have been reported [17, 18]. This has been largely attributed to the damage incurred by the vessel wall during inflation of the balloon.

The last line of defense is bypass surgery where a piece of a vein from the leg is grafted around the occlusion to re-establish blood flow. This is an open chest procedure and involves severe trauma to the patient. There is also an increased risk of re-occlusion due to thrombosis of the vein graft.

1.2.2 Thrombosis of cerebral arteries

The term "stroke" is used to describe a number of brain disorders with a common feature of a defect in the cerebral vasculature. Strokes are classified according to whether they are ischemic or hemorrhagic. Most strokes are due to arterial occlusion with brain ischemia (oxygen deprivation) leading to cerebral infarction or transient ischemic attacks [4].

Similar to the pathogenesis of acute coronary syndromes, thrombosis over a disrupted plaque can play a key role in cerebrovascular occlusions [12]. However, intracranial hemorrhage and embolism may also be involved; common sources for the thrombus embolus are the heart and the carotid arteries. Transient ischemic attacks result from progressive narrowing of the vessel leading to reduction of blood flow or from a transient occlusion by a thrombus. Cerebral infarction arises from total occlusions.

Early studies of therapies for acute stroke show benefit at a high price [19]. It is clear

that cerebral perfusion has to be re-established within 3–6 hours to restore normal neurological function. The treatment is to infuse the patient with thrombolytics and agents that dissolve thrombus and increase cerebral perfusion. This treatment modality is not always successful, and sometimes the occlusion is not cleared in time. The thrombolytic tPA has recently been approved by the Food and Drug Administration for the treatment of embolic stroke. Mechanical intervention has not been tried on large scale due to difficult access to the occlusion via the tortuous bends in the arteries. Also, the arteries of the brain are more fragile, increasing the risk of vascular injury and vasospasm. A major problem in the treatment of stroke is the recurrence of stroke. This is particularly true of strokes that are embolic in nature. In such cases the underlying cause of the stroke has to be treated where possible.

1.2.3 Thrombosis of peripheral arteries

Claudication is the clinical term for pain in the muscles of the leg due to insufficient delivery of oxygen resulting from a proximal obstruction to blood flow. Peripheral arterial disease is frequently asymptomatic for long periods and often occurs together with coronary artery disease. The risk of a leg amputation is relatively low ($\sim$5%); however, life expectancy is generally reduced [20]. A large number of patients die of cardiovascular causes.

Smokers demonstrate a higher incidence of fibrous, calcified, and ulcerated plaques in the aorta and in the iliofemoral circulation [12]. Diabetes is also commonly associated with disease of the iliofemoral and distal arteries of the leg. Major acute arterial occlusion is often due to fibrin-rich emboli arising from the heart or occasionally from venous thromboembolism through a patent foramen ovale (an abnormal communication between chambers in the heart). Microemboli causing digital infarction may arise from cardiac sources or from fragmentation of a proximal thrombus during vascular intervention.

In most patients with intermittent claudication, conservative therapy is usually lifestyle advice to exercise regularly and to reduce smoking. In acute cases the primary treatments are reconstructive surgery and catheter recanalization procedures. Arterial bypass grafts and percutaneous transluminal angioplasty are the most common procedures performed [21]. Systemic thrombolysis with drugs has a low success rate and a significant risk of bleeding. Local thrombolysis delivers drugs via a catheter and has a higher success rate. Nevertheless, the use of thrombolytics is frequently not the treatment of choice for peripheral arterial disease.

1.2.4 Thrombosis of bypass grafts

Bypass surgery is generally performed for diffuse atherosclerotic disease resulting from a chronic build-up or when there has already been a previous intervention. It is also done when arterial disease develops at multiple sites. Basically, a piece of the saphenous vein in the leg is grafted and implanted to bypass the occlusion.

A problem plaguing bypass surgery is thrombosis of the vein graft cutting off blood flow again. Disease of vein grafts is a form of accelerated atherosclerosis that begins with acute vascular injury, mural thrombosis, and proliferation of smooth muscle cells in the vessel wall. Injury to the vein graft results from procurement of the vein from the leg, surgical handling, delays before insertion, and from the increased shear forces of the pulsatile arterial system. There is platelet deposition and secretion of growth factors for smooth muscle cells and white cells. Recent bypass procedures have used a graft from the internal mammary artery that is more protected from generalized injury and platelet deposition. This is probably due to previous adaption to arterial shear forces.

There is no satisfactory treatment for thrombosed vein grafts. Mechanical intervention like angioplasty is not preferred because of problems and embolization at lesions to distal coronary arteries [22]. Thrombolytics ease the thrombus burden in about 50% of the cases, but the re-occlusion rate is around 30% [3, 23]. Because platelet deposition starts as soon as blood flows through the vein graft, perioperative antithrombotic therapy is critical.

1.2.5 Thrombosis of deep veins

Deep vein thrombosis is a common and potentially dangerous complication of a primary illness in hospitalized patients. It may lead to pulmonary embolism that can be fatal. When venous thrombi dislodge, they can reach the pulmonary arterial circulation and may adhere to the bifurcation of the pulmonary artery. The thrombus generally forms in post-operative patients who are under extensive bed rest. It is also common in people who spend extended periods of time in a sedentary position.

Venous thrombosis develops when stasis in the deep veins of the legs occurs at times of increased coagulability of the blood [12]. This combination leads to local generation of thrombin that is the crucial event in the pathogenesis of the disease. Since the clot forms under static conditions of blood flow more red blood cells are trapped and the clot appears red. Vessel wall injury is less likely to be involved. Deep vein thrombosis can also go undetected for some time,

and they can be several weeks old before turning symptomatic.

Prevention of deep vein thrombosis is a critical part of post-operative care. This involves elimination of stasis and fighting blood coagulation. Although anticoagulant therapy is highly effective, two thirds of the patients who die from pulmonary embolism succumb abruptly or before the therapy can take effect. Thrombolytic therapy is generally more rapid than anticoagulants in thrombus removal. Contra-indications again appear in the form of bleeding.

Surgical intervention for venous thrombosis consists of either thrombectomy or venous interruption. The role of thrombectomy remains controversial. There are several techniques for the interruption of the inferior vena cava that is the main blood vessel carrying blood from the legs back to the heart. One example is a variety of external clips designed to partially compress the vein so that emboli floating in the stream are filtered [24]. However, compromised cardiac output due to inadequate venous return led to low acceptance of these techniques in clinical practice.

1.3 Laser thrombolysis

The disadvantages of current techniques to rapidly clear large thrombus burden in occluded arteries led to the search for an alternative method that did not endanger the vessel wall. The potential for laser energy to remove atherosclerotic obstructions (plaque) was described as early as 1963 [25]. Since then most investigations have concentrated on the removal of plaque in a technique called laser angioplasty [26]. In 1983 Lee *et al.* used an argon laser to vaporize human thrombus *in vitro* [27]. If the arterial occlusions is a combination of plaque and thrombus, it is essential to remove both for effective therapy.

1.3.1 Continuous wave laser thrombolysis

Early studies of both laser angioplasty and laser thrombolysis used continuous wave laser to remove the arterial obstruction. Crea and Abela attempted to recanalize thrombosed coronary arteries in dogs using an argon ion laser [28]. The wavelengths used were $488\,\text{nm}$ and $514\,\text{nm}$, and the laser energy was transmitted via 140 or $200\,\mu\text{m}$ cleaved silica fibers. The results were not encouraging with recanalization reported in only 1 of 9 dogs. Perforation of the arterial lumen was observed in 7 of 9 dogs. Minimal thrombus was removed and there was evidence of charring at the laser delivery sites.

The results of several subsequent studies have demonstrated the limitations of both continuous laser energy and delivery by hard silica fibers [29, 30, 31, 32]. Irradiation by a continuous wave

laser does not confine the heat produced to the target area. The diffusion of heat out of the target area can result in thermal necrosis and even charring in the surrounding tissue. These factors also lead to intense vasospasm and thrombosis [33]. It has been reported recently that accelerated intimal hyperplasia can be attributed to thermal injury [34]. Intimal hyperplasia is a condition where the smooth muscle cells in the vessel wall proliferate and cause closure of the vessel.

Bare silica fibers are generally stiff and have sharp edges. Tortuous bends in the vascular system are difficult to navigate and therefore limit access to the occlusion. The sharp edges of the fiber pose considerable hazards to the vessel wall, and arterial perforations and fracture of fibers have been reported in animal trials. The fiber tip was then covered with a metal cap ("hot-tip") in an attempt to reduce the sharp profile of the fiber [35, 36, 37, 38, 39]. While results from animal trials were promising, an unacceptable number of thermal injuries during angioplasty in human coronary arteries were reported. Consequently, most attempts at laser angioplasty and thrombolysis using continuous-wave lasers were abandoned.

1.3.2   Pulsed laser thrombolysis

Srinivasan *et al.* reported their experience using ultrashort excimer laser pulses to produce precise cuts in polymers without adjacent thermal effects [40]. This approach of using pulsed lasers to limit thermal effects can also be be used to ablate tissue. The limiting pulse length would be determined by the thermal relaxation time of the material. This is the time for heat to diffuse out of the irradiated volume and is determined by the thermal diffusivity of the tissue and the dimensions of the volume. When laser energy is deposited in pulses shorter than the thermal relaxation time, heat accumulates and high temperatures are achieved. The ablative event can then occur before the heat diffuses out of irradiated volume. This confinement of heat can reduce the thermal damage incurred by adjacent tissue [41, 42].

For vascular structures the thermal relaxation time is of the order of milliseconds, so lasers with pulse durations less than 1 ms are likely to produce little thermal injury [43, 44]. Pulsed lasers from the ultraviolet [45, 46, 47, 48, 49], visible [50, 51, 52, 53, 54, 55], and infrared [56, 57, 58] have been investigated for both angioplasty and thrombolysis. Notable among these are the excimer (308 nm, 351 nm, 100–200 ns), tunable pulsed-dye (400–600 nm, 1 μs), and the Ho:YAG (2.1 μm, 250 μs) lasers. The excimer and holmium lasers are popular because of the potential for a single laser system to treat both plaque and thrombus. The excimer laser targets the tissue

proteins, while the holmium energy is absorbed by tissue water. Both these chromophores are present in both plaque and thrombus.

Excimer laser thrombolysis

Excimer laser angioplasty systems emitting 308 nm light in 100–200 ns pulses are being tested for thrombus removal in animal and clinical trials [47]. These systems were designed for and have had extensive evaluation for the treatment of atherosclerotic obstructions.

The laser energy is delivered via a catheter made of bundles of 50–100 μm core diameter fused silica fibers circumferentially arranged around a central guidewire lumen. Conventional angioplasty guidewires are pushed through the thrombus into the distal part of the vessel. The laser catheter is brought over the guidewire to the thrombus, and pulse energies of 40–50 mJ/mm^2 are delivered at a repetition rate of 10–30 Hz. Balloon angioplasty immediately after the laser procedure is generally required to open the vessel further.

Ultraviolet light of 308 nm is strongly absorbed by the tissue protein in the clot; the depth of penetration is about 30 μm. This would theoretically allow for precise etching of clot similar to that demonstrated in atherosclerotic tissue and polymers. However, the results have been conflicting [59, 60]. The clinical excimer laser is configured to principally treat plaque. Refining the laser and delivery systems, technique, and case selection specifically for treatment of thrombi may improve the efficacy of the excimer laser for thrombolysis. However, ultraviolet photons have sufficient energy to break certain carbon bonds and may result in unwanted photochemical reactions.

One feature that was noted was that the ablative event was different from previous continuous-wave ablation studies. Ablation was initiated by explosive vaporization of the tissue and the subsequent formation of a vapor bubble. The dynamics of this rapidly expanding and collapsing bubble exert mechanical forces on the clot leading to removal of more clot. This bubble formation occurs almost always when tissue is ablated under a liquid with a pulsed laser. The removal of thrombus under these conditions is usually more efficient but less controlled.

Holmium laser thrombolysis

Holmium/thulium:YAG lasers emitting 2.1 μm radiation have been successfully used for angioplasty and are now being tested for thrombolysis [56]. Other applications include cutting bone and intervertebral discs. The pulse duration is 250 μs in the free running mode and 1 μs in a

Q-switched mode. Water has an absorption peak at $2.1\,\mu$m, and the penetration depth of the holmium radiation in water-containing tissues is about $300\,\mu$m.

The holmium laser is a solid state device and is favored for its smaller size and ease of operation. The clinical laser for angioplasty and thrombolysis is configured to emit $250\,\mu$s pulses. The energy is delivered to coronary artery thrombi via a catheter similar in design to the one for the excimer laser. The catheter is 1.4–1.7 mm in diameter and delivers 250–600 mJ pulses at a repetition rate of 5 Hz.

The results of holmium laser thrombolysis are fair. In one study the majority of the thrombus was cleared and the residual stenosis was less than 30% in all cases [61]. No acute adverse procedural complications were reported. However, balloon angioplasty was still required as a follow-up procedure.

There is some reservation regarding the holmium laser for thrombolysis. Stress wave effects and the formation of vapor bubbles have been shown to induce damage to adjacent tissue [62]. Hassenstein *et al.* reported formation of thrombotic occlusions during holmium laser angioplasty [63]. Another potential disadvantage is the inability of the holmium laser to selectively target thrombus without ablating the vessel wall. Since water is present in roughly the same proportions in all tissues, the holmium laser does not discriminate between an arterial occlusion and healthy vessel wall. This presents the danger of perforations caused by inadvertent ablation of arterial tissue.

1.3.3 Selective thrombolysis

A laser system capable of selectively targeting the thrombus is therefore desirable. This capability is offered by lasers emitting in the ultraviolet and visible regions, where the absorption by thrombus is much higher than that by artery. The principal chromophore of thrombus in the visible waveband is hemoglobin present in the red blood cells. Since higher absorption coefficients require less energy per unit area to achieve ablation, the ablation threshold for artery is higher than that for clot. Pulsed lasers operating in this waveband at radiant exposures between the thresholds for artery and clot can therefore selectively remove clot.

Prince *et al.* reported that differential absorption of light of selected wavelengths between plaque and arterial wall resulted in differences in ablation thresholds [64, 65, 50]. LaMuraglia *et al.* conducted spectrophotometric studies to determine the absorption spectra of thrombus and normal arterial tissue in the 400–600 nm waveband [53]. An increase in absorption of nearly two

orders of magnitude between clot and artery due to the presence of hemoglobin was observed (Figure 1.2).

Based on these tissue spectrophotometric studies, a pulsed-dye laser system was developed. The wavelength of emission is tunable between 400–600 nm, and the pulse duration is 1–2 μs. A longer pulse could potentially work as long as it stayed below the thermal relaxation time of tissue ($\sim$1 ms). The lasers currently configured in clinical settings operate at 480 nm with pulse widths of 1–2 μs [55, 66]. The ablation thresholds for acute arterial thrombus and normal arterial tissue measured with this laser *in vivo* and *in vitro* were approximately 15 mJ/mm^2 and 1500 mJ/mm^2 respectively [67, 54].

1.3.4   Catheter system

Light delivery is achieved with a fluid-core light guide, that is essentially a tubing of low refractive index filled with an optically transparent fluid of higher refractive index (Figure 1.3) [67, 68]. Light propagation is similar to that of a regular optical fiber. The light is launched from the laser into an optical fiber contained within the fluid catheter. The fiber in turn launches the light into the optical fluid that finally delivers it to the target. Further, the catheter is open-ended at the distal end allowing the fluid to flow out of the catheter. The advantages over delivery by regular optical fibers are:

- increased flexibility and reduced risk of perforations because of the soft material of the tubing;

- removal of blood and ablation debris by the flowing fluid to clear the path for laser delivery to the thrombus;

- contact with the target is not necessary because light can be transmitted past the end of the catheter, and this feature may reduce mechanical injury to the vessel wall;

- the optical fluid used is radiographic contrast used in conventional angiography. Being radio-opaque, contrast gives the additional capability of monitoring laser thrombolysis progress in real time using fluoroscopy.

The laser catheter is fitted with a Y-adapter. The optical fiber is inserted into the catheter tubing through one leg of the adapter. The distal end of the fiber is kept about 20 cm from the distal part of the catheter. A fluid injector injects the contrast media through the other leg of

the Y-adapter. The catheter can be inserted into the femoral artery in the leg and advanced to the occlusion in the coronary artery over a monorail guidewire.

The initial pulse energy at the output end of the fiber is approximately 80 mJ. The transmission through the optically clear fluid is about 75% resulting in an output energy of 60 mJ. The internal diameter of the optical channel is 1.1 mm that results in a laser spot diameter of similar dimensions. The pulse repetition rate is 3 Hz. The fluid injector maintains the contrast flow between 0.3–0.5 m/s that provides adequate light transmission up to 1 cm from the tip of the catheter. The tip of the catheter is marked with a gold band for visualization during fluoroscopy.

1.3.5 Initial results

The pulsed-dye laser thrombolysis technique was tested on a canine model with promising results [67]. Coronary artery thrombi were removed in all of 22 dogs without perforation, vasospasm, or other untoward incidents. All thrombi were removed within 600 pulses. The patency rate of the vessels 90 minutes after the procedure was 80%.

Based on these favorable animal studies of laser thrombolysis and approval from the Food and Drug Administration, a pilot study of laser thrombolysis in acute myocardial infarction in humans was performed. The criteria for patient selection was contra-indications to or failure of thrombolytic drugs. The procedures were performed at St. Vincent Hospital, Portland, Oregon and at St. Joseph's Hospital, Atlanta, Georgia. Effective thrombus removal was demonstrated in 16 of 18 patients [69].

1.4 Goals

All the pulsed laser thrombolysis systems described above are prototypes and are in early phases of experimental and clinical investigation. Laser thrombolysis appears feasible but is yet to be established as an adjunct or stand-alone therapy for the various types of vascular disease. This requires further research into the following areas: (*i*) physics of the ablation process, (*ii*) engineering of laser and delivery systems, and (*iii*) *in vivo* clinical trials.

Laser thrombolysis is initiated by a light pulse delivered through the fluid catheter. The temperature of the thrombus increases as it absorbs the light reaching levels sufficient for vaporization. Vapor bubbles expand and collapse and disrupt the thrombus. The relationship between these phenomena and their contribution to thrombus removal is not clear. Investigation and quantification of the basic mechanism will serve as a basis for maximizing the efficiency of the

procedure. Briefly, the areas addressed by this thesis are as follows:

- Optimal laser parameters for efficient ablation are identified.

- Ablation threshold exposures for thrombus and artery are estimated.

- Vapor bubble formation and its role in the ablation process are studied.

A qualitative and quantitative understanding of the ablation process will provide insight into the physical phenomena associated with the process and help provide design parameters for laser and catheter systems.

1.4.1   Visualization studies

A major goal is to determine and describe the phenomena that take place during pulsed laser ablation of thrombus and thrombus phantoms under water. This is done by visualizing the ablation process and the associated bubble action using flash photography. Two processes are active during pulsed ablation:

- volumetric heating due to absorption of light resulting in vaporization of the clot,

- the mechanical action of vapor bubbles formed as a result of vaporization.

The relative importance of each mechanism was unknown. Photographic visualization of ablation will achieve a qualitative understanding of the removal process. Quantification of mass removal and comparison with existing thermal ablation models will elucidate the significance of heating versus bubble dynamics in the ablation process. This will serve as a basis to maximize the efficiency and safety of laser thrombolysis by optimizing laser and light delivery parameters.

Bubble kinetic energies will be calculated based on size and lifetime of the bubbles. A calculation of bubble energies will yield estimates of the fraction of the total laser energy that is utilized in the creation of the vapor bubbles.

I shall also investigate the confining effects of boundaries (vessel walls and delivery catheter) on the bubble formation and ablation efficiency. The interaction of the bubble with the delivery catheter may result in adverse effects such as recoil and perforations of the vessel wall. Studies of boundary effects on bubble formation and ablation efficiency will help in maximizing thrombus removal and minimizing collateral damage to surrounding structures.

1.4.2   Optimization of laser parameters

Another major goal is to optimize the efficiency of ablation by identifying the ideal laser parameters for thrombolysis. Effects of wavelength, spot size, pulse energy, and repetition rate on the ablation efficiency will be studied. Ablation efficiency is characterized by mass removed per unit energy per pulse.

The selective ablation of thrombus is achieved by using a laser wavelength between 400–600 nm. However, the optimal wavelength within this waveband was not known. Wavelengths that are better absorbed than others may result in more efficient ablation, or vice versa. Also, dye lasers are currently used that emit microsecond pulses in the visible region. These lasers, requiring water and dye pumps, are too bulky and unwieldy for use in the operating theater. Identification of an optimal wavelength will not only result in efficient ablation, but it may simplify the design of a next-generation laser operating at a single wavelength.

The other laser parameters that are investigated in this work are the spot size, pulse energy, and repetition rate. The spot size is crucial in two aspects:

- It will largely determine the diameter of the delivery catheter.

- It will fix the threshold energies for ablation of thrombus and vessel wall, thus providing lower and upper limits respectively for the pulse energies to be used.

Higher pulse energies will obviously result in more mass removal. Identifying the relationship between delivered energy and efficiency may help to better understand the ablation process. Also, an upper limit for the pulse energy to be used is essential in the design of the laser system.

Finally, the pulse repetition rate will influence how long the laser thrombolysis procedure takes. If the amount of clot removed per pulse does not depend on the repetition rate, the laser pulses can potentially be delivered at a faster rate thus reducing the procedure time. Further, a fixed repetition rate will help in the design of the laser. However, the repetition rate influences the transmission characteristics of the liquid core catheter, and this may provide the upper limit for the pulse repetition rate. Also, the debris from the previous pulse has to be removed by the time the next pulse arrives.

All the ablation efficiency studies proposed above depend on an accurate measurement of mass removal of the order of micrograms. The ability to measure such small amounts is further complicated by the fact that the ablation takes place in a liquid environment. A major step towards the completion of the above studies therefore involved the development of a method to

accurately measure the ablation mass within 5% in an aqueous environment.

1.4.3   Ablation threshold studies

Increasing the radiant exposure above a certain threshold level will result in ablation of the vessel wall. Threshold radiant exposures for ablation of thrombus and artery at any wavelength have to be measured to provide a window of efficient and safe ablation. The threshold energy for ablation over a uniform spot depends on two factors:

- the optical absorption coefficient μ_a of the target tissue,

- the laser spot size on the surface

The spot size and the absorption coefficient determine the energy confined per unit volume and the rise in temperature. Barring stress confinement (where ablation can occur due to tearing), ablation is generally initiated when the heating per unit volume is sufficient for vaporization. The absorption in turn depends on the wavelength of light delivered. The wavelength and spot size studies outlined above will result in optimal wavelength(s) and spot size(s) at which thrombolysis can be performed. It is therefore necessary to be able to predict the ablation threshold radiant exposures (energy per unit area) for thrombus and artery at any wavelength.

In this study, thresholds were determined as a function of absorption and mapped onto the absorption spectra of thrombus and artery. Thresholds were measured by using mass-removal, optical, acoustic, and visualization techniques. Thermal signals from the surface were monitored at radiant exposures below and above threshold.

1.4.4   Thrombus phantoms

Laser thrombolysis is a complex process involving thermal and mechanical events. Investigations of these processes is further complicated when the target is a biological tissue such as clot. This is due to the inherent variabilities associated with tissue. To elucidate the physical mechanism of laser ablation, most experimental work reported here is done on gelatin tissue phantoms. The gel models are reproducible and allow comparative experiments using various optical properties and laser and delivery parameters. The results of the third chapter in this thesis suggest that ablation thresholds for gel and clot are similar at equivalent optical absorptions. This comparison is a rather limited validation of gel as optical model for clot. Also, their mechanical properties differ. Nevertheless the processes that take place in these controlled models should provide insight into

the phenomena that take place during ablation of clot. Gel has been used to model soft tissues by numerous researchers [70, 71, 72, 73, 74]. Selected gel experiments will be validated with real thrombus.
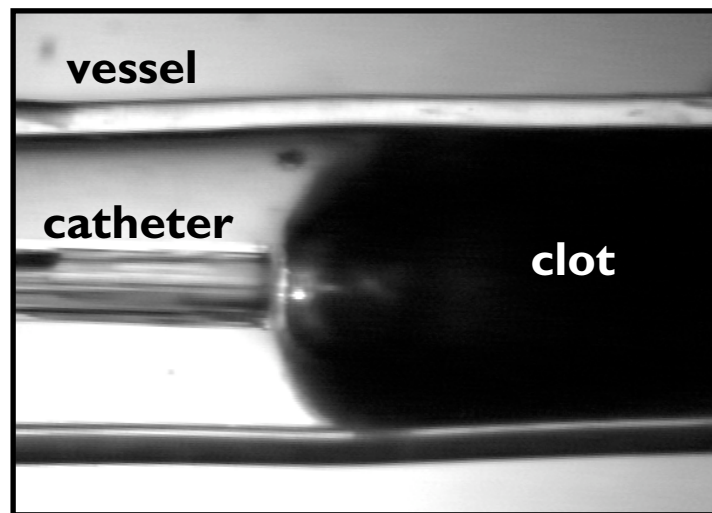
Figure 1.1: Microsecond ablation of porcine clot in a $3\,\text{mm}$ silicon tube. The tube simulates the cylindrical geometry of a blood vessel. Light is delivered by a fluid-core catheter. The clot absorbs the light and a portion is vaporized. A vapor bubble is formed that expands and collapses causing the clot to be further disrupted.
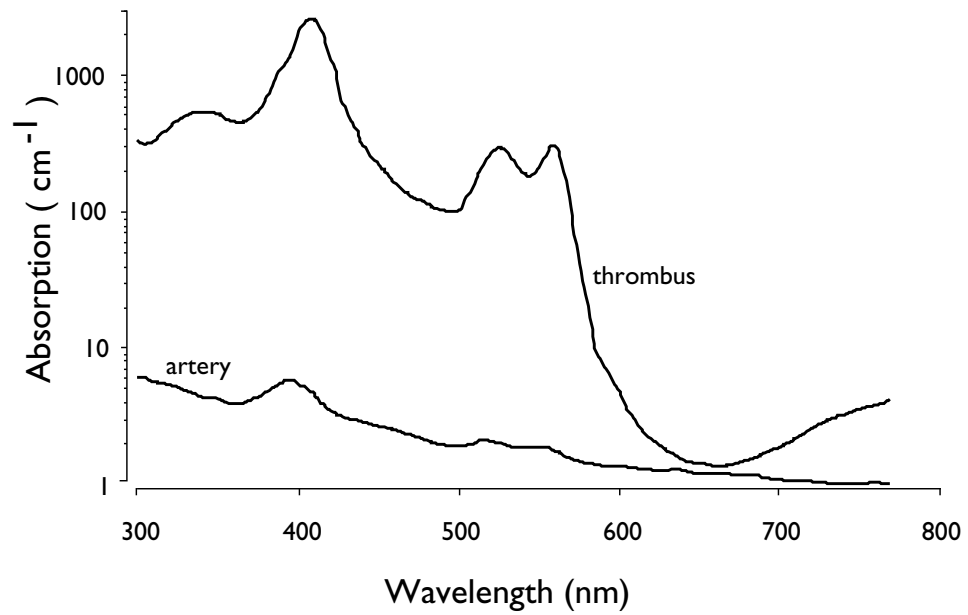
Figure 1.2: Absorption spectra of human thrombus and vessel wall. A wavelength in the visible region is selected for laser thrombolysis to selectively ablate thrombus without incurring injury to the vessel wall.

vessel

blood

solid optical fiber

optically clear fluid (refractive index n_1)

tubing (refractive index $n_2 < n_1$)
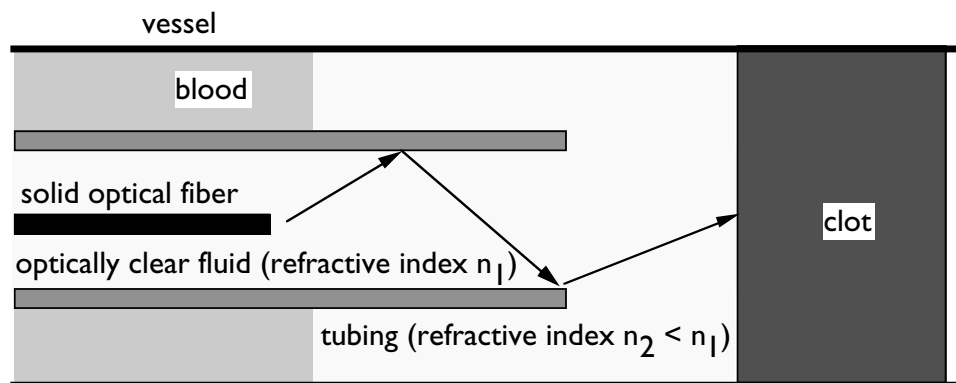
clot

fluid stream carries laser light to the clot

Figure 1.3: Schematic representation of the fluid-core catheter used to deliver microsecond laser pulses to the clot during laser thrombolysis. The laser energy is launched from the laser into an optical fiber contained in a catheter. The fiber in turn launches the light into an optically clear liquid that transmits the light to the target by total internal reflection. The distal tip of the catheter is open-ended so that the fluid can flow out of the catheter and wash away the blood in front of the clot. A clear path for direct laser delivery to the clot is thus established. Another important advantage of the catheter over a bare solid fiber is that the fiber does not extend all the way to the end but ends roughly 20 cm from the distal open end. The distal part of the catheter is therefore softer and more flexible and therefore less traumatic. Finally, the fluid is optically clear but radio-opaque that makes live monitoring by angiography possible.

Chapter 2

Laser parameters for efficient ablation

This chapter describes experiments carried out to determine the optimal wavelength, spot size, pulse energy, and repetition rate for laser thrombolysis.[1] The clot was simulated by gelatin containing a light-absorbing dye. Arteries were simulated by 3 mm inner diameter plastic tubes, and the gel was ablated under water. Laser parameters were deemed optimal when the maximum amount of gelatin was removed per pulse per unit energy (ablation efficiency). A unique spectrophotometric method was developed to measure the mass removed. Wavelength studies were conducted by varying the absorption of gelatin between $10-2000\,\mathrm{cm}^{-1}$ corresponding to clot absorption in the $400-600\,\mathrm{nm}$ range. Laser energy was delivered via optical fibers of $300-1000\,\mu\mathrm{m}$ core diameter to investigate the effect of spot size. The pulse energies ranged from $25-100\,\mathrm{mJ}$, and the repetition rate was varied from $1-10\,\mathrm{Hz}$. The results of this study suggest that any wavelength between $410-590\,\mathrm{nm}$ can be used for effective thrombolysis. The mass removed per pulse depends on the total energy delivered rather than on the radiant exposure. The pulse repetition rate did not strongly influence the total mass removed. The high ablation efficiencies suggest a dominance of the mechanical action of vapor bubbles over thermal events in the ablation process.

2.1 Tissue optics

Generally, light transport in tissue is governed by three intrinsic parameters of the material: absorption μ_a, scattering μ_s, and anisotropy g. Both absorption and scattering have dimensions of inverse length and represent the average number of absorption and scattering events undergone by a photon traversing a distance of unit length in the medium. The anisotropy g is the average cosine of the angle between the directions of a photon prior to and after a scattering event. The

---

[1]This chapter is a part of the paper "Threshold and ablation efficiency studies of microsecond ablation of gelatin under water" to be published in *Lasers in Surgery and Medicine*, 19:3, 1996.

g value of an isotropic scatterer is zero, while a highly forward scattering medium would have a g value close to unity. Based on the scattering coefficient μ_s and anisotropy g, an effective or reduced scattering coefficient $\mu_s' = \mu_s(1-g)$ can be defined. A highly forward scattering medium such as blood therefore has a low effective scattering.

The light distribution within the tissue is a complex function of μ_a, μ_s, and g and is described by the integro-differential radiative transport equation [75]. Numerous analytical, numerical, and statistical models have been developed to solve the radiative transport equation [76, 77, 78, 79, 80, 81]. Analytical models include the Beer's law, Kubelka-Munk, and diffusion theories. The validity of each model depends amongst other factors on the relative magnitude of the absorption and effective scattering coefficients. Statistical models such as Monte Carlo simulations are considered exact but tend to be time-consuming.

The radiant exposure $E(z)$ in mJ/mm^2 at depth z in an absorbing only medium is given by Beer's law:

$$E(z) = E_0 \exp(-\mu_a z) \tag{2.1}$$

where E_0 is the incident radiant exposure. This equation is exact for an absorbing only medium and is a reasonably good approximation for materials where absorption greatly dominates scattering. Blood is a strong absorber in the visible region ($\mu_a \sim 100$–$1000\,\mathrm{cm}^{-1}$) with a low effective scattering coefficient ($\mu_s \sim 300\,\mathrm{cm}^{-1}$, $g \sim 0.99$). Therefore Beer's law can be used to calculate light distribution in blood and blood clots.

At irradiation levels where non-linear effects like dielectric breakdown can be neglected, the ablative effect of a high power laser pulse on tissue is largely determined by its duration and how deep it penetrates into the material. The optical penetration depth δ is defined as the depth at which the radiant exposure in the medium drops to $\frac{1}{e}$ of the incident radiant exposure. In a medium where Beer's law applies, this is simply given by:

$$\delta = \frac{1}{\mu_a} \tag{2.2}$$

The absorbed fraction of the light can be converted into heat, photochemical reactions, or re-emitted light. Typically, most of the light is converted into heat. If all the absorbed light is converted into heat, the volumetric heating produced is given by $\mu_a E(z)$ with dimensions of J/cm^3. The rise in temperature at depth z is given by:

$$\Delta T = \frac{\mu_a E(z)}{\rho c} \tag{2.3}$$

where ρc is the heat capacity of the material.

It is not clear how the absorption affects the total mass removed. At lower absorption coefficients the light penetrates deeper (equation 2.2) and larger volumes are heated that could result in more mass being removed. However, a low absorption may also cause insufficient heating for ablation to take place (equation 2.3). Higher temperatures are achieved at higher absorption coefficients. This means the threshold radiant exposure to ablate the tissue will be lower, and suggests that any extra energy can be utilized for ablating more material. However, that does not necessarily have to be true. Light does not penetrate deeply into highly absorbing tissue. This means that the high temperatures are confined to a shallow depth of tissue, and the the extra energy might just be overheating that layer. Therefore, there may exist an optimal absorption at which the mass removed per unit energy may be maximized.

2.2   Goals

The goals of the experiments described in this chapter were to study the effects of wavelength, spot size, pulse energy, and pulse repetition rate on ablation efficiency. Efficiency is defined here as the total mass removed per pulse per unit energy. While a range of safe wavelengths for laser thrombolysis has been identified, the relative efficiency of each wavelength between 400–600 nm is not known (figure 1.2). It is also not clear whether the ablation efficiency depends on the radiant exposure (mJ/mm^2) or on the total energy delivered. No complete parametric study of microsecond ablation of a soft target under a liquid has been undertaken yet. The spot size is also important in determining the size of the catheter delivering the laser energy. The repetition rate will be a major factor influencing the total procedure time in a clinical setting.

Since the wavelength determines the absorption and hence the penetration depth into the tissue, it has been theorized that an optimal wavelength for laser thrombolysis would be found at an optimal penetration depth. Early studies have speculated that deeper penetrating wavelengths in the 400–600 nm waveband would result in higher ablation efficiency since a larger volume would be heated [52], for example 480 nm. Another reason for favoring 480 nm was its good absorption by beta-carotene present in atherosclerotic plaque [50]. Later studies suggested that primarily the 410 nm and to a lesser extent the 450–500 nm wavelengths were among the most effective for laser thrombolysis since they provided the highest degree of selectivity in absorption between thrombus and vessel wall [53]. However, there is no experimental evidence available to positively justify the choice of a particular wavelength.

The question then arises: *how important is light absorption in mass removal at energies*

above threshold? Laser thrombolysis is done in a fluid medium, and an important phenomenon influencing removal of tissue under a liquid is cavitation or the formation and collapse of a vapor bubble [71, 82, 83]. The contribution of the bubble dynamics to the ablation process may be comparable to or even overshadow the absorption-dependent thermal effects. It is therefore important to estimate the relative significance of the absorption coefficient in the ablation process at energies above threshold.

In this parametric study, gelatin was used to model clot. A dye was added to the gelatin to absorb the laser light. The use of the thrombus model eliminated the biological variability of thrombus. Another important advantage of the model was that the absorption could be controlled by just changing the amount of dye in the gelatin. This facilitated the use of a single laser in the wavelength studies. An absorption range of 10–$2000 \, \mathrm{cm}^{-1}$ was studied that corresponded to the waveband between 400–$600 \, \mathrm{nm}$ on the absorption spectrum of thrombus (figure 1.2).

Since laser thrombolysis is performed under an aqueous medium of saline and contrast, the gelatin was ablated under water. An important aspect of laser thrombolysis is the constraining cylindrical geometry of the vessel wall. In these experiments, the gelatin was confined in plastic tubes to simulate the cylindrical boundaries of the arterial wall. Solid glass fibers were used to deliver the laser energy. A unique spectrophotometric method was developed to accurately measure the ablated mass within 5%. The radiant exposure was varied by varying both the pulse energy and irradiated spot size, and ablation efficiency was characterized as the amount of gelatin ablated per pulse per unit energy.

2.3 Materials and methods

2.3.1 Thrombus model

The thrombus was modeled using 3.5% by weight gelatin (175 Bloom, Sigma Chemicals, St. Louis, MO) in water containing a photostable absorbing dye as the chromophore (Direct Red 81 from Sigma, 75% dye content). The bloom number is a measure of the stiffness of the gel and is supplied by the manufacturer: a higher bloom number represent stronger gels. Gelatin of this strength and concentration was chosen because it appeared to be closest in mechanical strength to fresh arterial clot. No rigorous mechanical testing was carried out to validate the choice of these parameters.

Young's modulus is one useful measurement of the strength of a material. Samples of gel

and porcine clot (many weeks old) were compressed using a Liveco V1000 universal tester. The average Young's modulus for the gel was found to be 18 kPa, and the value for clot varied between 5–15 kPa depending on the site of the measurement. While this correlation is acceptable, the dynamic mechanical properties of the materials may very well be different under the explosive conditions of microsecond ablation. The conclusions of this study do not depend on the mechanical properties of the model, and should therefore still have valid implications for laser thrombolysis.

The gelatin-water mixture was heated to 60°C to dissolve the gelatin and sufficient chromophore was added to achieve the desired absorption coefficient at the laser wavelength used. Liquid gel samples were drawn into and cured by cooling in Tygon tubes (Norton) simulating coronary arteries (figure 2.2). The tubes had an inner diameter of 3 mm and a wall thickness of 1.5 mm. The absorption coefficients of the samples had a linear relationship with the concentration of chromophore in the gelatin solution: 0.089 g of chromophore in a solution of 1.4 g gelatin and 40 cm^3 water gave an absorption coefficient of 100 cm^{-1} at 577 nm. The absorption coefficients ranged from 10 cm^{-1} to 2000 cm^{-1}.

Figure (2.1) shows the absorption spectrum of 6 μg/ml direct red solution measured in a 1 cm cuvette. The absorption coefficient μ_a was calculated from absorbance A and path length d using the relation:

$$\text{transmission} \equiv 10^{-A} = e^{-\mu_a d} \tag{2.4}$$

2.3.2   Laser delivery

A 1.3 μs (FWHM) pulsed dye laser (Palomar Medical Technologies, Beverly, MA) operating at a wavelength 577 nm was used for ablation. In subsequent experiments that included the pulse repetition rate studies the laser wavelength was changed to 506 nm. This was done because 506 nm is close to the absorption peak of the Direct Red dye (figure 2.1), and therefore smaller amounts of dye were required to achieve desired absorption coefficients. Quartz fibers of 300, 600, and 1000 μm core diameter were used to deliver the laser pulses to the gelatin targets. Solid glass fibers were used to instead of a fluid core catheter because they were easier to use. Since the focus of these experiments were the effects of laser parameters on the ablation efficiency, the actual delivery device was not important.

The fiber tip was maintained at a distance of 1 mm from the gel surface. A steady flow of water at 0.3 m/s was established by a fluid injector (Medrad Mark V) and directed around the

fiber to target site (figure 2.2). The flow served to collect the ablated gel and also to clear the path for laser delivery to the target area. The flow rate of $0.3\,\mathrm{m/s}$ corresponds to the flow used in the fluid core catheters in clinical settings.

Ten pulses were fired on each sample and the ablated gel was collected by the flowing water in $1\,\mathrm{cm}$ cuvettes. The steady flow was continued after the last pulse until $4\,\mathrm{ml}$ of liquid was collected; this was sufficient to collect all the ablated gel. The above procedure was repeated on control samples without light delivery to account for the gel removed by the flow of water alone. The ablated gel was dissolved completely in the water by shaking, and its mass was determined by the spectrophotometric method described below. The ablation efficiency was then calculated as the mass removed per unit energy per pulse.

Absorption studies were conducted by delivering pulse energies of 25–$100\,\mathrm{mJ}$ via a $1000\,\mu\mathrm{m}$ fiber to gels with absorption coefficients varying from 10–$2000\,\mathrm{cm}^{-1}$. Radiant exposure studies were conducted by delivering pulse energies of 25–$100\,\mathrm{mJ}$ via 300, 600, and $1000\,\mu\mathrm{m}$ fibers to gels with an absorption of $300\,\mathrm{cm}^{-1}$. An absorption of $300\,\mathrm{cm}^{-1}$ was chosen in the radiant exposure studies since thrombus has this absorption at $577\,\mathrm{nm}$ which is one of the wavelengths used in clinical trials of laser thrombolysis. Absorption and radiant exposure studies were done at a pulse repetition rate of $3\,\mathrm{Hz}$ which is currently used in clinical settings. Values of $1\,\mathrm{Hz}$, $3\,\mathrm{Hz}$, $6\,\mathrm{Hz}$, and $10\,\mathrm{Hz}$ were used in the repetition rate studies with $100\,\mathrm{mJ}$ pulse energy delivered via a $1000\,\mu\mathrm{m}$ fiber to a $100\,\mathrm{cm}^{-1}$ target. An absorption of $100\,\mathrm{cm}^{-1}$ was chosen since thrombus has this absorption at $480\,\mathrm{nm}$ which is another wavelength used for laser thrombolysis.

Ten samples and five controls were used for each data point. Pulse energies were measured with a joulemeter (Molectron). The effective spot sizes produced $1\,\mathrm{mm}$ from fiber end were determined by ablating fiber polishing paper under water and measuring the resulting burn diameters under a microscope. The spatial profile of the laser spot was measured using a CCD camera focused $1\,\mathrm{mm}$ from the fiber output end and is shown in figure (2.3).

2.3.3 Spectrophotometric mass removal measurement

Since the mass of the ablated material was small and ablation took place in a fluid environment, conventional methods of measuring mass were not suitable. I therefore devised a method in which the absorbance of the solution was compared with the absorbance of a known concentration of dye solution to determine the mass of the ablated gel.

The method is based on the following argument: The absorbance $A(\lambda)$ of a dye solution at a

particular wavelength λ is proportional to the concentration C of the dye solution with the path length kept constant

$$A(\lambda) \propto C. \tag{2.5}$$

If the volume of water is not changed, the absorbance is proportional to the mass M of the dye dissolved,

$$A(\lambda) \propto M \tag{2.6}$$

or

$$A(\lambda) = K(\lambda)M. \tag{2.7}$$

A calibration experiment measuring the absorbance of known dye concentrations will determine the proportionality constant $K(\lambda)$. The amount of dye M_{xd} in the total ablated mass M_x can therefore be calculated by measuring the absorbance $A_x(\lambda)$ and using equation (2.7). For a particular absorption μ_a, the exact amount of dye M_d that went into the gel preparation is known. M_w and M_g are the masses of water and gelatin used for dye preparation. The total mass of gel prepared is therefore:

$$M_{gel} = M_w + M_g + M_d \tag{2.8}$$

If the amount of dye M_{xd} in the total ablated gel M_x is determined by measuring the absorbance $A_x(\lambda)$ of the ablated material, M_x can be calculated using:

$$M_x = \frac{M_{xd}}{M_d} \, M_{gel} \tag{2.9}$$

Substituting for M_{xd} using equation (2.7),

$$M_x = \frac{A_x(\lambda)}{K(\lambda)} \, \frac{M_{gel}}{M_d} \tag{2.10}$$

Absorbance $A(\lambda)$ was measured at $510\,\mathrm{nm}$ that corresponded to the absorption peak of the Direct Red chromophore (figure 2.1). The calibration curve was established by measuring absorbances of 0–$50\,\mu$g of the dye dissolved in $4\,\mathrm{ml}$ water. Five measurements were made for each data point to obtain an error estimate. There was a linear relationship between absorbance and dye mass which validated equation (2.7).

Two wavelengths

The measured absorbances in the calibration experiment had relatively large errors associated with them ($\sim$10–20%). This was probably due to the low dye concentrations used and variations

in the plastic cuvettes used to measure absorbance on the spectrophotometer.

$$A'(\lambda) = A(\lambda) + \epsilon(\lambda) \tag{2.11}$$

Here $A'(\lambda)$ and $A(\lambda)$ are the measured and true absorbances respectively, and $\epsilon(\lambda)$ is the error.

To reduce the calibration error, absorbances at two wavelengths were measured and the difference was calculated.

$$A'(\lambda_1) - A'(\lambda_2) = [A(\lambda_1) - A(\lambda_2)] + [\epsilon(\lambda_1) - \epsilon(\lambda_2)] \tag{2.12}$$

If the errors are not strongly dependent on wavelength, the subtraction will reduce the error, and the measured difference in absorbances will approach the true value.

The slope of the calibration line now becomes

$$S(\lambda_1, \lambda_2) = K(\lambda_1) - K(\lambda_2) \tag{2.13}$$

and the mass of the ablated gel is calculated by

$$M_x = \frac{A_x(\lambda_1) - A_x(\lambda_2)}{S(\lambda_1, \lambda_2)} \frac{M_{gel}}{M_d} \tag{2.14}$$

Absorbance was measured at $510\,\mathrm{nm}$ and $800\,\mathrm{nm}$ offering the largest dynamic range (figure 2.1). The error in the data points in the calibration experiment was of the order of 5%. The calibration line is shown in figure (2.4). The slope was determined to be $0.009\,\mu\mathrm{g}^{-1}$.

Finally, corrections due to material collected by washing, given by the control samples, were made.

$$\text{total mass ablated} = \frac{(A_s^{510} - A_s^{800}) - (A_c^{510} - A_c^{800})}{S(\lambda_1, \lambda_2)} \frac{M_{gel}}{M_d} \tag{2.15}$$

where A^{510} and A^{800} are the absorbances at $510\,\mathrm{nm}$ and $800\,\mathrm{nm}$ respectively. Subscripts 's' and 'c' refer to laser ablated samples and controls.

A direct correlation to the calibration and ablation experiments is possible since the ablated material was also collected in $4\,\mathrm{ml}$ of water. The ablation efficiency for each absorption coefficient and laser energy was calculated as the average mass ablated per laser pulse per unit energy.

2.4   Results

Ablation of gelatin was characterized by a snapping sound and visible removal of material. The ablated gelatin was removed in small chunks that quickly dissolved in the water. All the ablated material was collected in the mass removal experiments. The spectrophotometric method of

measuring the ablation mass proved accurate and reproducible with an error estimate of less than 5%. An increase in crater depth with multiple pulses was observed. Control samples showed that gelatin collected by the washing action alone typically accounted for less than 3% of the total mass removed.

2.4.1 Effect of absorption

At pulse energies of 25, 50, and 100 mJ, no material was removed at an absorption coefficient of $10\,\text{cm}^{-1}$ (figure 2.5). No snapping sound could be heard and gross visual examination revealed no craters. Pulse energies of 50–100 mJ resulted in ablation efficiencies of less than $1\,\mu\text{g/mJ}$ at $30\,\text{cm}^{-1}$. Acoustic signals were muted or absent. At higher absorption coefficients the ablation efficiency increased and remained roughly constant between 2–$3\,\mu\text{g/mJ}$ from 100–$1000\,\text{cm}^{-1}$ for all three pulse energies. Ablation in this region was accompanied by a loud snapping sound indicating explosive removal of material. Visual examination of the craters after 10 pulses showed the diameter to be within 10% of the spot size made by the fiber and the depth to vary from 4–6 mm. Above $1000\,\text{cm}^{-1}$ the ablation efficiency reduced slightly.

2.4.2 Effects of radiant exposure and repetition rate

More gelatin was removed with larger fibers at the same energy. The $1000\,\mu\text{m}$ fibers ablated about twice as efficiently as $300\,\mu\text{m}$ fibers (figure 2.7). Loud snapping sounds were heard for all the ten pulses fired through the $1000\,\mu\text{m}$ fibers, but the acoustic signals were muted after about five shots using the $300\,\mu\text{m}$ and $600\,\mu\text{m}$ fibers. The ablation efficiency was roughly constant at all pulse energies for a *single* spot size.

The spot sizes made by 300, 600, and $1000\,\mu\text{m}$ fibers one millimeter from polishing paper under water were measured to be 520, 650, and $1070\,\mu\text{m}$ in diameter respectively. Radiant exposures were calculated by dividing the pulse energy by the spot size made by the fiber. Energies of 50 mJ and 85 mJ through $300\,\mu\text{m}$ and $600\,\mu\text{m}$ fibers respectively produced iso-radiant exposures of about $250\,\text{mJ/mm}^2$, but resulted in different ablation efficiencies. Larger spot sizes resulted in greater ablation efficiencies at similar energies although the radiant exposures were lower. Ablation efficiency was slightly lower at higher repetition rates (figure 2.8).

2.5   Discussion

This study was carried out to find a suitable wavelength, radiant exposure, and repetition rate for microsecond laser ablation of thrombus. Since the choice of wavelength governed the absorption coefficient of thrombus, the effect of absorption on the ablation efficiency was studied using a gelatin-based thrombus model. The gelatin was ablated in Tygon tubes under water and ablation masses were measured.

Gelatin was ablated under simulated conditions of cylindrical geometry and a unique, yet simple method to accurately measure the ablation mass was presented. This method is based on the spectrophotometric signature of the ablated chromophore and allows the effects of various laser parameters and irradiance conditions on ablation under water to be investigated.

2.5.1   Effect of absorption on ablation efficiency

To find an optimal wavelength for laser thrombolysis, gelatin of various absorption coefficients was ablated and the mass removed was measured. At low absorption coefficients of $10\,\mathrm{cm}^{-1}$, pulse energies of 25, 50, and 100 mJ (radiant exposures of 28, 56, and $112\,\mathrm{mJ/mm}^2$ respectively) are below ablation threshold since no material was removed. This is confirmed in the next chapter where threshold radiant exposures are measured as a function of absorption (figure 3.7).

The ablation efficiency increases as the absorption increases from a low value of $10\,\mathrm{cm}^{-1}$ to about $100\,\mathrm{cm}^{-1}$ due to the decreasing threshold energies to below 25 mJ which was the lowest energy used in the ablation mass experiments (figure 2.5). However, at $100\,\mathrm{cm}^{-1}$ and above, when all three pulse energies were above threshold, the ablation efficiency did not change much with absorption. The slight decrease in efficiency at high absorption coefficients may be the result of overheating the target material. The comparable mass removal between 100–$1000\,\mathrm{cm}^{-1}$ indicates that ablation efficiency does not strongly depend on the optical penetration depth (10–$100\,\mu\mathrm{m}$) at energies above threshold.

Figure (2.6) shows the same data as figure (2.5), but it relates the pulse energy to the threshold energy at the corresponding absorption coefficient. The x-axis value for each data point is obtained by dividing the pulse energy by the threshold energy for the corresponding absorption coefficient. The threshold values for the various absorption coefficients were taken from chapter 3, where the threshold experiments are described in detail. Slight mass removal is observed at energies just below threshold. This was probably due to melting of the gelatin and not due to explosive ablation. The mass removal curves for the three pulse energies become flat when the

pulse energy reaches threshold. In other words, the mass removed does not depend on whether the delivered energy is just at threshold or well above it. It does however depend on the total energy delivered; a 100 mJ pulse removes twice as much as a 50 mJ pulse.

It has now been shown that absorption has little effect on the mass removal in the absorption region of 100–1000 cm^{-1} at pulse energies of 25–100 mJ. This has a direct implication for the choice of wavelength for laser thrombolysis as seen in figure (2.9), with the caveat that a change in ablation efficiency can be expected due to the different mechanical strengths of thrombus and gelatin. Thrombus has an absorption range of 100–1000 cm^{-1} in the waveband between 410–590 nm, and therefore any wavelength in this range can be chosen without significantly compromising the efficiency. Selectivity would still be retained since vessel wall absorption is less than 10 cm^{-1} in this waveband.

Two main theories have been proposed to model pulsed laser ablation of tissue. The steady-state model assumes a constant ablation velocity during the laser pulse [84]. The blow-off model assumes that ablation commences after the laser pulse [85]. Both models describe mass removal in air and assume that material is removed as a result of heating and vaporization of tissue. The vaporized volumes predicted by the two models are:

$$V_{ss} = \frac{Q(E_0 - E_{th})}{\rho(c\Delta T + L_v)} \tag{2.16}$$

$$\frac{V_{bo} = \frac{Q}{\mu_a} \ln(E_0}{E_{th})} \tag{2.17}$$

E_0 is the incident radiant exposure (mJ/mm^2), E_{th} is the threshold radiant exposure, and Q is the area of the irradiated spot (mm^2). ΔT in equation (2.16) is the temperature rise to boiling (100°C), and the radiant exposure needed to achieve that rise is given by equation (2.3). L_v is the latent heat of vaporization (J/g).

Both the steady-state and blow-off models predict a strong dependence of the mass removal on the absorption coefficient as seen in equations (2.16) and (2.17) [84, 86]. However, this study has shown that the total mass removal under water is fairly independent of absorption at energies above threshold. This implies that vaporization is not the dominant factor in the mass removal under a liquid at energies much above threshold. The dominant factor in mass removal under a liquid is some mechanical action which is most likely the result of expansion and/or collapse phases of the vapor bubble.

2.5.2 Effect of radiant exposure

Radiant exposures produced by a $300\,\mu$m fiber ($520\,\mu$m spot size) were about four times those produced by a $1000\,\mu$m fiber ($1070\,\mu$m spot size) at similar energies, and yet ablation per unit energy was more efficient with the larger fiber. Also, iso-radiant exposures did not result in similar ablation efficiencies. Thus there is no direct relationship between ablation efficiency and radiant exposure.

Some previous studies have reported a linear increase in mass removal with radiant exposure [86, 87, 88]. However, in those studies the tissue was ablated in air and in an unconfined geometry. Further, the radiant exposure was varied by varying the pulse energy while maintaining a constant irradiated spot size. We also observed a linear increase in mass removal with pulse energy (constant ablation efficiency) for a *single* spot size.

The vaporization models described in the previous section predict an increase in ablation mass at higher radiant exposures. The results I have reported here do not reflect such a trend. This again suggests that vaporization does not remove most of the material in the ablation process. A possible explanation for the higher ablation efficiencies with larger fibers at the same energies could be that the dynamics of the vapor bubbles formed are different once the energy is above threshold.

Etch depths were calculated on the assumption that the ablated mass was removed from a cylindrical volume with a diameter equal to the spot size. The density of the gelatin was assumed to be $1\,$g/cm^3. Figure (2.10) shows the etch depth per pulse as a function of pulse energy for the three fibers used. It suggests that while smaller spot sizes remove less mass than bigger spot sizes at similar energies, they dig deeper craters. This hints at another explanation for the smaller average efficiency of the smaller fibers. Since smaller fibers dig deeper holes, it is possible that the ablation debris from a laser pulse is not cleared completely by the time the next pulse arrives. The debris will then attenuate the energy delivered to the gel leading to decreasing mass removal per pulse with increasing pulses. This hypothesis is partially supported by the muted acoustic reports heard during the later pulses delivered by the smaller fibers. The amounts removed per pulse by the early pulses may therefore be similar with small and large fibers. However, it is clear that the total mass removed after 10 pulses is greater with the larger fibers. The efficiency of the later pulses could be increased by increasing the flow rate of the fluid stream.

The ablation efficiencies measured are in rough agreement with the ablation of calcified plaque and normal artery under saline as reported by Prince *et al.* [89]. However, they are about

an order of magnitude higher than the results of other investigators who ablated tissue in air [86, 50]. This again suggests that most of the work in the ablation process in a liquid is cause by some mechanical action resulting from the vapor bubbles. Earlier studies have suggested the participation of the vapor bubble in tissue removal and damage [71, 70]. Van Leeuwen *et al.* and Jansen *et al.* investigated vapor bubble formation during excimer and holmium laser angioplasty. They found that the pressure transients generated by bubble expansion and collapse within arteries could cause dissections in the vessel wall. Vogel attributed retinal damage incurred during intraocular surgery to bubble formation [105]. However, they did not measure mass removal. There is little doubt that pulsed laser ablation of tissue in a liquid is an explosive process, partly due to the cavitation effects. The bubble activity has both beneficial effects by removing unwanted tissue, and detrimental effects by inducing damage to collateral tissue. The hypothesis that the bubble is principally responsible in mass removal is investigated in chapter 4.

2.5.3 Effect of pulse repetition rate

Ablation efficiencies were largely independent of the pulse repetition rate between 1–10 Hz. This means that the ablative events last for less than 100 ms which was the shortest time interval between consecutive pulses. Ablation efficiency decreased slightly at higher repetition rates (figure 2.8). Possibly the ablated material from a previous pulse was not cleared from the target area by the time the next pulse arrived. The laser energy would then be attenuated before reaching the gel surface.

2.5.4 Clinical Implications and Limitations

The results of this investigation indicate that laser wavelengths between 410–590 nm are most suitable for removing thrombus in vessels. Currently used wavelengths of 480 nm and 577 nm for laser thrombolysis were chosen because of good absorption by beta-carotene and hemoglobin respectively. As shown in this study, these are acceptable wavelengths from an ablation efficiency point of view. Choosing a wavelength must take other factors into consideration, e.g., cost and ease of design.

The higher ablation efficiencies with larger fibers at similar energies suggest that larger diameter catheters would be better at creating wider lumen during laser thrombolysis. Clearly, the size of the catheter constrained by flexibility requirements and the size of the vessel. Despite the

evidence that larger catheters would not dig as deeply into the thrombus as a small catheters at similar energies, this effect (30–40%) could be compensated by more pulses or greater pulse energies. Higher pulse energies result in greater ablation masses. The maximum energy that can be used with a particular spot size during laser thrombolysis would be limited by (i) the ablation threshold for the vessel wall, and (ii) big bubbles formed in thrombus that might cause dissections in the vessel.

The repetition rate currently in clinical use is $3\,\mathrm{Hz}$. The results of this study imply that laser thrombolysis can be done at about $10\,\mathrm{Hz}$ without seriously compromising the efficiency. The slight decrease in the ablation efficiency is compensated by the potential for reducing the total time of the ablation procedure. This conclusion is verified in the fifth chapter where porcine clot is ablated at different repetition rates.
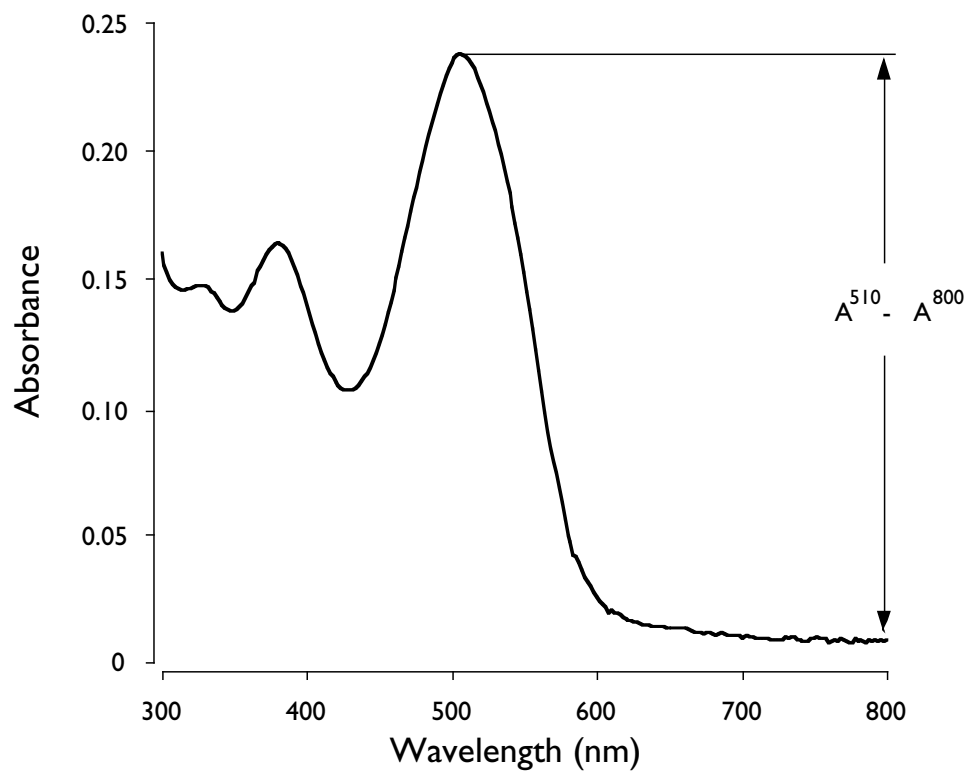
Figure 2.1: Direct Red absorption spectrum: The difference in absorbances at 510 nm and 800 nm of the ablated gelatin in solution gives a measure of its dye content from which the total mass of ablated material can be determined. Absorbance was measured in a 1 cm cuvette with 6 μg/ml dye concentration in water.

1 μs laser
pulses

fiber

water

1mm

gel

3mm

cuvette

ablated gel collected in 4 ml water
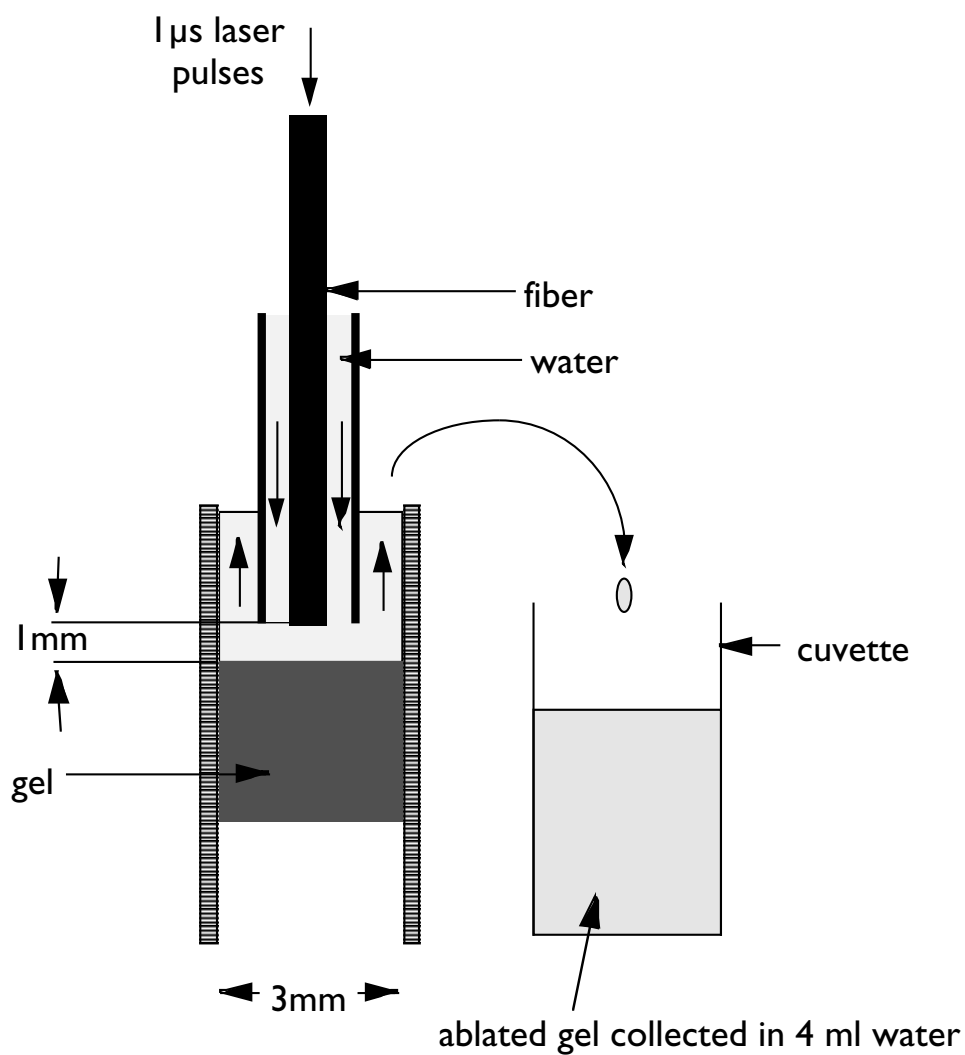
Figure 2.2: Gelatin containing an absorbing dye is confined in a 3 mm diameter tube. Laser energy is delivered in $1\,\mu$s pulses via a solid glass fiber at a distance of 1 mm to the gelatin. The ablated material is collected in 4 ml water and the absorbance is measured in a spectrophotometer.
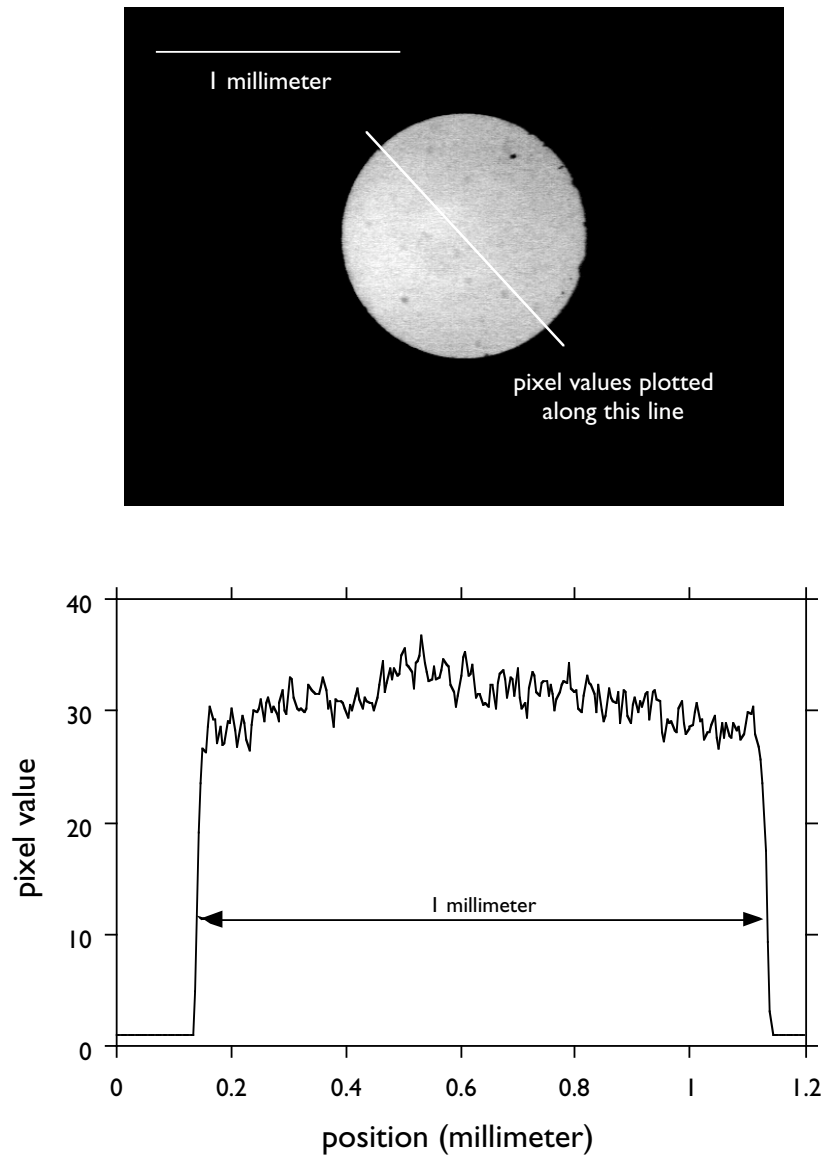
Figure 2.3: Laser spot 1 millimeter out of a $1000\,\mu$m fiber. The pixel plot indicates a uniform profile
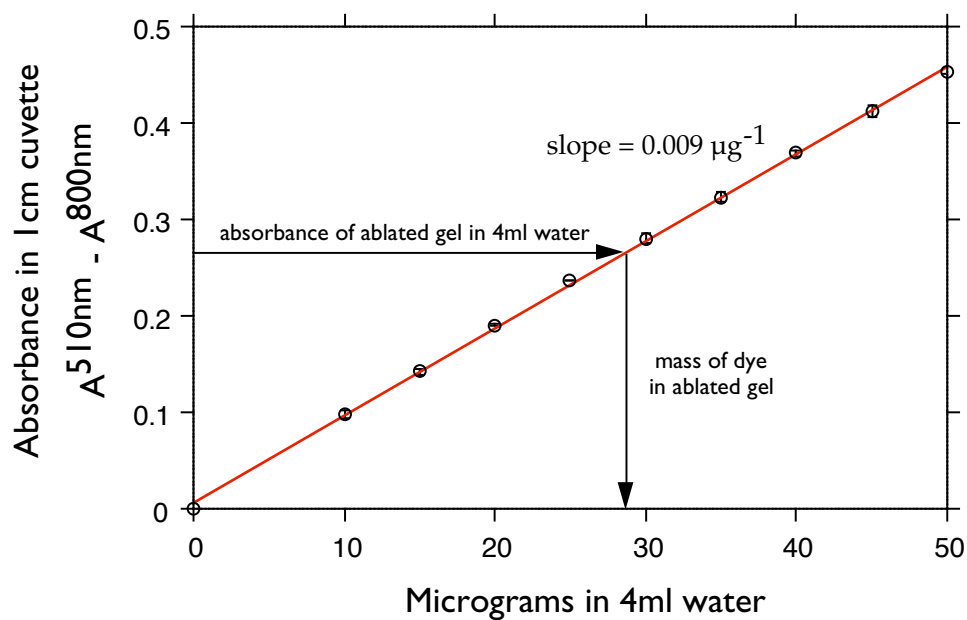
Figure 2.4: Calibration line for spectrophotometric mass removal measurements. Error bars are smaller than the symbols. The absorbance of the ablated material is measured and the mass of dye in the ablated mass is determined from the calibration line. The mass of dye is then converted to the total mass removed by using a multiplication factor.
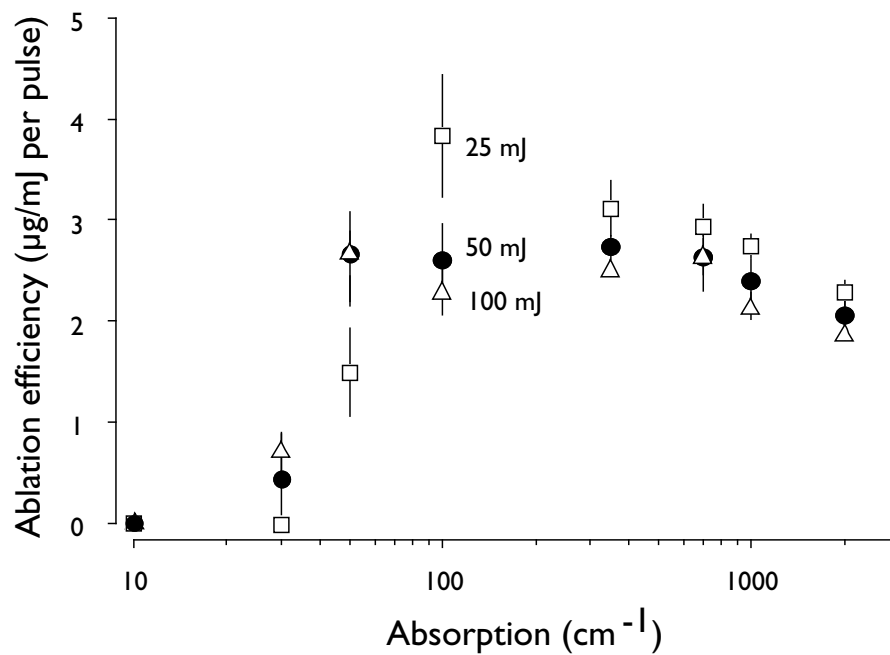
Figure 2.5: Ablation efficiency as a function of absorption at different pulse energies. The squares, circles, and triangles represent pulse energies of 25, 50, and 100 mJ respectively. A 1000 μm core diameter glass fiber was used for laser delivery. Values are averages of 10 pulses. Error bars denote standard deviation of 10 samples.
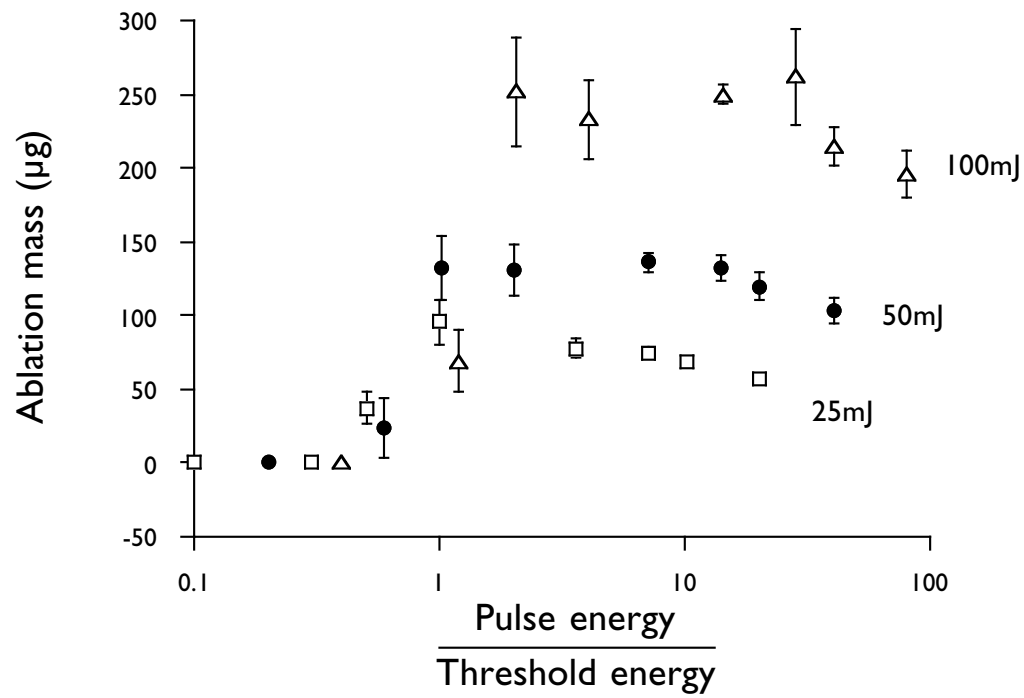
Figure 2.6: Mass removal at the pulse energies of 25 mJ, 50 mJ, and 100 mJ related to threshold energies for various absorption coefficients. Threshold values were taken from chapter 3. Mass removal seems to be quite efficient even when the pulse energy is just at threshold. At high absorption coefficients where the energy is well above threshold, mass removal decreases. This is probably due to overheating of the material.
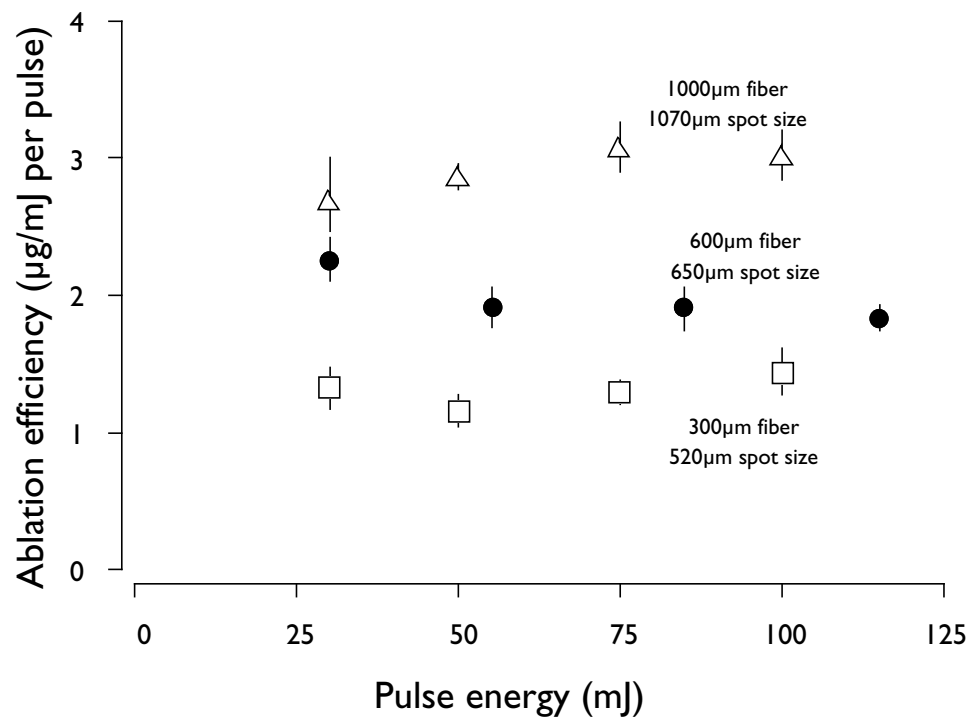
Figure 2.7: Ablation efficiencies at various pulse energies and spot sizes. The squares, circles, and triangles represent 300, 600, and $1000\,\mu$m fibers respectively. Absorption coefficient of the gelatin was $300\,\text{cm}^{-1}$. Values are averages of 10 pulses. Error bars denote standard deviation of 10 samples.
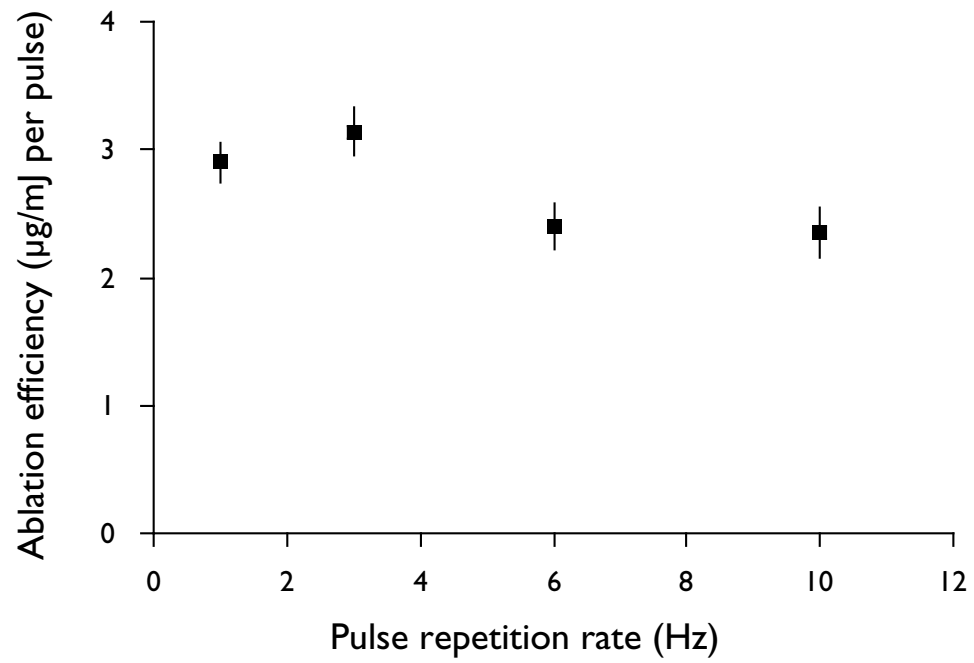
Figure 2.8: Effect of repetition rate on ablation efficiency. A $1000\,\mu$m fiber was used to deliver $100\,$mJ energy to a $100\,$cm^{-1} gel target.
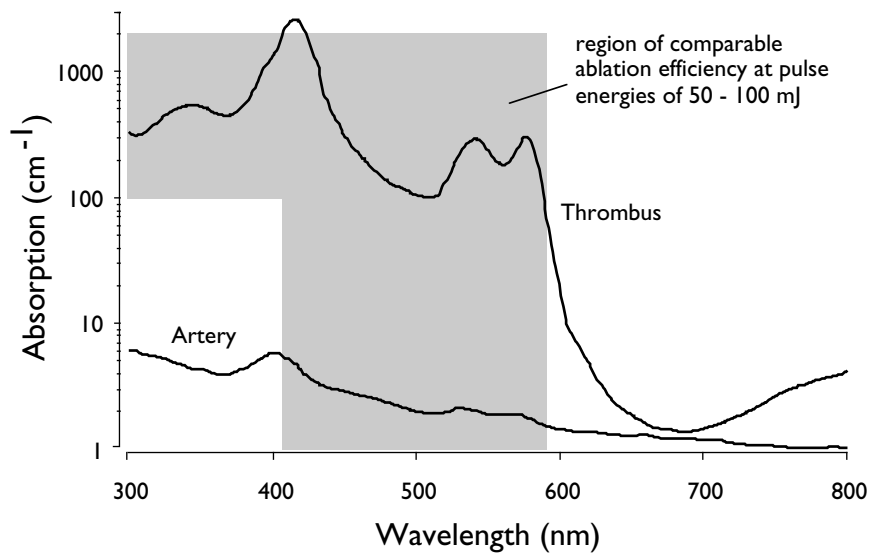
Figure 2.9: Wavelengths for laser thrombolysis: An absorption range of $100–1000\,\mathrm{cm}^{-1}$ corresponds to the waveband between $410–590\,\mathrm{nm}$ for thrombus absorption. Ablation efficiency is independent of wavelength in this range at pulse energies above threshold. Selectivity is still maintained due to low absorption by artery.
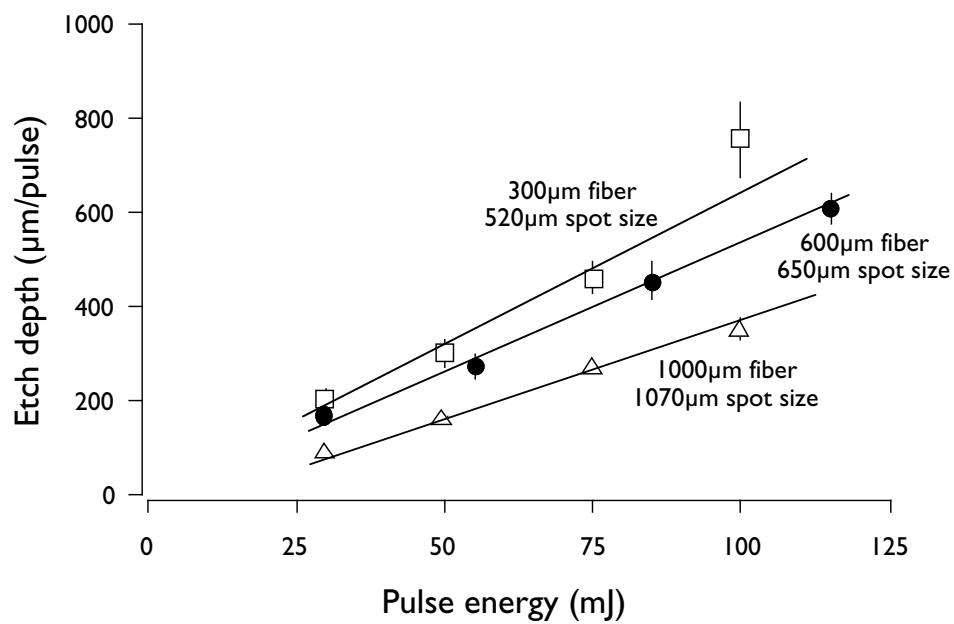
Figure 2.10: Calculated etch depths at various pulse energies and fiber sizes: Ablated mass is assumed to be removed from a uniform cylinder with spot size as diameter. Etch depths represented here are an average of ten pulses. Absorption was $300\,\text{cm}^{-1}$. Error bars denote standard deviation of 10 samples. Lines are visual best fits.

Chapter 3

Threshold radiant exposures for microsecond ablation

This chapter describes experiments to determine microsecond ablation thresholds at any wavelength.[1] Stress and thermal confinement issues pertaining to onset of ablation are presented. Thresholds are measured as a function of absorption and mapped onto the absorption spectra of thrombus and artery.

Laser pulses were delivered to gelatin-based clot models under water and in air. The pulse energy was increased until ablation was detected. Onset of ablation was detected both indirectly and directly. Surface temperatures were monitored at radiant exposures below and above threshold. Measured values were compared with those predicted by various ablation models.

Ablation thresholds for gel were found to be in good agreement with those available in literature for blood, atheroma, and vessel wall. Onset of ablation was governed by the radiant exposure rather than by the pulse energy. The threshold radiant exposure was roughly inversely proportional to the absorption coefficient. Visualization experiments showed that ablation commenced with the formation of a vapor bubble. There were no significant differences between thresholds under water and in air.

A calculation of temperature increase indicated that the surface temperature has to be increased to just above 100°C for ablation to commence. The latent heat of vaporization was not required. Microsecond ablation thresholds for thrombus under water can be estimated at any visible wavelengths.

---

[1]This chapter is part of the paper "Threshold and ablation efficiency studies microsecond ablation of gelatin under water" to be published in *Lasers in Surgery and Medicine*, 19:3, 1996.

3.1 Stress and thermal confinement

The absorption of a laser pulse by tissue causes heating; ablation can follow as a result of tissue tearing or vaporization [90]. Tearing can occur when the thermo-elastic expansion of the heated volume causes stress to build up in the optical zone. Large stresses develop when the heating is so rapid that the pressure transients do not have time to dissipate out of the irradiated volume. The time it takes for pressure waves to leave the irradiated volume is given by:

$$\tau_s = \frac{\delta}{\sigma} \tag{3.1}$$

where σ is the speed of sound in the tissue ($\sim$1500 m/s), and δ is the optical penetration depth. Stress confinement occurs when the laser pulse τ_p is shorter than τ_s [90].

Pulsed laser ablation may also proceed through vaporization. The laser energy is thermally confined when the pulse duration is shorter than the time required for heat to diffuse out of the irradiated volume during the laser pulse. This time is given by:

$$\tau_h = \frac{\delta^2}{\kappa} \tag{3.2}$$

where κ is the thermal diffusivity ($\sim$0.0014 cm^2/s). Temperature increases during the laser pulse until 100°C is reached. If more energy is deposited, then vaporization commences [70]. Ablation with longer pulses or continuous wave lasers is also initiated by vaporization [84, 85]. However, the energy required to reach vaporization temperature is higher due to diffusion of heat out of the irradiated volume during the laser pulse.

Times for stress confinement are shorter than those required for thermal confinement. Pulsed laser ablation of tissue can therefore be broadly divided into three regimes: stress confinement ($\tau_p < \tau_s$), thermal confinement ($\tau_s < \tau_p < \tau_h$), and no confinement ($\tau_h < \tau_p$). In the case of blood and thrombus, the optical penetration depth varies between 10–100 μm in the visible region. The microsecond pulse from the dye laser therefore does not meet stress confinement conditions. However, the absorbed energy is thermally confinement, and ablation should proceed through vaporization.

3.2 Goals

One of the goals of the preceding chapter was to find an optimal wavelength for laser thrombolysis. The results of those experiments suggested that almost all visible wavelengths were suitable for efficient ablation. They also showed that increasing the pulse energy resulted in more mass

removal. However, the energy cannot be increased indiscriminately since that will lead to ablation of the arterial wall. The radiant exposure therefore has to be maintained at a level that is both efficient and safe: above the ablation threshold for thrombus and below that for arterial wall. Threshold values for atherosclerotic plaque, thrombus, vessel wall, and blood are available in literature only at selected wavelengths [50, 52]. Since the choice of wavelength is largely flexible, threshold information for the entire visible region is crucial.

Determination of thresholds will also help understand the basic ablation process. The steady-state and blow-off thermal ablation models mentioned in the preceding chapter both predict ablation thresholds based on vaporizing tissue in a thermal confinement regime. The radiant exposure required to heat the tissue surface to $100°C$ and then vaporize it is given by:

$$E_{th} = \frac{\rho(c\Delta T_{100} + L_v)}{\mu_a}$$
(3.3)

Van Leeuwen *et al.* and Jansen *et al.* investigated bubble formation in a liquid during excimer and holmium angioplasty and proposed a partial vaporization theory. This theory suggests that at threshold for bubble formation, the temperature of the liquid needed to be raised to just above $100°C$ [71, 70]. The latent heat of vaporization for the phase change of the entire irradiated area was not required. Any extra energy would initiate vaporization at a few nucleation sites over the irradiated area.

$$E_{th} = \frac{\rho c\Delta T_{100}}{\mu_a}$$
(3.4)

It is not clear which is model is applicable to predict microsecond ablation thresholds for laser thrombolysis. The partial vaporization model may be more accurate since the results of the preceding chapter suggest that the mass removal is influenced by bubble formation.

3.3 Materials and methods

Gelatin containing a light-absorbing dye (Direct Red 81) was used to model clot and vessel wall. The absorption was controlled by varying the amount of dye in the gel. Since the laser wavelength determines the absorption of thrombus and artery, thresholds were measured as a function of absorption. The threshold at a particular wavelength would then be the value at the corresponding absorption.

Microsecond pulses were delivered to gel targets under water, and the pulse energy was increased until ablation was detected. Four different methods were used to detect ablation:

- acoustic signature of ablation

- deflection of a HeNe probe beam

- direct mass removal measurements

- direct visualization of ablation

The first two methods were indirect methods based on the assumption that an acoustic signal and the deflection of a probe beam were caused by an ablation-related phenomenon. To verify the results of these methods, thresholds were determined at selected absorptions by directly measuring mass removal and by visualizing the ablative process.

Surface temperatures at threshold were calculated using equation (2.3) to estimate the temperature necessary for vaporization. Infrared emission from the surface following pulsed irradiation below and above threshold were monitored to detect any changes in the surface temperature signals at threshold. Such a change would give an indication of the energy that goes into the phase change during vaporization.

3.3.1 Acoustic ablation signals

Ablation threshold energies at absorption coefficients from 10–$2000\,\mathrm{cm}^{-1}$ were determined by detecting an acoustic signal accompanying ablation in a semi-infinite medium under water (figure 3.1). Gel samples were prepared in a $250\,\mathrm{ml}$ beaker to form a $1\,\mathrm{cm}$ thick layer and covered with water. The beaker was then placed on a PVDF transducer (Hydrosonics) connected to a digital signal analyzer (Tektronix DSA 602A) through an amplifier (Hydrosonics). A photodiode detecting the laser light provided the trigger source for the oscilloscope.

Laser pulses were delivered from a distance of $1\,\mathrm{mm}$ to the gel surface via a $1000\,\mu\mathrm{m}$ fiber, and explosive ablation was accompanied by an acoustic signal that was detected by the transducer (figure 3.2). The threshold energy was the pulse energy required to produce a signal of $30\,\mathrm{mV}$ peak-to-peak on the signal analyzer. A value of $30\,\mathrm{mV}$ was chosen because it was the minimum signal differentiable from the background noise.

Each pulse was fired on a fresh target area to maintain surface geometry and fiber-to-target distance. Five measurements were taken for each absorption coefficient and radiant exposures were calculated by dividing the threshold energy by the spot size on the gelatin surface. Ablation threshold energies for $300\,\mathrm{cm}^{-1}$ gels were also determined using $300\,\mu\mathrm{m}$ and $600\,\mu\mathrm{m}$ fibers and threshold radiant exposures were calculated.

3.3.2   Deflection of He-Ne probe beam

Gelatin was prepared in 1 cm plastic cuvettes with transparent walls and covered with water. A HeNe beam was directed into the cuvette through one of the walls such that it just grazed the surface of the gelatin (figure 3.3). Upon exiting the cuvette through the opposite wall, the beam was detected by a photodiode and the signal was fed into the digital oscilloscope. The diameter of the beam was reduced with a $200\,\mu$m pinhole before entering the cuvette. A similar pinhole was placed in front of the photodiode such that only light along the straight path between the pinholes could be detected. A minor deflection in the HeNe beam would now manifest itself in a drop in the photodiode signal.

Laser pulses were delivered via a $1000\,\mu$m fiber with the tip 1 mm from the gel surface. The orientation of the fiber was such that its axis intersected the HeNe probe beam at $90°$. Any ablation event would then be initiated just under the probe beam and either deflect or block the beam. A photodiode detecting the laser light provided the trigger source for the oscilloscope. The threshold energy was the minimum pulse energy required to produce a drop in the photodiode signal (figure 3.4). Unlike the previous experiment with the acoustic transducer, this was an all-or-none experiment. The photodiode signal either dropped completely to zero, or it did not drop at all.

3.3.3   Mass removal measurements

Mass removal measurements were carried out in a similar manner as described in chapter 2. Gelatin was confined in 3 mm inner diameter tubes and light was delivered via a $1000\,\mu$m fiber (figure 2.2). Water was directed around the target site at a rate of 0.3 m/s using a fluid injector. Mass removal was measured using the spectrophotometric method. Pulse energies were increased from a low value at which there was no mass removal. Threshold was designated as the pulse energy at which mass removal commenced. Absorptions of $10\,\mathrm{cm}^{-1}$, $100\,\mathrm{cm}^{-1}$, and $1000\,\mathrm{cm}^{-1}$ were used.

3.3.4   Visualization of ablation

Flash photography was used to directly visualize the events occurring following laser delivery (figure 3.5). Gelatin was ablated in 1 cm cuvettes using a $1000\,\mu$m fiber, and the ablation process was captured using a CCD camera (CV-250, Motion Analysis, Eugene, OR) and a $1\,\mu$s strobe (Machine Vision Strobe, EG & G). The image was captured $5\,\mu$s after the laser pulse and the

delay was controlled by a delay generator. A photodiode detecting the laser pulse provided the trigger for the timing. A delay of $5\,\mu$s was chosen based on experimental determination that ablative events at threshold lasted for about $10\,\mu$s. The image was thus captured at roughly the midpoint of the sequence of events. A laser filter was placed in front of the camera to avoid blinding the CCD chip. Threshold was the minimum laser energy at which "something" visibly happened.

3.3.5   Surface temperature signals below and above threshold

The thermal response at the surface following pulsed laser irradiation was monitored with a fast infrared detector. Pulse energies below and above threshold were delivered, and the surface emission signal was analyzed for any change at threshold. An absorption of $100\,\mathrm{cm}^{-1}$ was used. This experiment was done in air instead of under water to avoid absorption of the infrared signal.

A $1\,$mm fiber delivered pulsed irradiation at right angles to the gel surface (figure 3.6). The fiber tip was $5\,$mm from the gel surface, and the resulting spot size on the surface had a diameter of $1.6\,$mm. The fiber was pulled back from the usual $1\,$mm distance for two reasons: the field of view of the infrared detector was not to be obstructed, and a larger spot size was desired to preclude significant diffusion of heat in the radial directions. Pulse energies of 15–$70\,$mJ were delivered which covered a range from subthreshold to supra-threshold radiant exposures.

A HeCdTe detector (EG & G, Judson) with an active area of $1\,\mathrm{mm}^2$ detected the infrared emission from the surface. The detection angle was about $45°$, and the optics included a telescope made of germanium lenses with a conjugate ratio of 1:1. The rise time of the detector was $500\,$ns, and the wavelength detection range was 8–$12\,\mu$m. The output signal was amplified by a preamplifier (PA-350, EG & G, Judson) with a bandwidth of DC–$1.5\,$MHz and stored on the digital signal analyzer.

Ablation pictures of the gel surface were taken at the same time using the flash photography setup described in the previous section. This was done to determine whether thresholds were different in air. The pictures were also taken at an angle of about $45°$.

3.4 Results

3.4.1 Threshold radiant exposures

Threshold radiant exposures ranged from $160\pm10\,\mathrm{mJ/mm^2}$ at $10\,\mathrm{cm^{-1}}$ to $8.5\pm0.5\,\mathrm{mJ/mm^2}$ at $1000\,\mathrm{cm^{-1}}$ (figure 3.7). Gross visual examination of the gelatin surface revealed craters at energies that produced an acoustic signal. Some surface deformation was observed in a few cases at energies below the designated threshold indicating minimal material removal. At high absorptions the threshold values were low, and the the laser output was unstable at low energies ($< 25\,\mathrm{mJ}$). The pulse energy had variations of sometimes up to 20%. Therefore the laser was run at higher energies with a calibrated neutral density filter in the path of the laser beam to attenuate the output energy. Output was then stable within 2%. Thresholds values measured with both the acoustic and HeNe probe beam methods agreed with each other within 20%.

The threshold values obtained were validated by spectrophotometric mass loss experiments using Tygon tubes at absorption coefficients of 10, 100, and $1000\,\mathrm{cm^{-1}}$. Threshold was designated as the energy at which mass loss commenced. Figure (3.8) indicates a threshold value of about 130–$170\,\mathrm{mJ/mm^2}$ for an absorption of $10\,\mathrm{cm^{-1}}$. The values obtained by the four methods at these absorption coefficients are shown in table (table:thresholds) and agree favorably with each other.

The spot sizes made by 300, 600, and $1000\,\mu\mathrm{m}$ fibers one millimeter from polishing paper under water were measured to be 520, 650, and $1070\,\mu\mathrm{m}$ in diameter respectively. Threshold energies of 4, 7, and $13\,\mathrm{mJ}$ were measured using 300, 600, and $1000\,\mu\mathrm{m}$ fibers respectively on $300\,\mathrm{cm^{-1}}$ gelatin. The radiant exposure was calculated in each case by dividing the threshold energy by the corresponding spot size. This resulted in a threshold radiant exposure of $18\pm3\,\mathrm{mJ/mm^2}$.

The flash photography experiments show the formation of a vapor bubble at pulse energies close to those designated as threshold in the previous experiments (figure 3.9). No bubbles or any other discernable ablative events were observed at lower energies. Since the bubble was formed at the gel-water interface, only the top half was clearly visible. The bubble shape at threshold was oval with a base diameter equal to that of the $1\,\mathrm{mm}$ spot size and a height of about 200–$300\,\mu\mathrm{m}$. Bubble sizes increased with pulse energy and the shape became more spherical. Material removal was observed during and after the bubble lifetime.

3.4.2 Estimates of threshold surface temperatures

Surface temperature increases $\Delta T(0)$ at threshold were estimated using equations (2.1) and (2.3).

$$\Delta T(0) = \frac{\mu_a E_0}{\rho c} \qquad (3.5)$$

E_0 is the incident radiant exposure at threshold. The heat capacity ρc was assumed to be that of water $(4.184 \, \mathrm{J/(cm^3 \, °C)})$ which should be a valid approximation given the high water content of the gel. Room temperature was (25°C) added to obtain absolute temperatures (figure 3.10).

3.4.3 Surface thermal signals below and above threshold

Following absorption of the laser pulse, the surface heated up and emitted infrared radiation. The amplitude time course of the surface photothermal signal scaled with the delivered pulse energy at all times after the laser pulse (figure 3.11). This experiment was done at an absorption of $100 \, \mathrm{cm^{-1}}$, and threshold radiant exposure was measured to be about $20 \, \mathrm{mJ/mm^2}$ using the methods described above. No change in the surface emission profile was observed between radiant exposure levels below and above threshold.

The photothermal signals shown in the figure (3.11) were averaged over sixteen shots at $1 \, \mathrm{Hz}$ to reduce the noise level. Averaged signals were randomly compared to single-shot signals to check if multiple shots caused a change in the time course of the signal. No such change other than the noise level was observed. No calibration experiment was performed to convert raw voltage into real temperatures for lack of a suitable calibrated thermal source.

Simultaneous flash photography of the gelatin surface showed a tiny vapor bubble being formed at a pulse energy of about 35–40 mJ over a 1.6 mm spot (figure 3.12). Images were captured at $5 \, \mu\mathrm{s}$ after the laser pulse. Since multiple shots were fired, the bubbles formed by each shot were stored as a sequence on a video tape and made into a movie. No bubbles were seen at energies below threshold (15 mJ). The size of the bubble formed at threshold ($\sim$35 mJ) increased with each shot, and sometimes a discernable bubble was observed only after a few pulses. However, at energies well above threshold (70 mJ), a bubble was formed with the first shot, and the size of the following bubbles did not change with subsequent shots.

3.5 Discussion

This study was carried out to determine microsecond threshold radiant exposures for thrombus and artery at any wavelength in the visible region. The absorption of thrombus and vessel

wall vary between $0.1–1000\,\mathrm{cm}^{-1}$ in this waveband, and thresholds were therefore measured as a function of absorption. Gelatin containing an absorbing dye was used to model an absorbing soft tissue. Microsecond laser pulses were delivered with $300\,\mu\mathrm{m}$, $600\,\mu\mathrm{m}$, and $1000\,\mu\mathrm{m}$ fibers to gelatin both under water and in air. Thresholds were measured by detecting onset of ablation using direct and indirect methods. The indirect methods were detection of an acoustic signal accompanying ablation, and the deflection of a HeNe probe beam due to an ablation related event. Direct methods included measurement of ablation mass and visualization of ablation. Though the acoustic signal was probably degraded by acoustic mismatches at the gelatin-glass and glass-transducer boundaries, the mere presence or absence of a signal was sufficient to differentiate between ablation and non-ablation. No attempt was made to quantitatively analyze the signal.

The threshold values obtained with all the four methods agreed with each other within 20%. This suggests that onset of ablation is not affected by the cylindrical confinement of the vessel. Measurements with 300, 600, and $1000\,\mu\mathrm{m}$ fibers on $300\,\mathrm{cm}^{-1}$ gelatin resulted in nearly equal threshold radiant exposures. This shows that the onset of ablation is governed by radiant exposure and not by energy.

The thresholds agree with those found by Prince *et al.* for microsecond ablation of atheroma and normal aorta at similar absorption coefficients ($68\,\mathrm{mJ/mm^2}$ at $54\,\mathrm{cm}^{-1}$ and $160\,\mathrm{mJ/mm^2}$ at $26\,\mathrm{cm}^{-1}$ respectively) [50]. LaMuraglia *et al.* reported a threshold radiant exposure of $11\,\mathrm{mJ/mm^2}$ for the ablation of fresh thrombus at a wavelength of $482\,\mathrm{nm}$. The absorption of thrombus at this wavelength is $\sim100–200\,\mathrm{cm}^{-1}$, and according to the measurements on gel the threshold radiant exposure for this range lies between $15–20\,\mathrm{mJ/mm^2}$ (figure 3.13). The experimental values reported here also agree with thresholds measured by de la Torre *et al.* for bubble formation in lysed blood at various hematocrits within 10% [91]. This close correlation goes towards the validity of gelatin as an optical model for soft tissue. Evidently the threshold radiant exposure depends mainly on the absorption coefficient and is relatively independent of material.

It is now possible to predict microsecond ablation thresholds for both thrombus and vessel wall at any wavelength in the visible region. The thresholds can be read off the graph in figure (3.14) at the corresponding absorptions. Thresholds were not measured at very low absorptions ($\sim1\,\mathrm{cm}^{-1}$) corresponding to a wavelength of about $600\,\mathrm{nm}$ due to energy output limitations of the laser. However, the inverse relationship between thresholds radiant exposure and absorption evident in figure (3.7) can be extrapolated back to obtain a value of about $2000–3000\,\mathrm{mJ/mm^2}$

at $1\,\mathrm{cm}^{-1}$. It is also highly unlikely that such a poorly absorbed wavelength would be used for laser thrombolysis.

The experimental threshold values reported in this paper are about an order of magnitude lower than those predicted by both the steady-state and the blow-off models. They are, however, of the same order of magnitude as theoretically calculated by the partial vaporization model. The partial vaporization theory describes the formation of a vapor bubble during pulsed laser ablation under a liquid. It predicts that at threshold, the temperature of the liquid needed to be raised to just above $100°\mathrm{C}$ [71, 70]. Vaporization was then assumed to be initiated at a few nucleation sites. The visualization experiments under water confirm that ablation is initiated by the formation of a vapor bubble. The bubble expands and collapses, and material is removed. The acoustic signal detected is probably the result of bubble expansion and collapse during ablation.

The measured thresholds at very low absorptions ($\sim 15\,\mathrm{cm}^{-1}$) are slightly lower than those predicted by the partial vaporization model. A possible explanation could be that a microsecond pulse comes close to being stress confined at those low absorption coefficients ($\tau_s \approx 0.67\,\mu\mathrm{s}$). Therefore pressure transients could be participating in the initiation of ablation. Also, at high absorption the measured values are higher than those predicted by the partial vaporization model. Since the microsecond pulse is well within the thermal confinement regime ($\tau_h \approx 800\,\mu\mathrm{s}$), it is unlikely that the higher thresholds are due to heat diffusion out of the irradiated volume during the laser pulse. I propose two possible reasons for the discrepancy, both experimental:

- Absorption greater than $500\,\mathrm{cm}^{-1}$ were not measured directly due to limitations of the spectrophotometer. Instead, dye concentrations required for moderate absorptions ($\sim 100\,\mathrm{cm}^{-1}$) were extrapolated to calculate the concentrations needed for high absorptions. This was based on the assumption that absorption had a linear relationship with dye concentration. Any small error in absorption measurement would get multiplied by the extrapolation. Therefore, there is an uncertainty associated with high absorption values.

- The dye-content of highly absorbing gels is high, and it was noticed that when the gel was covered with water some of dye diffused out of the gel into the water. A thin layer of dye solution of non-negligible absorption was formed over the gel surface. This layer may have attenuated the laser energy before it reached the gelatin thus increasing the threshold.

A calculation of threshold temperatures shows that the surface needs to be heated to about $100°\mathrm{C}$ for ablation to be initiated. The latent heat of vaporization has to be supplied for the phase change. If the whole disk under the irradiated area is to be vaporized, the additional energy

required for the latent heat is about an order of magnitude larger than that needed to raise the temperature to 100°C. The partial vaporization theory suggests that the whole disk need not be vaporized. Instead, once the surface has been heated to 100°C, any extra radiant energy is utilized to vaporize a fraction of the disk under the irradiated area [70]. The threshold radiant exposure would then be that required to raise the surface temperature to just above 100°C so that there is enough latent heat to initiate vaporization at a few discrete places over the irradiated spot. If vaporization is initiated at many sites, the multiple microbubbles formed coalesce to form a bigger bubble. Van Leeuwen *et al.* and Jansen *et al.* photographed the formation of such microbubbles at threshold produced $0.5\,\mu$s after delivering a Q-switched Ho:YAG laser pulse ($\tau_p \approx 1\,\mu$s) into water [71, 70]. The fact that the threshold surface temperatures calculated in this study are about 100°C lends credence to the partial vaporization model.

Infrared emissions from the surface were monitored to detect any change in the emission profile at threshold. It had been hoped that the explosive vaporization of the gelatin would emit a distinct thermal signature that could be analyzed to account for the energy going into the vaporization process. However, no change was evident. Surface signals at energies below, at, and above threshold were scaled to the energy (figure 3.11). The relative amplitudes of the scaled signals would then give an estimate of the relative efficiency of the energy coupling into the gelatin. All three scaled signals completely overlapped each other indicating equivalent energy coupling. The transition from sub-threshold to supra-threshold radiant exposures is not evident at all. At present there is no satisfactory explanation for this observation.

The radiometric experiments required ablation of gelatin in air to avoid masking of the infrared signal by water. The events following laser delivery were monitored by flash photography. An additional observation from these experiments was that threshold values did not change in air. The pictures show the formation of a small sub-surface vapor bubble at threshold (figure 3.12). These threshold bubbles were much smaller than the spot size indicating that vaporization did not occur over the whole irradiated spot. The size of the bubbles increased with multiple shots. This could have been due to the increase in the baseline temperature of the gel surface so that more energy was available for the phase change. Visual examination of the gel surface revealed pit marks that were probably due to the formation of multiple small bubbles. All these observations are consistent with the partial vaporization theory.

The parametric study described in the previous chapter concluded that absorption had little effect on ablation efficiency at radiant exposures above threshold. Some fraction of the material

is heated and vaporized to form a vapor bubble. That mass has been shown to be a very small fraction of the total mass removed (chapter 2). The rest of the mass is probably removed as a result of the mechanical expansion and collapse of the vapor bubble. This study has shown that while absorption may not be important in the total material removal above threshold, it is nevertheless crucial in determining the energies at which a bubble can be created.

In conclusion, microsecond ablation thresholds have been measured as a function of the absorption coefficient μ_a. Since the choice of laser wavelength determines the absorption coefficients of thrombus and vessel wall, ablation thresholds for thrombus and vessel wall at any wavelength in the visible region can now be predicted. The radiant exposure for laser thrombolysis can then be chosen such that it is above the threshold for thrombus, but below that of artery.

Current clinical trials use pulse energies of 50–60 mJ at a wavelength of 480 nm out of a 1 mm catheter. The absorption of thrombus at 480 nm is about $100 \, \text{cm}^{-1}$ and that of artery is less than $10 \, \text{cm}^{-1}$. The currently used radiant exposure range of 60–75 mJ/mm^2 is about thrice and half the ablation thresholds of thrombus and artery respectively.

However, it is important to note that the threshold values reported in this thesis were measured *in vitro*. The situation *in vivo* may be very different. For example, there may be a thin layer of blood on the inside of the vessel wall. A radiant exposure lower than the artery threshold may then result in ablation of the blood layer and lead to adjacent damage to the vessel below. Another factor to be considered is that the intravascular bubble formed during ablation of thrombus may be large enough to dilate the artery and cause dissections. The energy required to form such a large bubble may be less than that required to ablate artery directly thereby imposing a tighter restraint on the maximum energy used.

It should be emphasized that the thresholds reported here are applicable to pulse durations where only thermal confinement conditions are met. Shorter pulses may fall in the stress confinement regime, and lower threshold values can be expected. Longer pulses may need higher radiant exposures to reach threshold due to heat diffusion out of the irradiated volume during the pulse.
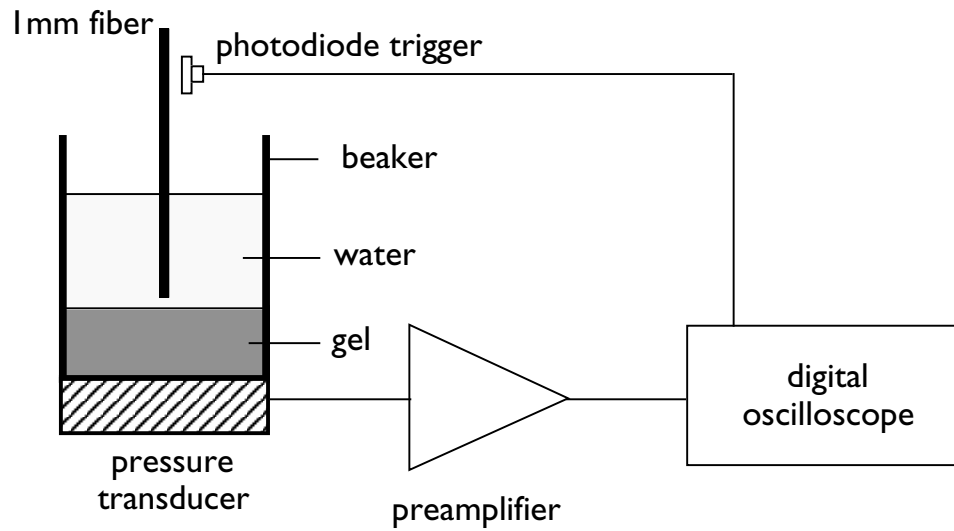
Figure 3.1: Ablation thresholds are measured by detecting an acoustic signal accompanying ablation. Light is delivered in $1\,\mu$s pulses, and the energy is increased until an acoustic signal is observed.
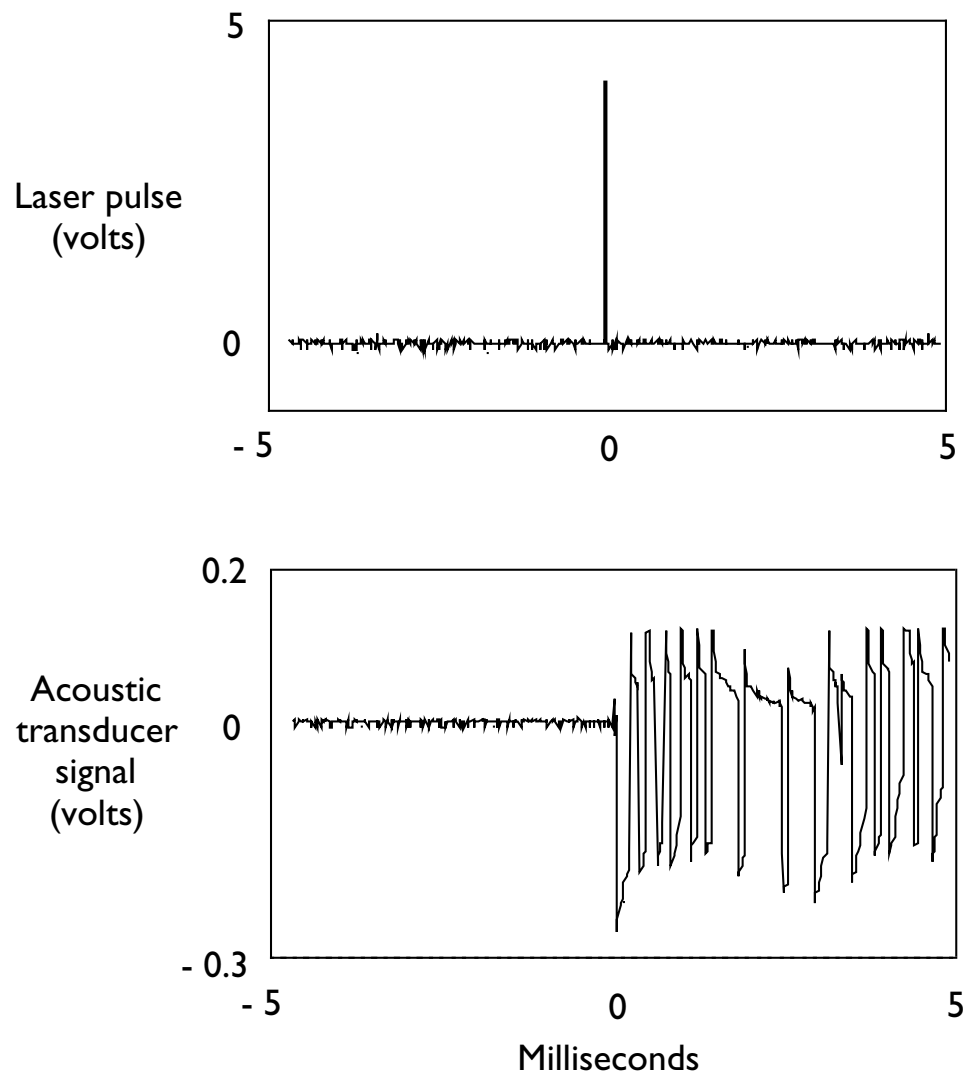
Figure 3.2: Acoustic signal due to ablation of gel under water by a $1\,\mu$s laser pulse. The acoustic signal is detected by placing the beaker containing the gel on PVDF transducer. The transducer signal is amplified and fed into an oscilloscope. The top graph shows the laser pulse detected by a photodiode that provides the trigger source for the oscilloscope. No acoustic signal is detected at sub-threshold radiant exposures.
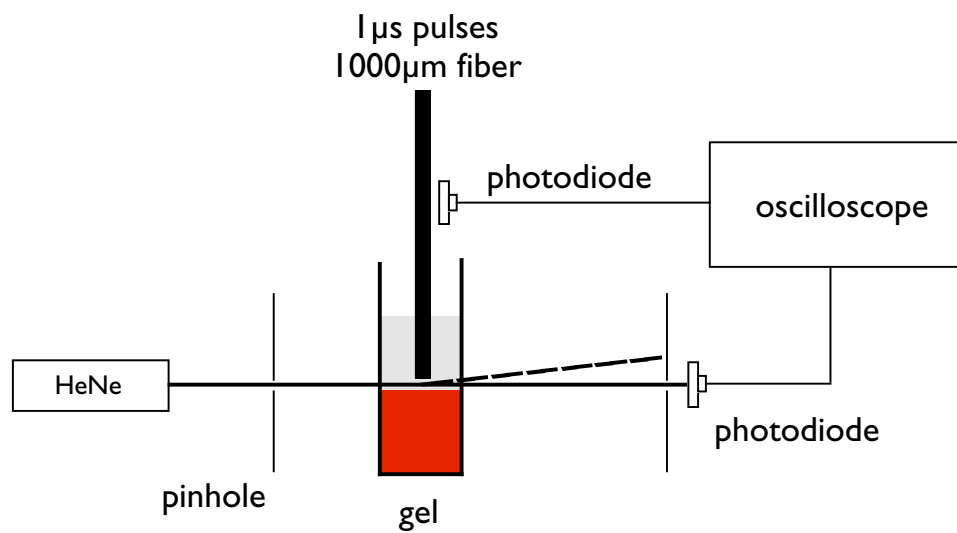
Figure 3.3: Ablation thresholds are measured by detecting a deflection of a HeNe probe beam due to an ablation event. Light is delivered in $1\,\mu$s pulses, and the energy is increased until a drop in the HeNe signal is observed.
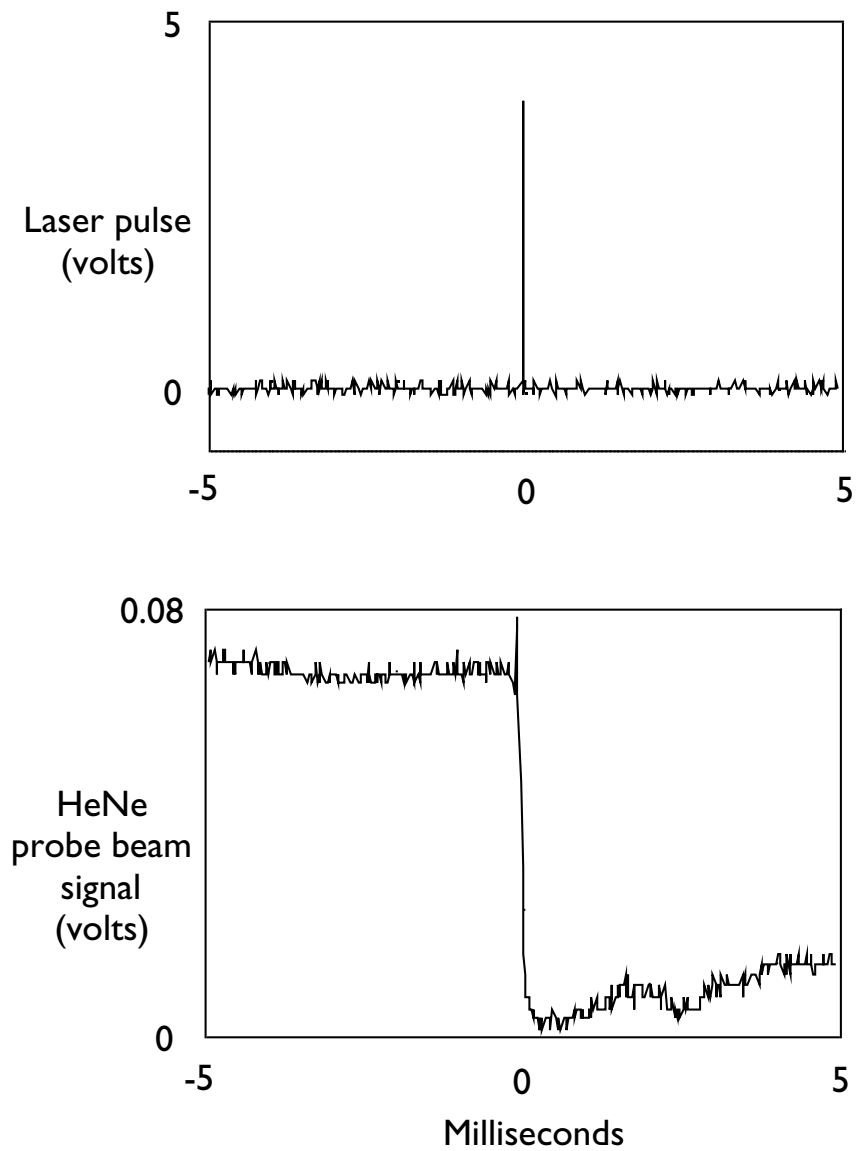
Figure 3.4: Deflection of the HeNe probe beam due to ablation of gel by a $1\,\mu s$ laser pulse. The HeNe probe beam is directed along the surface of the gel directly over the target area. Vapor bubble formation and/or ablation debris following ablation deflect the probe beam. No deflection is observed at sub-threshold radiant exposures.
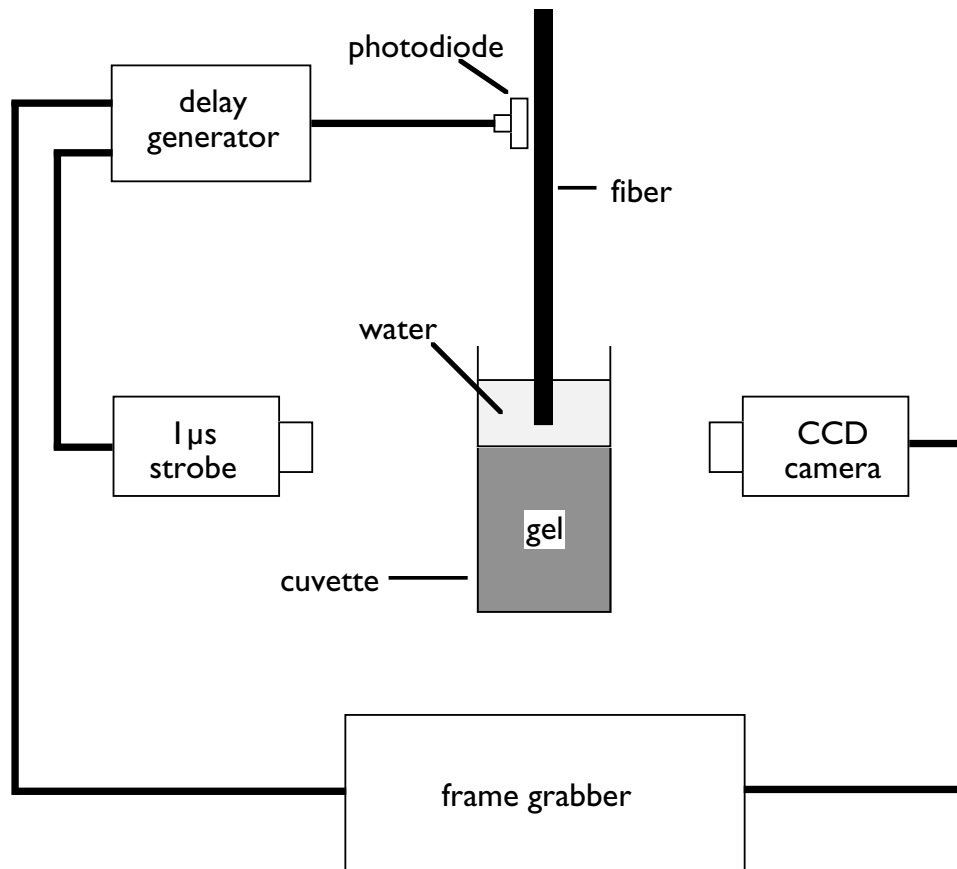
Figure 3.5: Gelatin was ablated in 1 cm cuvettes and was visualized using the CCD camera. The moment of image capture was controlled by the delay generator. Pulse energies were increased until ablation was detected.
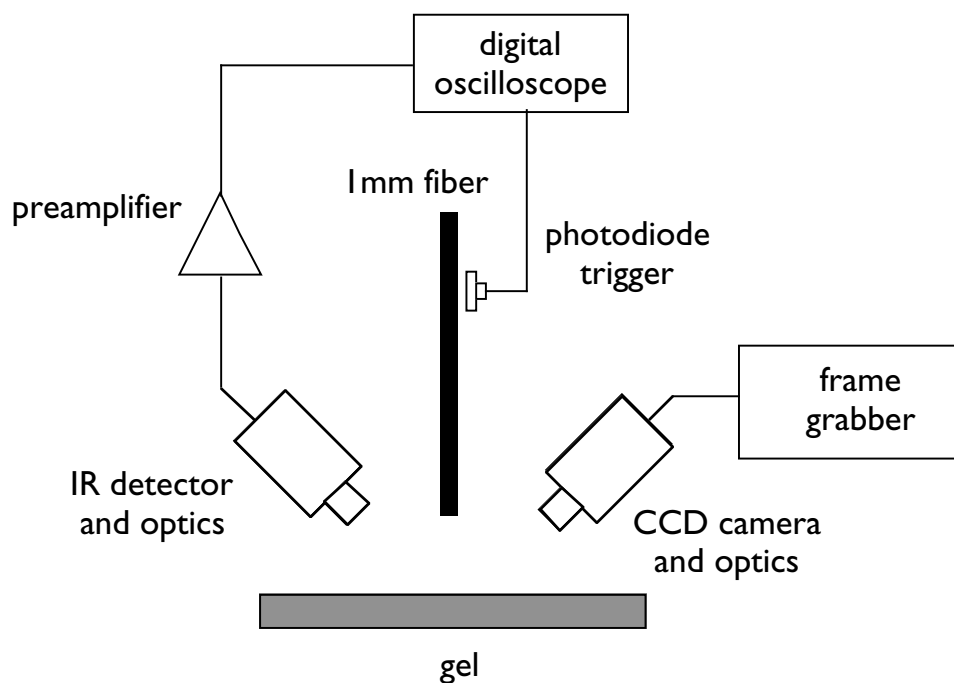
Figure 3.6: Gelatin was ablated in air and infrared emission from the surface was monitored with a HgCdTe detector. Microsecond laser pulses were delivered via a $1000\,\mu$m fiber $5\,$mm from the gel surface. Pulse energies ranged from below to above threshold. Ablation events at the surface was monitored by a CCD camera. Timing was achieved using a delay generator and microsecond strobe (not shown) similar to the flash-photography setup in figure 3.5. Absorption of the gelatin was $100\,\mathrm{cm}^{-1}$.
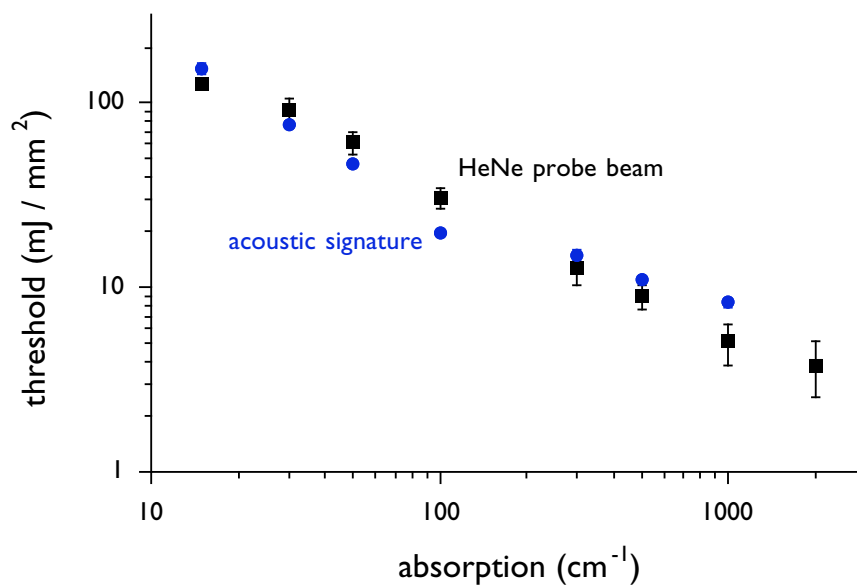
Figure 3.7: Threshold radiant exposures for gels of different absorption coefficients measured by detecting an acoustic signature and a deflection of a HeNe probe beam. Laser delivery was via a $1000\,\mu$m fiber and maintaining a 1 mm distance from the gelatin surface under water. Error bars are smaller than some symbols.
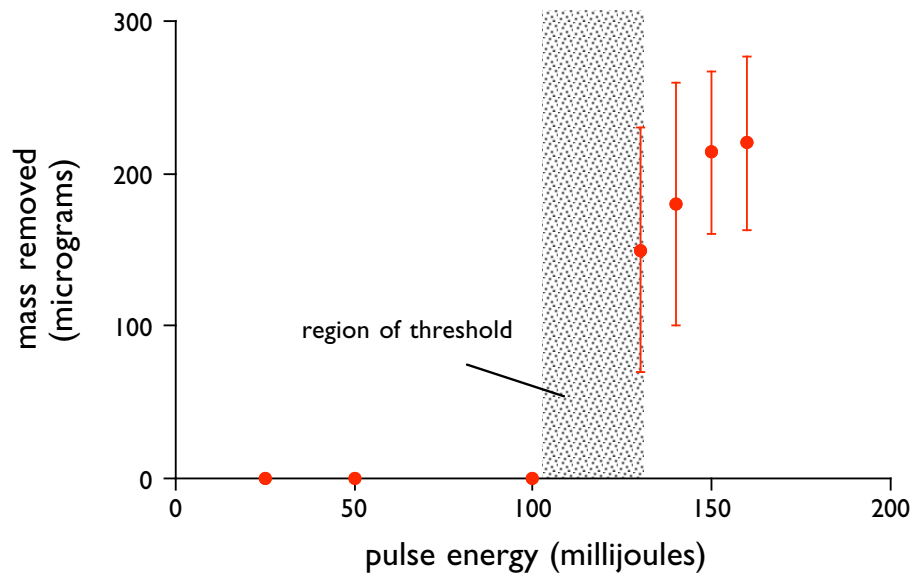
Figure 3.8: Threshold values obtained by the acoustic and HeNe methods were validated by direct mass removal measurements. Threshold was designated as the energy at which mass removal commenced. In this case, threshold is between 100–130 mJ. Gelatin was ablated in 3 mm tubes; absorption in this case was $10\,cm^{-1}$. Mass removal was measured by the spectrophotometric method. Laser delivery was with a $1000\,\mu$m fiber.
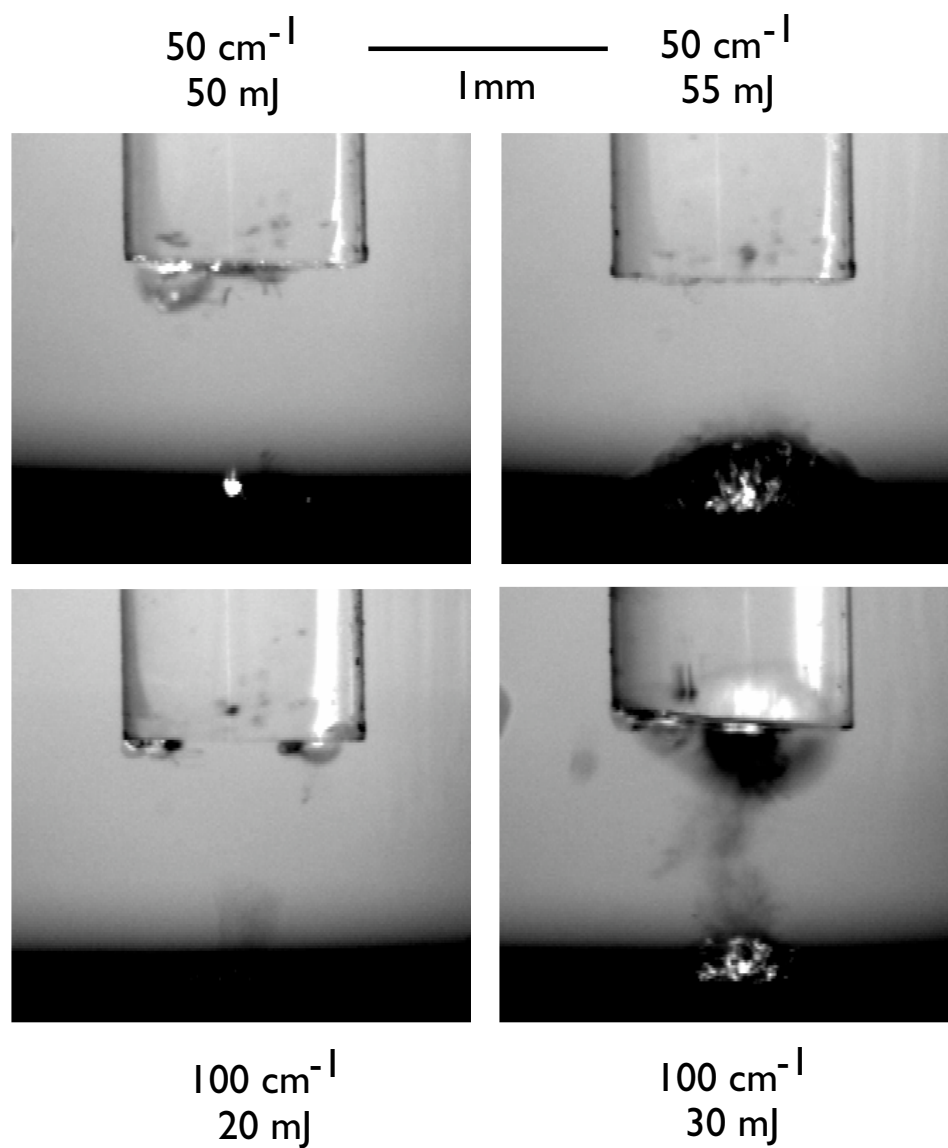
Figure 3.9: Ablation under water was visualized with flash photography. At threshold a vapor bubble is formed and material is removed. Pictures were taken $5\,\mu s$ after the laser pulse.
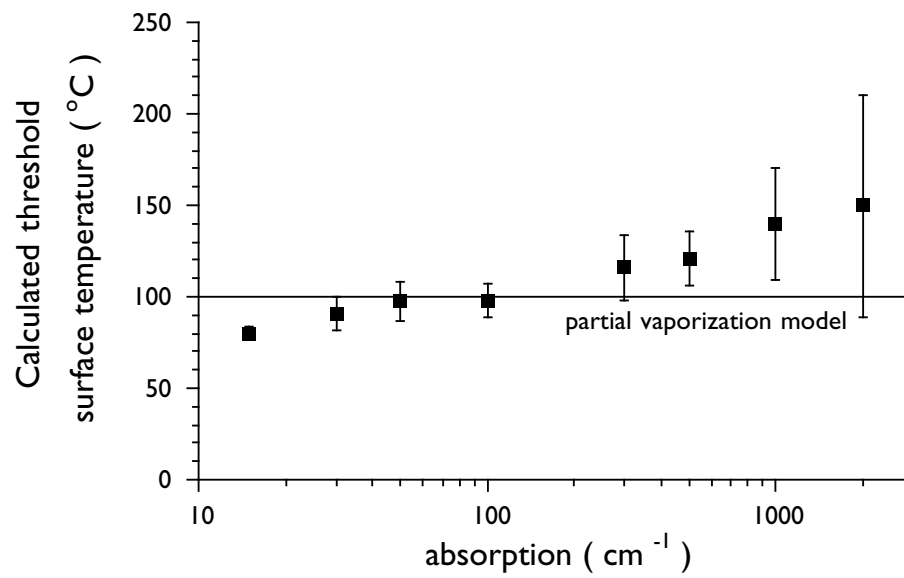
Figure 3.10: Surface temperatures at threshold were calculated. Rise in temperature is given by $\frac{\mu_a E_0}{\rho c}$. E_0 is the incident radiant exposure and ρc is the heat capacity. Ambient temperature was assumed to be 25°C.
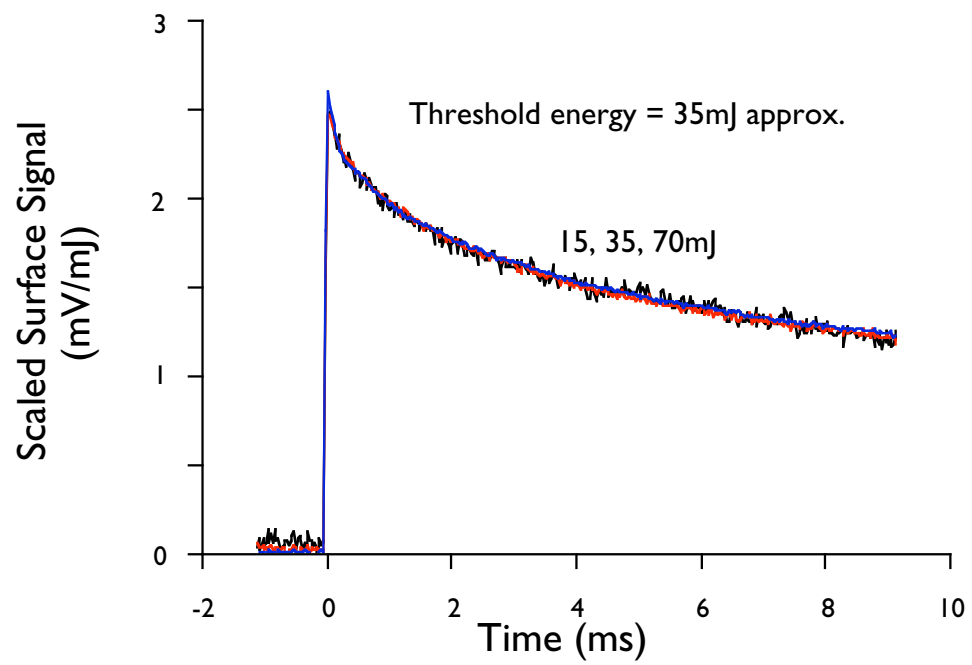
Figure 3.11: Infrared emissions from the surface following pulsed laser irradiation. Absorption was $100\,\mathrm{cm}^{-1}$. Surface signals have been scaled to the pulse energy. Pulse energy varied from below to above threshold. No change indicating vaporization is evident in the signal profiles.
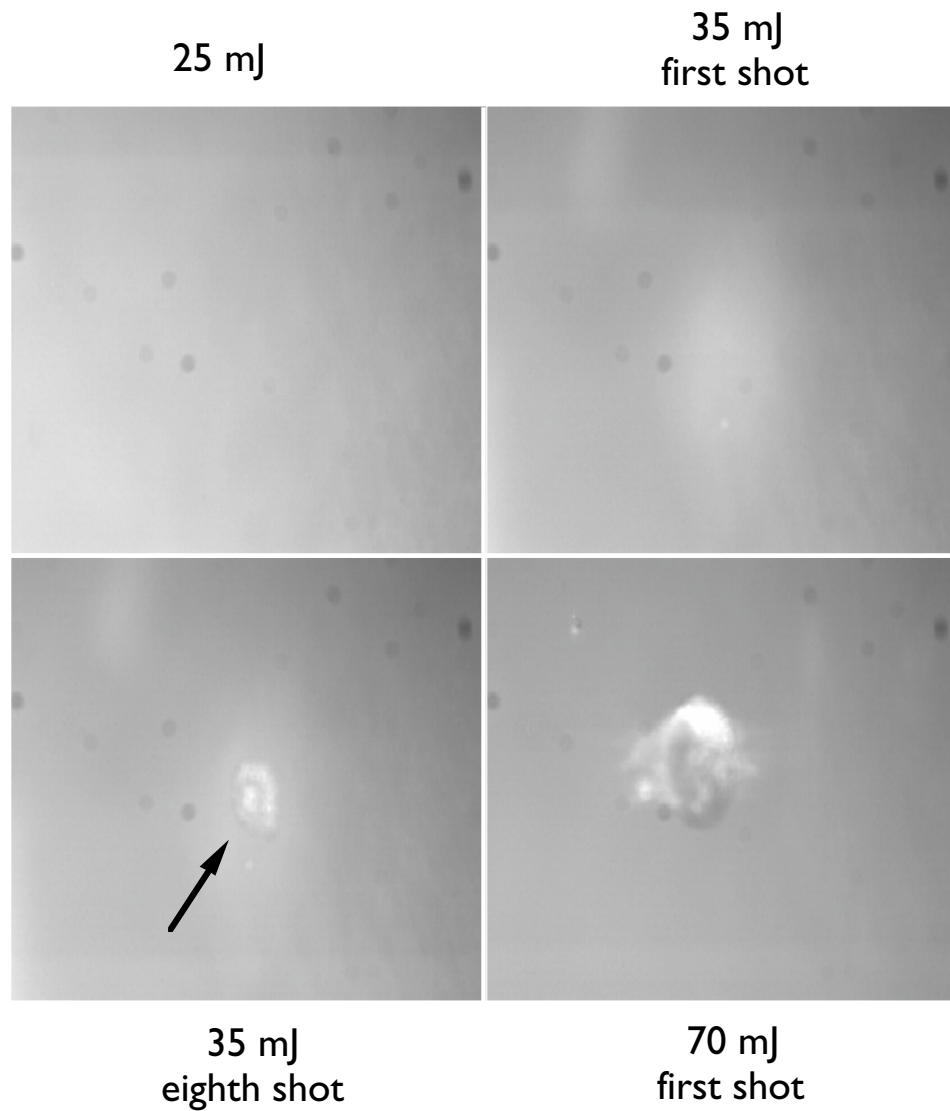
Figure 3.12: Ablation of gelatin in air. Absorption was $100\,\mathrm{cm}^{-1}$. Laser delivery was with a $1000\,\mu\mathrm{m}$ fiber $5\,\mathrm{mm}$ from the surface. The spot size was $1.6\,\mathrm{mm}$ in diameter. There is no effect at a pulse energy of $25\,\mathrm{mJ}$. At $35\,\mathrm{mJ}$ a small bubble starts to form at around the fifth shot on the same spot. The bubble grows with each subsequent shot; one after the eighth shot is shown here with the arrow pointing to the bubble. At pulse energies well above threshold ($70\,\mathrm{mJ}$), a bubble is formed with the first shot and does not change size with subsequent shots.
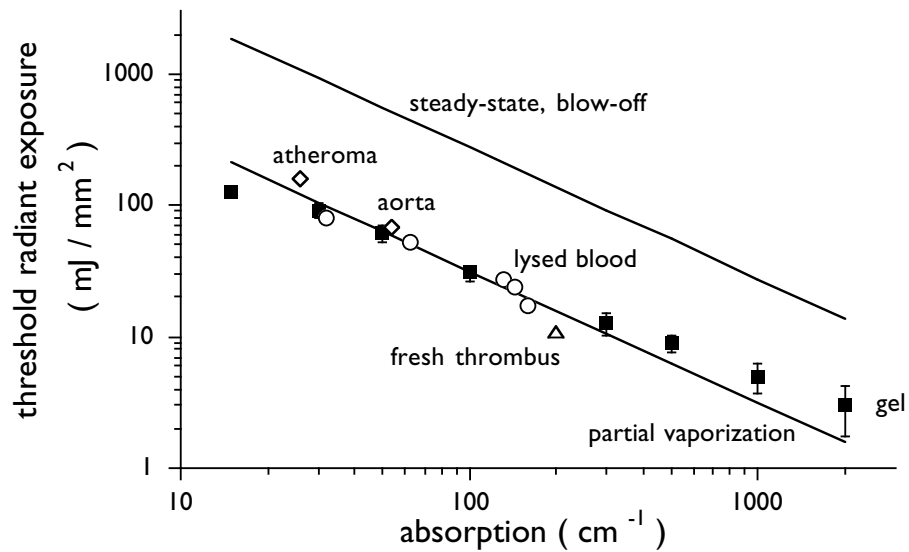
Figure 3.13: Threshold radiant exposures measured on gel are compared with those for tissue from literature. Thresholds for atheroma and aorta were measured by Prince *et al.* at 482 nm. LaMuraglia *et al.* measured the ablation threshold for fresh thrombus at 482 nm. Thresholds for lysed blood were measured by de la Torre *et al.*. at 577 nm for various hematocrits. Also are shown the thresholds predicted by the steady-state and blow-off models (upper line). The values measured in this study agree well with the partial vaporization model (lower line).
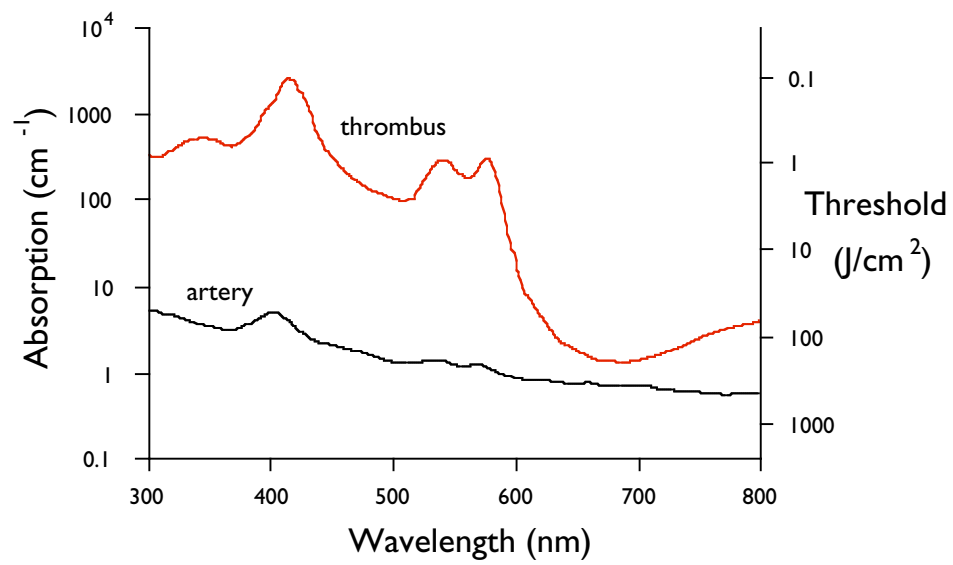
Figure 3.14: Threshold as function of absorption mapped onto the absorption spectra of thrombus and artery. Thresholds at any wavelength in the visible region can be read from this graph.

absorption coefficient (cm^{-1})	mass removal threshold ($\mathrm{mJ/mm^2}$)	visual threshold ($\mathrm{mJ/mm^2}$)	acoustic threshold ($\mathrm{mJ/mm^2}$)	HeNe threshold ($\mathrm{mJ/mm^2}$)
10	130 ± 10	140 ± 10	160 ± 10	130 ± 10
100	14 ± 3	28 ± 5	20 ± 1	31 ± 4
1000	6 ± 2	not available	8.5 ± 0.5	5 ± 1

Table 3.1: Ablation thresholds were measured by detecting an acoustic signature and the deflection of a HeNe beam as a result of ablation. Threshold values were validated by direct mass removal measurements and by visualization of ablation. Fiber diameter was 1 mm with the tip 1 mm from the gel surface.

Chapter 4

Bubble dynamics during microsecond ablation of gelatin under water

In this chapter, experiments are described to study the formation and collapse of vapor bubbles during pulsed laser ablation under a clear liquid.[1] Bubble dynamics during pulsed laser ablation of gelatin are chronicled and material removal is recorded. The effects of absorption, spot size, and pulse energy are studied. Bubble energies are estimated using Rayleigh's analysis of a collapsing spherical cavity. Mass removal is measured and correlated with bubble energies.

A microsecond laser was used to ablate a submerged gelatin-based thrombus model containing an absorbing dye. The gelatin was ablated without the confining effects of vessels in a large fish-tank and in $1\,$cm cuvettes. Pulse energies of 25–$100\,$mJ were delivered via 300–$1000\,\mu$m fibers. Flash photography was used to capture ablation events, and the mass removed was measured using a spectrophotometric method. Bubble energies were calculated based on maximum size and lifetime.

Vapor bubbles up to $5\,$mm in diameter lasting for 500–$600\,\mu$s were formed on gelatin in semi-infinite space. Material removal was observed after the collapse of the bubble. Smaller bubbles with shorter lifetimes were created in the $1\,$cm cuvettes. Ablation efficiency was roughly the same with both the $300\,\mu$m and the $1000\,\mu$m fibers.

Bubble energy estimates show that less than 5% of the total pulse energy goes into bubble formation at all times. Ablation mass increased roughly linearly with bubble energy. It did not have a direct relationship with radiant exposure.

---

[1]Part of this chapter was published in the paper "The effect of spot size, pulse energy, and repetition rate on microsecond ablation of gelatin under water" in SPIE *Laser-Tissue Interaction VI*, volume 2391, pages 336–344, 1995.

4.1 Cavitation

The results of the parametric ablation study described in the second chapter suggest that mechanical effects dominate over thermal effects for three reasons. First, the total mass removed was about an order of magnitude greater than predicted by heating and vaporization. Second, the absorption did not influence the ablation efficiency at pulse energies above threshold. Third, larger fibers were more efficient at removing material. The mechanical effects were suspected to be caused by the dynamics of a vapor bubble formed when some of the material was vaporized. Indeed, the visualization experiments in the third chapter show vapor bubble formation at ablation threshold and none below threshold.

The formation and activity of bubbles in a liquid is called cavitation. The phenomenon of cavitation was first rigorously investigated when the erosion of ship propellers was traced to the formation and collapse of water vapor bubbles on the blades [92]. These bubbles were formed due to low pressures in the water behind the curved blades of the propeller. A vapor bubble in a liquid can be produced by:

- pressure variations in a flowing liquid;

- sound waves in a liquid causing pressure variations;

- absorption of light, laser-induced breakdown, or by spark gaps;

- underwater explosions.

Hydrodynamic and acoustic cavitation are brought about by tension in the liquid; optical cavitation is achieved by local deposition of energy. While the dynamics of a cavitation bubble generally depends on the source of the cavitation, there are some features common to most bubbles [93]. The bubble grows from a small volume to a maximum size due to high pressures and temperatures inside the bubble. Equilibrium conditions are achieved when the forces within the bubble are matched by the forces exerted by the surrounding liquid on the bubble. Inertia causes the expanding bubble to overshoot its equilibrium size, and the outside forces overcome the forces inside. The bubble then proceeds to collapse to a small size until the pressure the inside the bubble again increases to a point when it is greater than the hydrostatic pressure outside. Depending on the geometry of the bubble and the proximity of solid boundaries, the bubble may re-expand to a size smaller than its initial maximum size. This may be repeated to produce a damped oscillatory motion. Multiple expansion and collapse phases have been recorded during

cavitation in a free liquid far away from any solid boundaries [94, 95]. The bubble dissipates energy in each expansion-collapse cycle and reaches a final collapse stage when there is no energy left to re-expand. The total lifetime of the bubble depends on its maximum size; a 5 mm bubble generally has a lifetime of the order of hundreds of microseconds. The presence of boundaries can have significant effects on the bubble dynamics. The bubble geometry is usually distorted, and the bubble may not re-expand upon collapse. The degree of distortion usually depends on the distance from the bubble center to the boundary [96, 97].

The high pressure transients during the expansion and collapse phases of the bubble have been shown to cause damage to nearby boundaries [98, 99, 100, 101]. Differential equations describing the motion of the bubble have been widely used to determine the pressure and velocity fields in the surrounding medium [93, 102]. However, bubble dynamics is influenced by numerous factors such as content of the bubble, heat conduction, viscosity, compressibility, and surface tension. The physics of the process is therefore complex. In 1917, Rayleigh considered the problem of an empty spherical cavity and obtained an elegant solution for the bubble wall velocity and time of complete collapse using energy considerations [103]. This analysis is used later in this chapter to estimate the energies of the bubbles formed during pulsed laser ablation of gelatin.

The vapor bubbles formed when soft tissue is ablated under a liquid using a pulsed laser is a form of optical cavitation. The absorption of the laser energy leads to heating and vaporization of part of the target. Due to confinement by the surrounding liquid, the expanding vapor forms a bubble. Strong pressure transients can be generated during both the expansion and collapse phases leading to additional material removal. These transients can also cause unwanted damage to collateral tissue. Van Leeuwen *et al.* and Jansen *et al.* investigated bubble formation during holmium laser angioplasty as a possible source of vessel wall dissections [71, 70]. Vogel *et al.* extensively studied the disruptive capabilities of bubbles during intra-ocular surgery [104, 96, 83, 105]. Picosecond and nanosecond laser pulses are used in intra-ocular surgery, and the bubbles are formed as a result of stress confinement or laser-induced breakdown of the medium.

The content of a bubble formed by vaporization depends on the material being ablated; in most soft tissues it is water vapor derived from the extracellular matrix of the tissue [106]. This is often the case even when the principal chromophore absorbing the laser energy is not water. The absorbing chromophore heats up and quickly transfers the heat to the surrounding tissue water [71, 107, 108]. For example, during excimer laser angioplasty, the target is plaque and the chromophore is the tissue protein. However, van Leeuwen convincingly demonstrated that the

content of the vapor bubble formed was water vapor by measuring a threshold temperature of 100°C for vapor bubble formation.

This is supported by the findings of the previous chapter where bubbles were formed at a threshold surface temperature of 100°C. The content of bubbles formed during laser thrombolysis can therefore be reasonably assumed to be water vapor. Bubble dynamics during thrombolysis may however be different from those during angioplasty and intra-ocular surgery because of several factors. First, the pulse length is different which could result in different bubble shapes and lifetimes. Second, the geometry of bubble formation is different since the bubble is formed on the target surface. Figure (4.1) illustrates the difference. The differences in bubble dynamics may result in different ablation processes and efficiencies.

4.2   Goals

The goals of the experiments in this chapter are to study formation of the vapor bubbles during pulsed laser ablation relevant to laser thrombolysis. Specifically, the questions to be answered are:

- How does material removal correlate with the bubble dynamics?

- How much of the total laser energy goes into the bubble action?

- How does bubble formation and collapse vary with absorption?

- Are bigger or more energetic bubbles formed with bigger fibers?

- What is the effect of pulse energy?

Relating the moments of material removal with the bubble dynamics may provide information about the relative importance of the expansion and collapse phases of the bubble. This is largely an academic question and goes towards understanding the basic ablation process. Of more practical interest would be correlating the ablation mass with bubble sizes and energies. Are bigger and more energetic bubbles needed to remove more material? To answer this question, bubble energies have to be calculated.

An estimate of the total energy going into the bubble action will also be helpful in reaching an energy balance for the ablation process. It was initially thought that the ablation mechanism was largely thermal with most of the energy going into heating. However, it has now been

shown that thermal ablation is not a significant factor. The energy seems to be channeled into predominantly mechanical effects including the bubble dynamics. Also, during pulsed ablation, an audible "pop" is evident indicating that some of the energy is converted to acoustic transients. It is not clear how much of the energy goes into the formation of the bubble and how much goes into just acoustic transients. Experiments in this chapter will provide data for estimating bubble energies.

The ablation efficiency does not depend strongly on the absorption coefficient. If bubble action is indeed a principal factor in ablation, bubbles of similar sizes are probably formed. The bubble size and lifetime would then also not depend strongly on the absorption. Another observation from the previous chapters was that bigger fibers were more efficient in removing material. This could be because (i) bigger and more energetic bubbles are formed or (ii) the bubble dynamics are affected by the physical dimensions of the fiber.

4.3   Materials and methods

Flash photography was used to record bubble dynamics on gel targets of various absorption coefficients. Pulse energies of 25–100 mJ were delivered via glass fibers of 300–1000 μm core diameter. The gelatin was ablated in a large fish-tank and in 1 cm cuvettes. Ablation efficiency was measured by the spectrophotometric method.

The targets were 3.5% gelatin containing Direct Red dye as the chromophore. The gel preparation is described in detail in chapter 2. The laser wavelength was either 577 nm or 506 nm. In either case, sufficient dye was added to the gel to achieve the desired absorption at the laser wavelength.

4.3.1   Flash photography

A standard flash photography setup was used in all the visualization experiments described in this chapter. A photograph of the bubble action is taken at various moments after the laser pulse (figure 4.2a). Figure (4.2b) shows the different targets. The flash or moment of image capture is controlled by a delay generator. Once a bubble has been photographed, a new bubble is created for the next image. Successive images of bubbles can then be pieced together to form a montage showing the complete evolution of bubbles. Since this method only captures a bubble at one particular moment, the history of a single bubble cannot be recorded. However, figure (4.3) showing pictures of two separate bubbles taken under identical conditions proves the

reproducibility of the method.

The laser pulse provides the timing source for the whole system. The energy pulse is delivered to the target via a glass fiber or a fluid catheter. A photodiode detects the light passing through the fiber and triggers a delay generator (Stanford Research Systems DG535). The delay generator has output ports AB and CD that are used to trigger a CCD video camera and an illumination source after an adjustable delay. The illumination source is a white light microsecond strobe. The CCD camera is attached to a stereoscope (Olympus SZ-60) for magnification. A laser filter is inserted in front of the microscope to avoid blinding the camera. The video frame from the camera is recorded on a frame grabber card. The total system delay was about $5\,\mu$s.

A Sony XC-57 CCD camera was used in the initial experiments. This camera was not triggerable and operated in a live mode—continuously feeding 30 frames per second to the frame grabber card. To capture an image at a particular time the frame grabber card was triggered from the delay generator. The card then captured the particular $32\,$ms frame fed to it by the camera at the triggering moment. All illuminated events in that $32\,$ms will be recorded. Later experiments used a CCD (Motion Analysis) camera capable of being triggered asynchronously. The exposure time was also adjustable from $1\,\mu$s to $10\,$ms. The trigger signal from the delay generator was then fed directly to the camera. A factory-set exposure of $280\,\mu$s was used. The software controlling the frame grabber card was NIH Image.

4.3.2   Ablation in semi-infinite space and cuvettes

The first set of experiments consisted of investigating the effect of absorption on the bubble dynamics. This was done by ablating a large piece of gelatin in a fish tank to avoid any boundary effects. The absorption was varied from 60–$500\,$cm^{-1}. Microsecond laser pulses were delivered via a $1000\,\mu$m fiber with the tip $1\,$mm from the gel surface. The pulse energy was $100\,$mJ. Each shot was delivered on a fresh target area. Bubble action was captured at various times after each shot using the flash photographic technique described above. The images were then arranged in a chronological order to depict bubble expansion and collapse. Three photographs were taken for each delay to test for reproducibility. Bubble dimensions were measured and plotted against time. Bubble energies were calculated using Rayleigh's analysis described later in this chapter.

The mass of gelatin was not measured since the aim had been to just investigate the effect of absorption on the bubble dynamics. It has already been shown that ablation efficiency is not seriously affected by μ_a at energies above threshold. Those initial ablation experiments had been

done in tubes. Simultaneous mass removal measurements and flash photography were done to correlate bubble energies with ablation efficiencies.

Gelatin was ablated in $1\,\mathrm{cm}$ cuvettes to facilitate collection of the mass removed and yet avoid confinement effects. The gelatin was cured in the cuvette and topped off with water. The absorption was fixed at $300\,\mathrm{cm}^{-1}$. Pulse energies of 30–$100\,\mathrm{mJ}$ were delivered with $300\,\mu\mathrm{m}$ and $1000\,\mu\mathrm{m}$ fibers to study the effects of spot size and pulse energy on the bubble dynamics and ablation efficiency. The ablated material dissolved in the water above the gel. After laser delivery the solution was carefully syringed out, and the mass removed was measured using the spectrophotometric method. Ten pulses were fired to collect enough material to be measured reliably. The repetition rate was $3\,\mathrm{Hz}$. Flash photographs were taken only of the first bubble formed. A fresh sample was used for each time delay. No light was delivered to control samples to account for gel that dissolved naturally in the water. Bubble energies were calculated based on size and lifetime measurements and correlated with mass removal.

4.4   Results

4.4.1   Ablation in semi-infinite space

Ablation was accompanied by a loud snapping sound and visible removal of material. Bubbles up to $5\,\mathrm{mm}$ in diameter were formed. The lifetimes of the bubbles formed were of the order of 400–$600\,\mu\mathrm{s}$. Higher pulse energies produced bigger bubbles with longer lifetimes. The size and shape of the bubbles were very reproducible except at times close to collapse. Bubble expansion and collapse occurred at roughly similar rates. A tiny bubble was observed even when the delay on the delay generator was set to zero. That was almost certainly due to the system delay of about $5\,\mu\mathrm{s}$ in the photography setup.

Figure (4.4a) shows an incipient bubble formed on $100\,\mathrm{cm}^{-1}$ gel $10\,\mu\mathrm{s}$ after the laser pulse. The radius is already about $1\,\mathrm{mm}$ indicating a fairly rapid growth. The bright spot at the center is fluorescence emitted by the dye following absorption of the laser wavelength. The fluorescence lasts for nanoseconds and is over by the time the delay generator sends out the trigger for image capture. However, since it is an luminous event it is still recorded on the $32\,\mathrm{ms}$ video frame. This artifact is overcome in later sets of pictures by using the triggerable CCD camera. That camera starts exposure only after it gets the trigger signal from the delay generator.

Another interesting feature is the halo around the fiber tip (figure 4.4). This halo is barely

discernable in the $10\,\mu$s picture but is clearly evident in the $30\,\mu$s picture. It is most probably due to vortices around the tip caused by pressure transients generated by the expanding bubble. This halo-like feature was reproducible.

At $50\,\mu$s after the laser pulse the upper bubble wall has reached the fiber tip. At this point the bubble wall is still intact, and careful examination reveals invagination of the wall around the tip. The white arrow indicates the level of the fiber tip. The bubble continues to grow and the wall is pierced at around 150–$200\,\mu$s. The maximum size of about $5\,$mm in diameter is reached at about 250–$300\,\mu$s (figure 4.5). After that the bubble begins to shrink and collapses completely at $500\,\mu$s (figure 4.6). No significant material removal is observed up to this point except the amount vaporized to form the bubble. However, about $20\,\mu$s *after* the bubble has completely disappeared, significant amounts of material are ejected (figure 4.7). This ejection of material continues for almost a hundred microseconds. Figure (4.8) is a montage of individual pictures showing the bubble history.

Bubble sizes and lifetimes were not strongly influenced by the absorption (figure 4.9). Particularly, bubble dynamics with $100\,$cm^{-1} and $300\,$cm^{-1} gel were almost identical. Slightly smaller bubbles were formed on the $60\,$cm^{-1} and $500\,$cm^{-1} gels. The small error bars on the bubble dimensions indicate the reproducibility of the experiment. The expansion-collapse curves for all the bubble are fairly symmetric about the time of maximum size. Bubble wall velocities were calculated by numerically differentiating the bubble growth curve. Highest velocities of around $20\,$m/s were calculated at early expansion and final collapse.

4.4.2 Ablation in cuvettes

Gelatin was ablated in $1\,$cm cuvettes so that the ablated material could be collected and correlated with bubble energies. Absorption was $300\,$cm^{-1}, and pulse energies of 30–$100\,$mJ were delivered.

Bubbles of maximum diameter of 1–$3\,$mm were formed and collapsed 200–$400\,\mu$s after the laser pulse. There were no significant differences in bubble sizes and lifetimes produced with the $300\,\mu$m and $1000\,\mu$m fibers at $100\,$mJ (figure 4.10). This was well above the threshold for both fibers, $4\,$mJ and $14\,$mJ respectively. Larger bubbles were produced with the $300\,\mu$m fiber at $30\,$mJ. This was about twice the threshold energy for the $1000\,\mu$m fiber, but 7–8 times the threshold for the $300\,\mu$m fiber. Similar amounts of gelatin were removed with the $300\,\mu$m and $1000\,\mu$m fibers (figure 4.11).

4.5 Discussion

This study was carried out to visualize bubble action during pulsed laser ablation of a soft target under a clear liquid and to help understand its role in material removal. Gelatin was ablated under water with microsecond laser pulses delivered by 300μm and 1000μm fibers. The effect of light absorption and pulse energy on the bubble dynamics were studied. Bubble dimensions and lifetimes were measured.

4.5.1 Bubble dynamics

Fairly large bubbles (diameter $\sim$5 mm) were formed on the gel surface at energies of 100 mJ. Bubble expansion was very rapid in the very early stages ($\sim$10 μs). This can also be seen in the early pictures where the bubble wall appears blurred indicating fast motion. The calculated wall velocities were of the order of 20 m/s. Some studies have reported a jet formation at the end of the collapse of a bubble in the vicinity of a boundary [96, 97]. These jets had velocities of hundreds of meters per second and attained great impact pressures leading to erosion of the boundary. From the flash photographs taken in this study it is not clear if such a jet is formed. The bubble geometry became very indistinct towards the end, and it was difficult to measure wall velocity and to distinguish any other features. More sophisticated recording techniques such as particle image velocimetry may be useful in capturing bubble action during collapse [97].

A damped oscillatory motion has been reported by almost all investigators studying bubble action. The bubble lost energy with each collapse but retained enough for re-expansion until there was none left. No secondary bubble expansion after collapse was observed in this study. Possible reasons could be the geometry of bubble creation and the target material. The bubble is created at the interface of gelatin and water with roughly equal halves in both media. This interface may disrupt the continuity of the wall as the bubble starts collapsing. Also, in many cases the wall had already been breached by the fiber tip during the expansion phase providing an outlet for releasing pressure during collapse. In his work on laser lithotripsy, Rink ablated stones with a microsecond laser in a very similar geometry [109, 110, 82]. He observed a secondary re-expansion and collapse, and sometimes even a third. The stone target in his experiments was much harder than the soft gel, and the bubble probably expanded mainly into the water retaining much of its geometry.

An interesting feature that was always observed was significant mass removal after the bubble collapsed. The ejection of material usually commenced within 20 μs after the final bubble collapse.

This indicates that bubble collapse is important in mass removal. However, it is still not clear whether the expansion phase is any less important. It may be that the bubble expansion loosens the material while the collapse removes it. The material probably takes time to recover from the impact of the collapse, and that may explain the delay before ejection. Acoustic measurements of expansion and collapse pressures may better demonstrate the relative importance of bubble expansion and collapse. No pressure measurements have been made in this study for lack of suitable measuring devices.

In the next section, the model proposed by Lord Rayleigh to describe bubble collapse is presented. The applicability of the model to the experimental results of this chapter is tested. Finally, estimates of bubble energy are made based on measurements of maximum size and lifetime.

4.5.2 Rayleigh's equations for a collapsing cavity

In 1917, Lord Rayleigh proposed a simple model relating the maximum size of a cavitation bubble to its collapse time based on energy considerations [103]. Numerous investigators have used this model to calculate the work (pressure $\times$ volume) done by the bubble during its expansion and collapse [96, 97, 105, 109, 110, 82, 71, 70]. Rayleigh's equation relating the maximum radius R_{max} and the time of collapse from the maximum size T_c is:

$$T_c = 0.915 R_{max} \sqrt{\frac{\rho}{p_{stat} - p_v}} \qquad (4.1)$$

ρ is the density of the liquid, p_{stat} is the hydrostatic pressure, p_v is the vapor pressure. The energy content of a bubble can be calculated as:

$$E_B = \frac{4}{3}\pi R_{max}^3 \cdot (p_{stat} - p_v) \qquad (4.2)$$

Rayleigh's model assumed a perfectly spherical bubble collapsing in an infinite medium. It also assumed no energy loss during the collapse and predicted an undamped oscillatory motion. The bubbles created in the experiments described in this chapter were not perfectly spherical and were distorted by the boundaries of the fiber and the gel surface. Also, the bubble did not expand after the first collapse implying that energy is lost at collapse.

Given these factors, the applicability of the Rayleigh model to estimate bubble energies in this case is suspect. One way to test the applicability of the model is to validate equation (4.1) since experimental data on the collapse time and maximum radius is available. Figure (4.12) compares the experimental radii and collapse times with the Rayleigh model represented by equation

(4.1). Given the limitations of the Rayleigh model, there is reasonable agreement between model and experiment, particularly for the bubbles formed in semi-infinite space (absorption studies). The measured collapse times of the bubbles formed in the cuvettes (spot size and pulse energy studies) are slightly longer than those predicted by the Rayleigh model. This is probably due to the additional influence of the cuvette walls. Stretching of collapse time due to the presence of boundaries has also been reported by other investigators [97, 109, 110].

4.5.3 Bubble energies and the effect of absorption

Changing the absorption coefficient did not seriously affect the maximum bubble sizes and lifetimes. Slightly smaller bubbles were formed at $\mu_a =$60 cm^{-1}; this may be because 100 mJ was just twice the ablation threshold for 60 cm^{-1}. In all other cases the pulse energy was 5–10 times the threshold energy. Using Rayleigh's equations bubble energies may be calculated (figure 4.13). Two things are to be noted in this graph. First, the energy of the bubble does not change much as the absorption is varied. This may be the reason that absorption does not strongly influence the total mass removed as shown in the second chapter. Once the pulse energy is well above threshold, similar sized bubbles are formed irrespective of the absorption. The bubble then seems to the principal factor involved in the ablation process.

The other point of interest is that only about 2% of the total laser pulse energy is converted into the pressure-volume work done by the bubble. It is not clear what happens to the bulk of the energy. Obviously, the initial coupling of the pulse energy into the target is thermal due to absorption. The heated material expands and some energy is released into pressure transients. Part of the material is vaporized and forms the bubble. The energy content of the bubble is the pressure-volume work given by equation (4.2). The bubble dissipates this energy in its expansion and collapse phases in the form of acoustic transients [111]. It is yet to be determined how much of the total laser energy goes into the initial pressure transients, and how much is wasted as heat.

Other researchers have also reported low coupling efficiencies of the pulse energy into the bubble. Vogel *et al.* investigated bubble formation by laser-induced breakdown during intraocular surgery. He estimated a large range of bubble energies between 1–25% of the total laser energy [101, 83, 105]. Rink *et al.* reported bubble energies of 10–30% of the pulse energy [82]. Ward *et al.* calculated the total energy going into bubble dynamics and acoustic transients to be about 18% of the laser energy. The coupling efficiency seems to depend on the pulse width, energy, and the target. Regarding the rest of the energy, the consensus seems to be that it is

wasted as heat. The interaction of a high power laser pulse with an absorbing sample under a liquid is complex and is a field of study at many centers. Numerical codes designed to model underwater explosions are now being used to clarify the energy balance issue [112, 111].

4.5.4 Effect of spot size and pulse energy

In the second chapter it was shown that larger fibers ablated gelatin in 3 mm tubes more efficiently than smaller fibers. A possible explanation had been that more energetic bubbles were formed at larger spot sizes. To either confirm or disregard this hypothesis, gelatin was ablated in 1 cm cuvettes to easily visualize the ablation process and chart the bubble dynamics. Laser energy was delivered via $300 \, \mu$m and $1000 \, \mu$m fibers. Ablation masses were measured and correlated to the bubble energies.

The surprising result of this experiment was that there was no significant difference in ablation mass at the two spot sizes at energies above threshold (figure 4.11). In chapter 2, the larger spot sizes were more efficient when the gel was ablated in tubes. The bubbles formed by the $300 \, \mu$m and $1000 \, \mu$m fibers in the tubes are probably of similar size. However, the larger fibers may produce a more confining effect in the tubes so that the bubble expands more into the gel than into the water above and therefore disrupt more gel. This hypothesis is investigated in the next chapter where bubble formation in tubes is photographed.

A linear increase in ablation mass with pulse energy was observed in this study. Bubbles of similar energies were formed with the two fibers, and there was a linear relationship between the calculated PV work and the pulse energy (figure 4.14). The coupling was less than that observed during bubble formation in semi-infinite space. This was because the boundaries of the cuvette walls decreased the maximum sizes and stretched the lifetimes.

The total mass removed is directly dependent on the energy of the bubble formed. The energy of the bubble is proportional to the pulse energy and not the radiant exposure. The coupling efficiency is less than 5%, and a large portion of the energy is not accounted for. This energy is most likely dissipated into heat and may or may not participate in the ablation process.
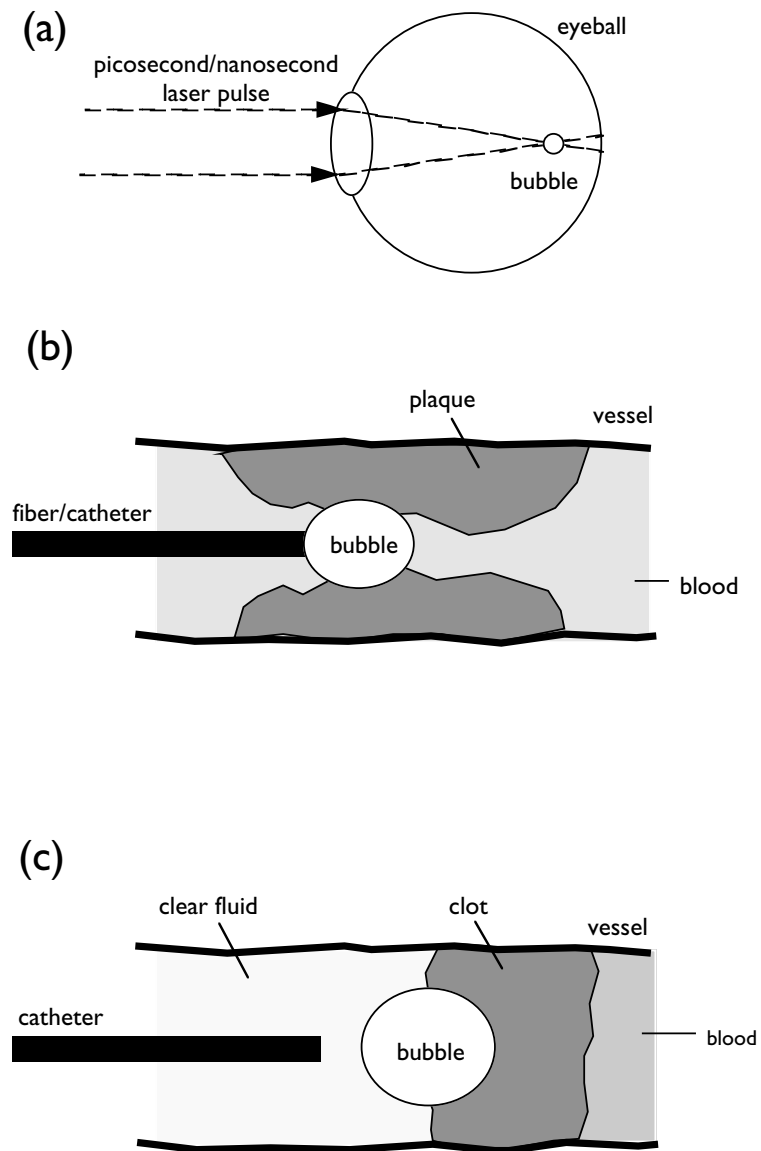
Figure 4.1: Three common geometries of bubble formation: **(a)** Intraocular surgery—bubble formation is due to optical breakdown at the focus with picosecond and nanosecond pulses. **(b)** Laser angioplasty—bubble formation is due to absorption of the pulse energy by the blood around the fiber tip. **(c)** Laser thrombolysis—bubble is formed at the thrombus surface.
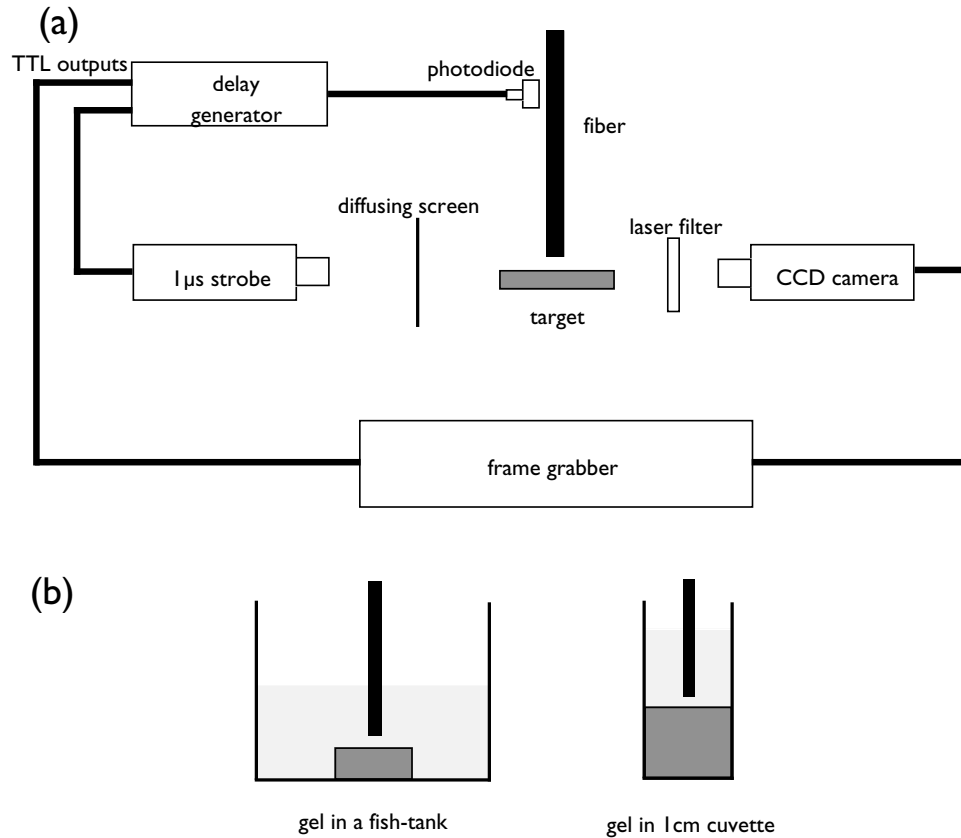
Figure 4.2: **(a)** Flash photography setup for imaging bubble action. Light is delivered by an optical fiber. A snap shot is taken at increasing delays after each laser pulse. The delay is controlled by the delay generator. The photodiode detects the laser light and provides the trigger for the delay generator. **(b)** The different target geometries used in the visualization experiments. The gel in the fish-tank provided a semi-infinite medium to visualize bubble dynamics without the influence of boundaries. The gel was ablated in 1 cm cuvettes to facilitate measurement of ablation mass and correlate it with bubble energies.
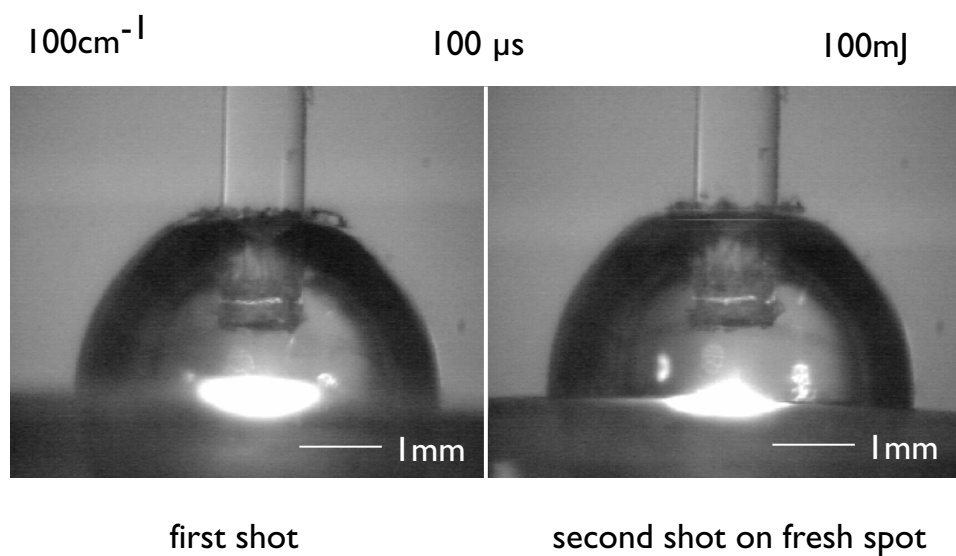
Figure 4.3: Two photographs taken of bubble formation under identical conditions using the flash-photography technique. Although the technique takes pictures of only individual events, it is reproducible.
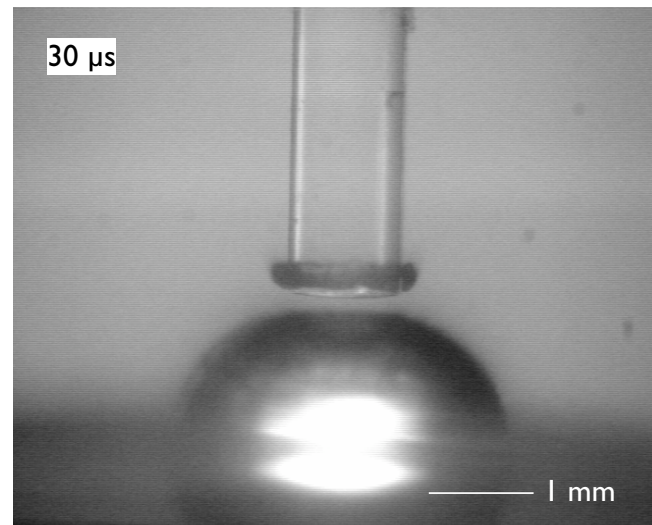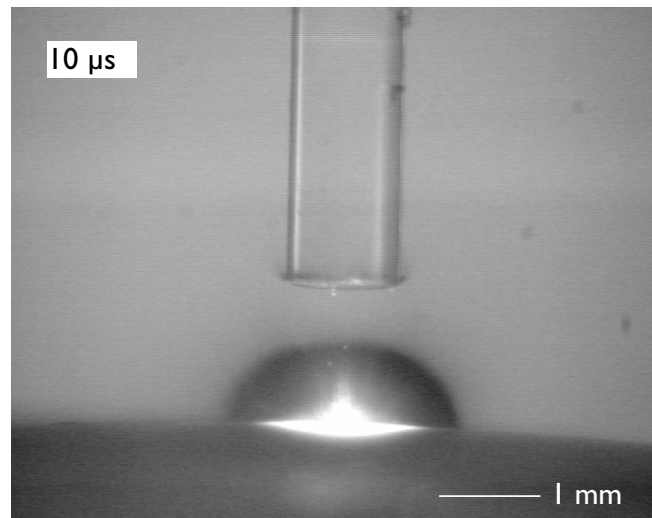
Figure 4.4: An expanding vapor bubble shown at $10\,\mu$s and $30\,\mu$s after the laser pulse. The pulse energy is $100\,$mJ delivered by a $1\,$mm fiber to $10\,$cm^{-1} gel in a fish-tank. The bright spot in the middle is fluorescence of the dye in the gel. A distinct halo can be observed around the fiber tip at $30\,\mu$s.
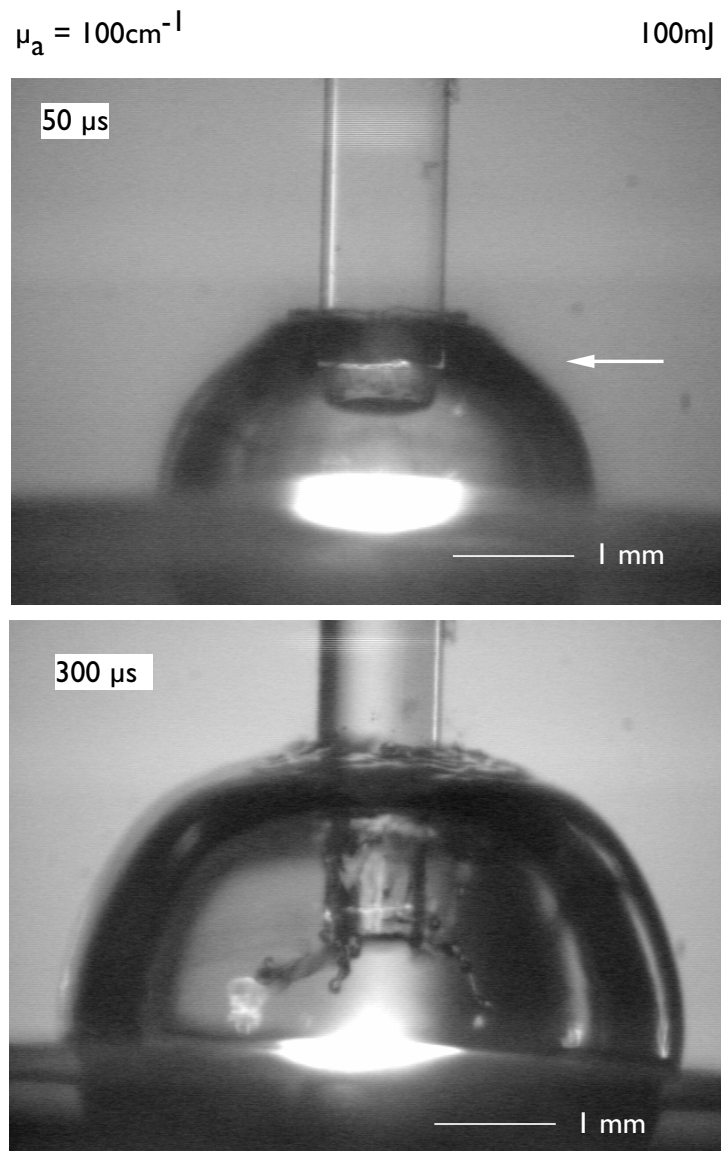
Figure 4.5: Bubble at 50 μs and 300 μs. At 50 μs the bubble wall has reached the fiber tip and engulfed it. The white arrow indicates the level of the tip. At 300 μs the bubble is at its maximum size. The fiber tip has breached the wall.
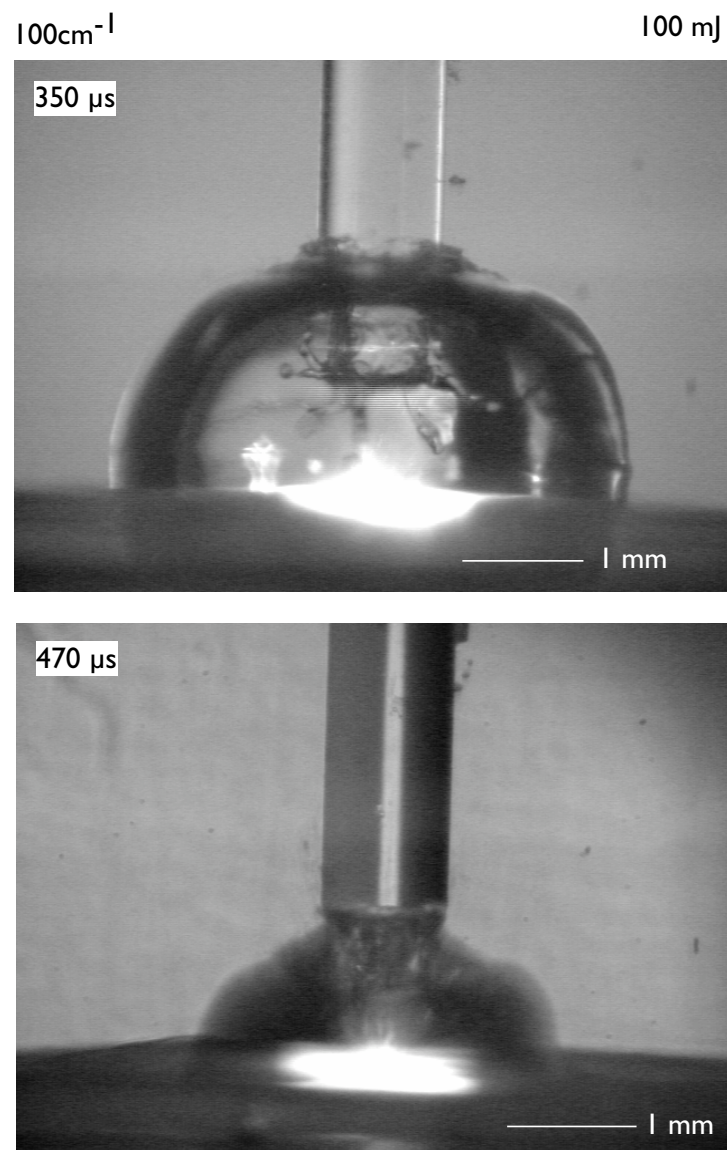
Figure 4.6: Collapsing bubble. Bubble wall velocity at collapse is about 20 m/s.
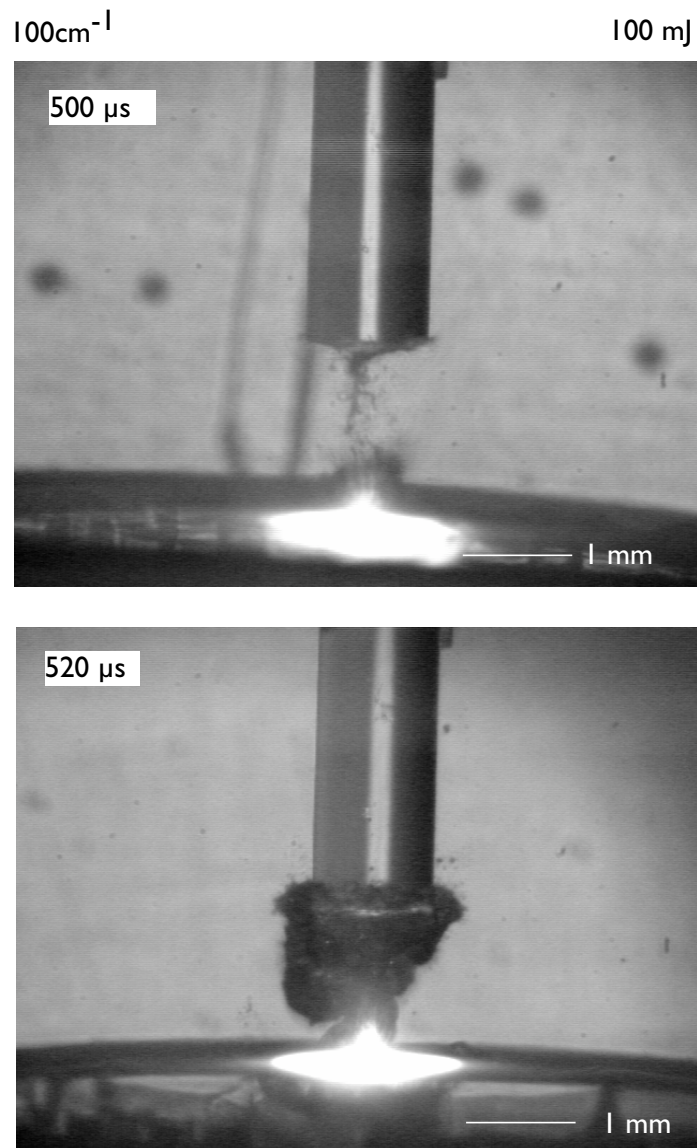
Figure 4.7: Significant material removal commences about $20\,\mu$s after the bubble has collapsed completely. The ejection continues for about $100\,\mu$s.
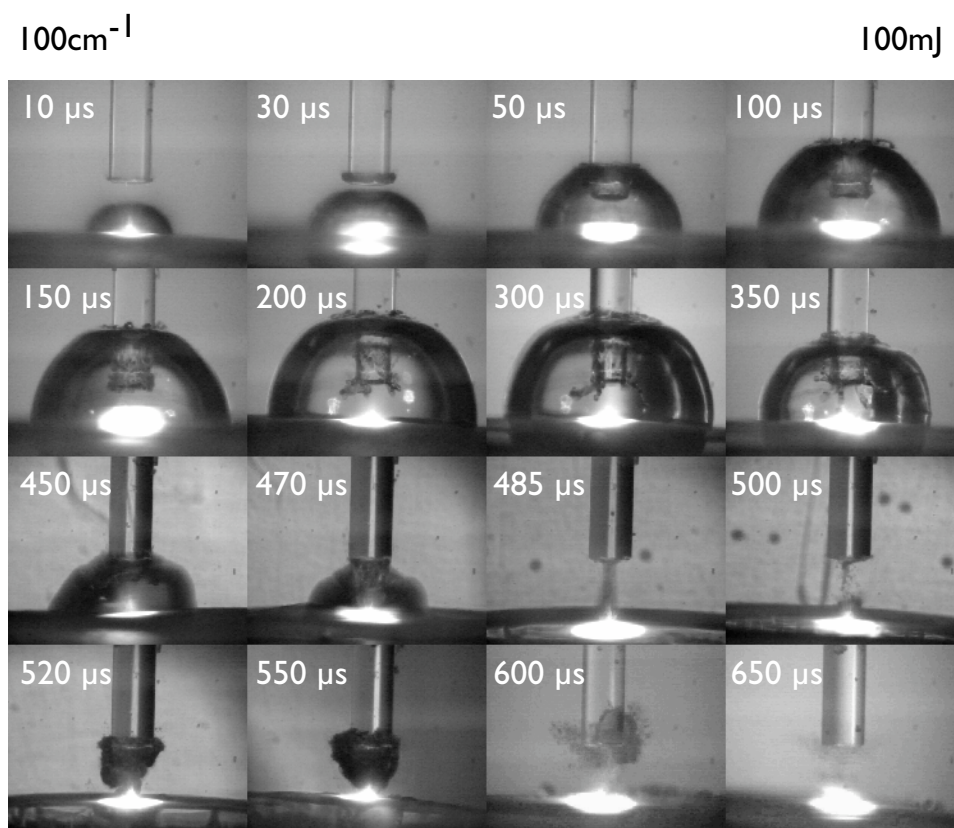
Figure 4.8: Montage of bubble pictures taken at different delays. Each bubble was an individual event and was formed by separate laser pulses.
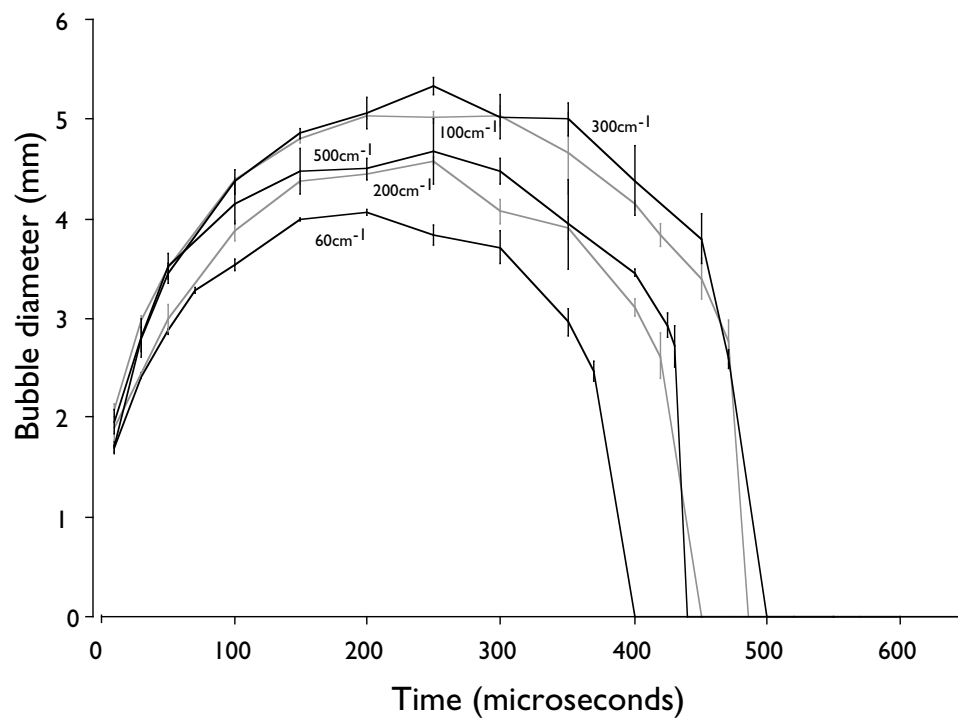
Figure 4.9: Bubble growth and collapse after the laser pulse. The bubble dimensions and lifetime are not strongly influenced by absorption.
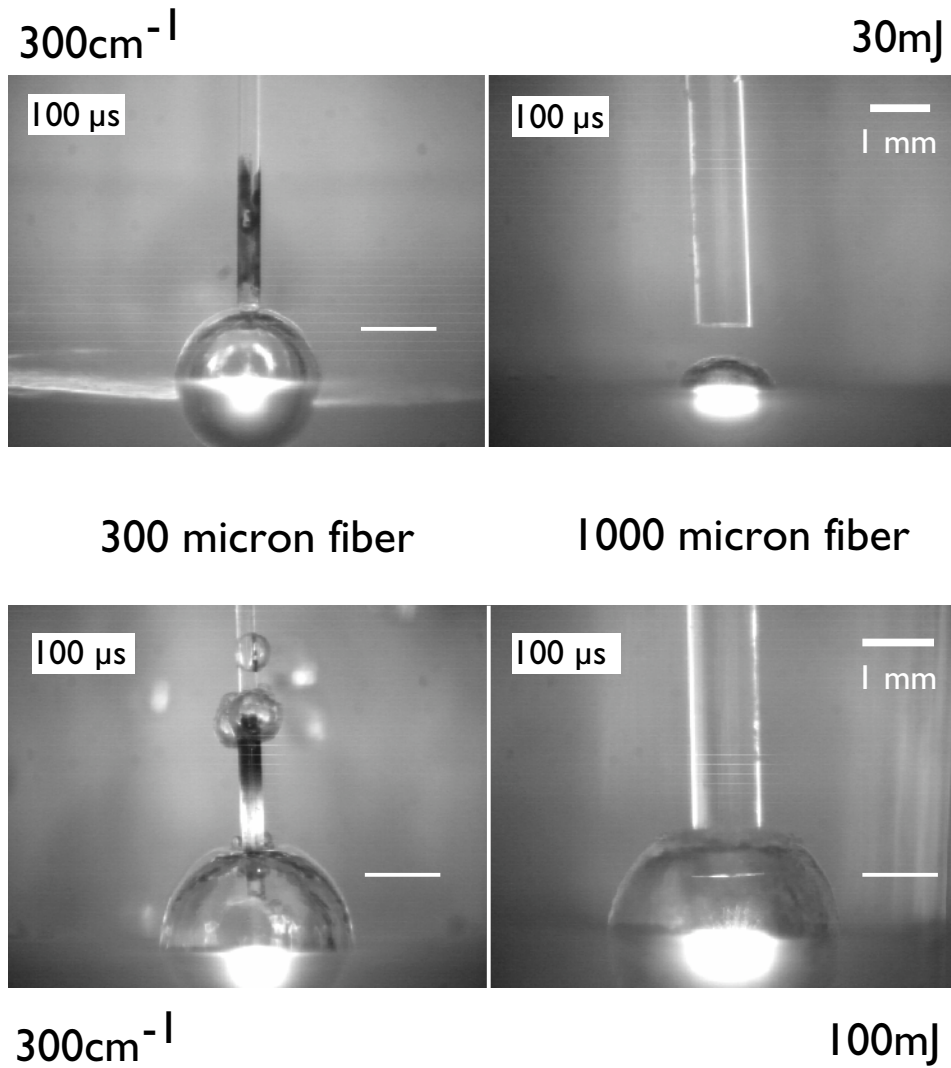
Figure 4.10: Bubbles formed on $300\,\mathrm{cm}^{-1}$ gel in cuvettes using $300\,\mu\mathrm{m}$ and $1000\,\mu\mathrm{m}$ fibers. A pulse energy of $30\,\mathrm{mJ}$ is just above the ablation threshold for the $1000\,\mu\mathrm{m}$ fiber, and the bubble formed is smaller than the one with a $300\,\mu\mathrm{m}$ fiber. However, similar sized bubbles are formed at $100\,\mathrm{mJ}$, well above the threshold energies for both fibers. The white bar indicates the level of the fiber tip. Small bubbles can be seen around the fiber in the lower left picture That is the place where the buffer of the optical fiber ends, and the bubbles are due to vortices around that discontinuity.
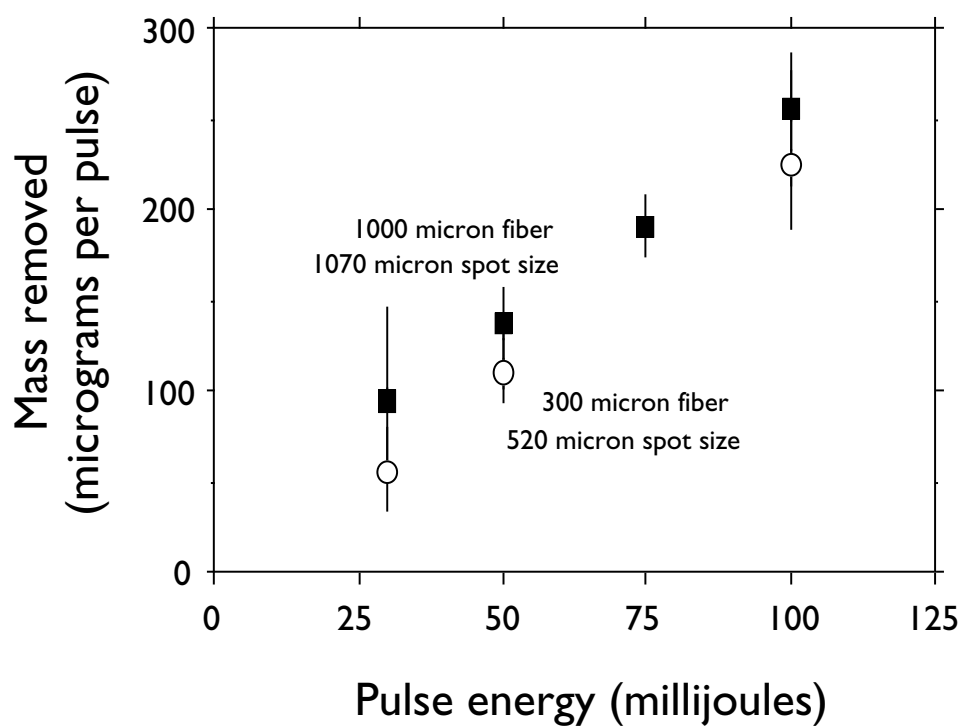
Figure 4.11: Mass ablated per pulse in $1\,\mathrm{cm}$ cuvettes using the $300\,\mu\mathrm{m}$ and $1000\,\mu\mathrm{m}$ fibers. Absorption was $300\,\mathrm{cm}^{-1}$.
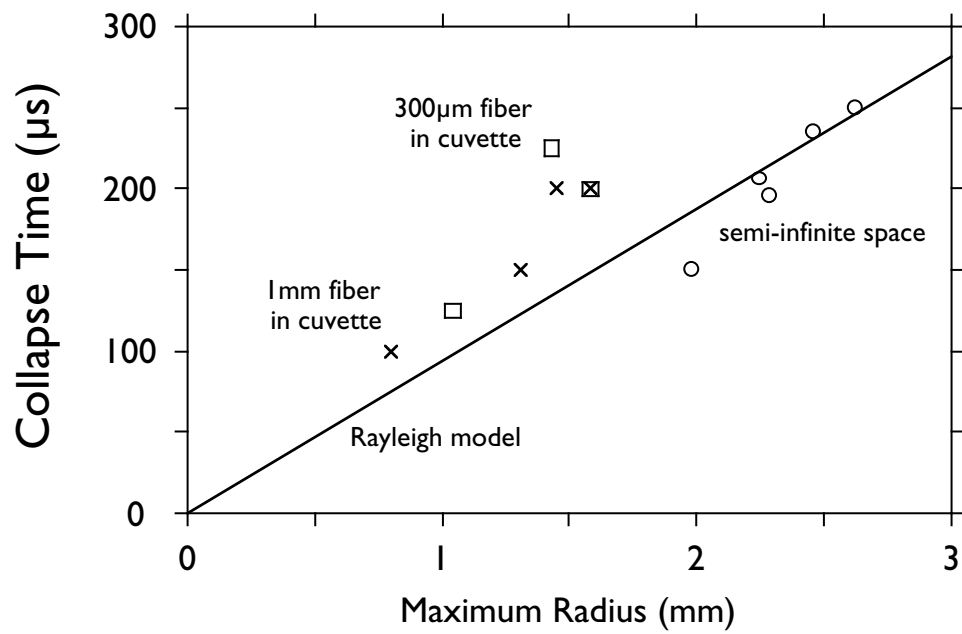
Figure 4.12: Collapse times measured from time of maximum size compared with those predicted by the Rayleigh model. The fairly reasonable agreement between the expected and measured values allows estimation of bubble energies using the Rayleigh model.
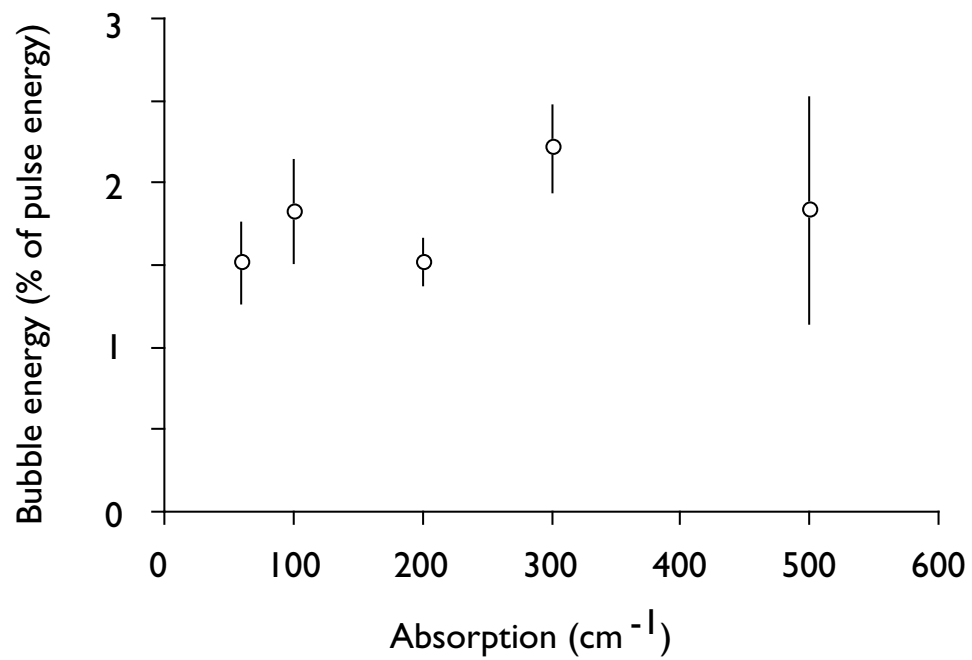
Figure 4.13: Ablation in fish-tank: Bubble energies calculated using Rayleigh's equations. A small percentage of the total laser energy goes into the pressure-volume work of the bubble at all absorptions. Pulse energy was $100\,\mathrm{mJ}$ delivered through a $1000\,\mu\mathrm{m}$ fiber.
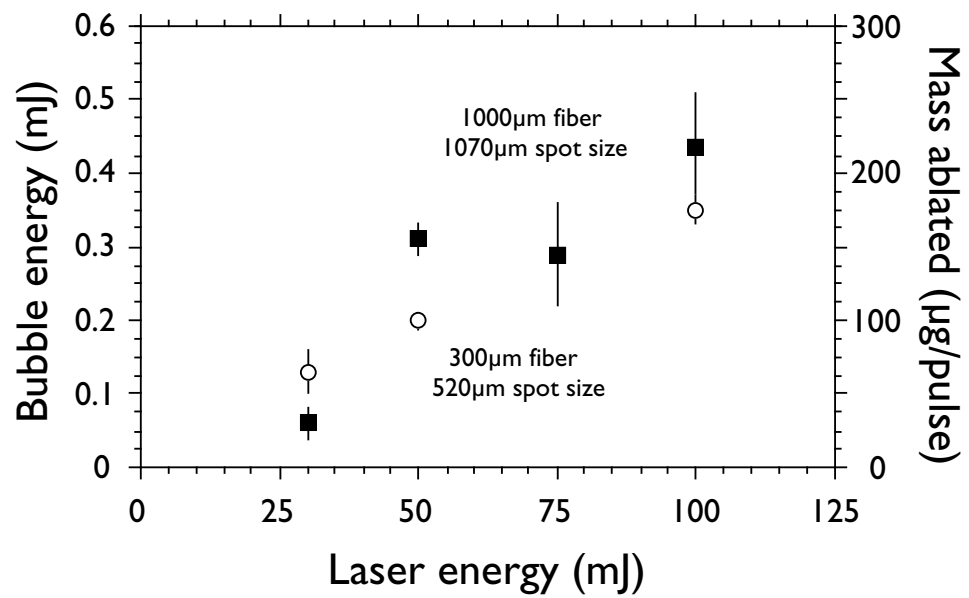
Figure 4.14: Ablation in cuvettes: The bubble energies are proportional to the laser pulse energy. The ablation mass also scales linearly with the laser energy.

Chapter 5

Visualization of ablation of gelatin and porcine clot in 3 mm tubes

This chapter investigates pulsed laser ablation under water in 3 mm tubes simulating coronary arteries.[1] Ablation of gel with different laser spot sizes is visualized. The effects of multiple pulses and repetition rate on the bubble dynamics are studied. Bubble formation and mass removal in gel are compared with ablation of porcine clot. The conclusion from the second chapter that laser thrombolysis is equally efficient at most visible wavelengths is tested. The differences between contact versus non-contact of the laser delivery device with the thrombus are investigated.

Initial experiments were conducted with a gel-based clot model confined in 3 mm inner diameter silicon tubes. Subsequent experiments used 24 hour old porcine blood clots. Quartz fibers of $300\,\mu$m and $1000\,\mu$m core diameter were used to deliver 100 mJ pulses. Bubble evolution was photographed. Laser pulses of 50 mJ pulse energy were delivered via a quartz fiber contained in a flushing catheter. Pulse repetition rates of 1 Hz, 3 Hz, and 6 Hz were used. Wavelengths of 506 nm and 577 nm were used to ablate clot. Bubble action was captured by flash photography using a CCD camera and recorded on video. The amount of material removed was measured using a spectrophotometric technique.

Bubbles of similar size and lifetime were formed with laser pulses delivered by $300\,\mu$m and $1000\,\mu$m fibers; yet more material appeared to be removed by the larger fiber. Ablation of clot and gel proceeded in a similar manner. No significant differences in bubble action or mass removal were observed at the three pulse repetition rates and the two wavelengths. Contact between the catheter and the clot did not result in a pistoning effect of the catheter at the pulse energy used.

---

[1] Part of this chapter was published in the paper "Visualization of microsecond ablation of porcine clot and gelatin under a clear liquid" in SPIE *Lasers in Surgery: Advanced Characterization, Therapeutics, and Systems VI*, volume 2671, 28–35, 1996.

5.1 Goals

In the second chapter, a parametric study was done to identify the optimal wavelength, pulse energy, and spot size for efficient ablation during laser thrombolysis. Larger fibers were shown to remove more mass than smaller fibers at similar energies. This was suspected to be due the formation of bigger and more energetic bubbles with the larger fibers. Experiments in the fourth chapter studied the formation and collapse of vapor bubbles leading to ablation. The results of these studies however showed that bubbles of similar size and lifetimes, and therefore of similar energies, were formed with different sized fibers. Also, the mass removed was similar. The only difference between the experiments in the second and fourth chapters was that in the visualization study, the gel was ablated without the confining effects of the 3 mm tubes. Obviously the geometry of ablation plays an important role in the efficiency of material removal. In this chapter, gel is ablated in tubes with 300 μm and 1000 μm fibers, and the process is imaged.

The parametric and visualization studies used gelatin as a clot model. This removed the biological variability of clots and also allowed the absorption at a single wavelength to be controlled. The results of the threshold studies in the third chapter showed that microsecond ablation thresholds for clot and gel were similar at equivalent light absorption. Also, the Young's moduli for the two materials were similar. However, more validation of the gel model was required before the results and their implications can be accepted as applicable to laser thrombolysis. One of the goals of this study is to validate some of the results of the parametric and visualization studies by comparing clot and gel ablation. In particular, clot is ablated at 506 nm and at 577 nm to test the conclusion that laser thrombolysis can be done at most visible wavelengths without compromising the ablation efficiency.

Laser thrombolysis currently uses repetition rates of 3 Hz. The vapor bubbles formed upon absorption of the laser energy have lifetimes of the order of hundreds of microseconds. This suggests that the efficiency of ablation should be relatively independent of repetition rate, since cavitation bubble dynamics are finished before the arrival of the next laser pulse. If this is indeed true, laser thrombolysis could possibly be done at a higher repetition rate thus reducing the total time for the procedure.

Early thrombolysis and angioplasty efforts used solid glass fibers to deliver the laser energy, and in a few cases arterial perforations and dissections were reported. These were suspected to be caused by a pistoning effect of the hard fiber when in direct contact with the clot. The pistoning or jack-hammer effect was thought to be due to explosive vaporization of the clot and

the subsequent bubble dynamics. Current laser delivery is achieved by a fluid core catheter that considerably minimizes the danger posed to vascular systems by the edges of the delivery device [68]. However, the concern about a pistoning effect due to direct contact with the clot remained because exact placement of the catheter *in vivo* is extremely difficult.

Porcine clot and gel were confined in 3 mm inner diameter silicon tubes to simulate coronary arteries. Pulse energies of 100 mJ were delivered through 300 μm and 1000 μm fibers to visualize the ablation process in the tubes. In the next set of experiments, a fluid catheter was used to deliver pulses at repetition rates of 1 Hz, 3 Hz, and 6 Hz. Vapor bubble formation was recorded using freeze-action flash photography. The total mass removed was measured to quantify ablation efficiency. The laser pulses were delivered with the catheter both in contact and non-contact modes. Both 506 nm and 577 nm were used to ablate clot to study the effects of wavelength on the ablation efficiency.

The results of the study show that bubble action is similar during ablation of clot and gelatin. Ablation of gel with the 1000 μm fiber appeared to remove more mass than delivery by a 300 μm fiber. No significant differences in the and mass removal were measured as a function of repetition rate for clot and gel. Contact did not result in pistoning. Both 506 nm and 577 nm were equally efficient in ablating clot.

5.2 Materials and methods

5.2.1 Targets

Gelatin of 100 cm^{-1} absorption was prepared in a manner similar to that described in chapter 2 and confined in 3 mm inner diameter tubes. The tubes were made of silicon rubber that is more flexible than the Tygon tubing used in earlier experiments. The wall thickness was 400 μm; the typical thickness of a coronary artery is $\sim$300 μm. However, a longitudinal tensile strength test showed the tube to have a significantly higher Young's modulus than an artery as seen in figure (5.1). Nevertheless, it was the best experimental model available at the time. Further, the silicon was transparent and that made it suitable for the flash photography.

The gel was cured in the tubes was topped off with water. The tube was immersed in a cuvette filled with water resembling a miniature fish-tank (figure 5.2). This was done to minimize the lensing effect of the tubes during flash photography.

Fresh non-heparinized blood was collected from domestic swine and allowed to clot in a

waterbath at 37°C for 24 hours. It was then cut into 0.5–1 cm pieces and confined in silicon tubes. Two microsecond lasers emitting at 506 nm and 577 nm were used to ablate the clot. The absorption coefficients of clot at these wavelengths were $100\,\mathrm{cm}^{-1}$ and $300\,\mathrm{cm}^{-1}$ respectively.

5.2.2 Ablation

Initial experiments involved the visualization of gel ablation with bare 300 μm and 1000 μm fibers. Single pulses of 100 mJ were delivered to the targets. The fiber tip was maintained 1 mm from the gel surface. The standard flash photography set-up was used to image bubble dynamics at various times after the laser pulse. Mass removal was not measured in this experiment.

In subsequent experiments, multiple pulses were delivered to the clot and gel targets. The repetition rate was variable between 1–10 Hz. The laser delivery device consisted of a 400 μm quartz fiber contained within a 1 mm flexible catheter. The tip of the fiber did not project out of the catheter and was maintained at 1 mm from the catheter tip. The pulse energy was 50 mJ out of the tip of the catheter.

Light was delivered through the catheter with its tip about 1 mm from the target surface for the non-contact experiments. Contact experiments had the catheter tip touching the target surface. A steady flow of water at 4 ml/min was established by a fluid injector and directed through the catheter to the target site. Pulse repetition rates of 1 Hz, 3 Hz, and 6 Hz were used. Thirty pulses were fired on each sample and the ablated material was collected by the flowing water in 1 cm cuvettes. The steady flow was continued after the last pulse until 4 ml of liquid was collected. The above procedure was repeated on control samples without light delivery to account for material removed by the flow of water alone. The ablated gel dissolved completely in the water, and the hemoglobin lysed from the removed clot in about 10 minutes.

The total mass removed was determined by measuring the absorption of the dominant chromophore in the ablated material. The chromophores are hemoglobin for clot and the dye Direct Red for gel. A calibration curve was used to convert the measured absorbance to the total mass removed. The calibration curves for clot and gel were established by measuring the absorbances of known masses of the material in 4 ml water. The curve was linear, and the slope of the line provided the necessary conversion factor. This method of measuring mass removal is described in detail in the second chapter.

5.2.3 Visualization

Flash photography was used to visualize the ablation phenomenon. Images were captured at $20\,\mu$s or $100\,\mu$s after the laser pulse using a CCD camera and recorded on video. The time of image capture was controlled by a delay generator and a microsecond strobe. The trigger signal was provided by a photodiode detecting the laser pulse (Figure 3.5).

The CCD camera (CV-250, Motion Analysis, Eugene, OR) captures a frame once it gets a trigger from the delay generator. It then sends that frame to an image capture card on a computer or to the video tape recorder. The camera has a frame memory option where it stores the captured frame in a buffer and keeps sending the same frame to the frame grabber card or video recorder until it gets another trigger and captures another frame. An individual frame can therefore be recorded for several seconds on tape. This option is useful for capturing the microsecond bubble action on video tape. The capture sequence is illustrated in figure (5.3).

5.3 Results

5.3.1 Ablation of gelatin with single pulse

Bubble sizes and lifetimes formed by single 100 mJ pulses delivered by the $300\,\mu$m and $1000\,\mu$m fibers were not significantly different (figures 5.4 and 5.5). However, visual observation showed more material removed with the $1000\,\mu$m fiber after bubble collapse. In this set of pictures, part of the bottom half of the bubble can also be seen. When the bubble was at its maximum size, some dilation of the tube can be observed.

5.3.2 Ablation of gelatin with multiple pulses

The gel was removed in small chunks which quickly dissolved in the water. All the ablated material was collected by the flowing water. There were no significant differences in the total mass ablated at pulse repetition rates of 1 Hz, 3 Hz, and 6 Hz (Figure 5.6).

Visualization of the ablation process showed clear bubble formation for the first 4–5 pulses. The images were captured $100\,\mu$s after the laser pulse. Figure (5.3) shows bubble formation at $100\,\mu$s in gel for a repetition rate of 1 Hz. The formation of a crater could be observed. The size of the bubble at $100\,\mu$s decreased with each pulse until no bubbles could be seen. However, a deepening crater was evident implying that ablation was still taking place. There were no significant differences in bubble action at $100\,\mu$s at the three repetition rates.

The gel was ablated with the catheter tip in contact with and 1 mm from the gel surface. The bubble action and total mass removed were similar for both cases. No pistoning of the catheter tip was observed (Figure 5.3).

5.3.3 Ablation of porcine clot

Ablation of clot was also characterized by a snapping sound and visible removal of clot. The ablated clot was removed in sizeable chunks of about 100–200 μm. The mass of clot removed was significantly higher than that of gel. The error in estimating the total mass was also higher. The three pulse repetition rates were equally efficient in ablating clot (Figure 5.6).

Ablation pictures were taken at 20 μs after the laser pulse (Figure 5.7). Bubbles were formed with each laser pulse delivered. Crater formation was not as clearly evident as with gel because the strobe light did not transilluminate the clot very well. However, a crater could be seen in the clot surface with a microscope. Ablation at higher pulse repetition rates seemed to be slightly more violent. However, mass removal measurements indicate equivalent ablation efficiencies.

The clot was ablated in contact and non-contact modes. Bubble behavior and mass removal were similar for both cases. No pistoning was seen with the catheter tip in contact with the clot surface.

Two wavelengths were used to ablate clot: 506 nm and 577 nm. The absorption of clot at these wavelengths is 100 cm^{-1} and 300 cm^{-1} respectively. The mass removal at both wavelengths was roughly equal indicating that the ablation efficiency is independent of absorption. Bubble action was also similar.

5.4 Discussion

In this study, microsecond ablation in 3 mm tubes simulating coronary arteries was studied. The effect of the fiber size on the bubble dynamics was investigated to better understand why ablation was more efficient with larger fibers in cylindrical geometry. Another goal was to visualize the process of clot ablation and to investigate the effect of pulse repetition rate on the total mass removed. The clot was ablated with a fluid catheter in contact with the clot surface to investigate a possible pistoning effect of the catheter tip. Pulse repetition rates of 1 Hz, 3 Hz, and 6 Hz were used to ablate porcine clot and gelatin (clot model) in both contact and non-contact modes. Images of bubble formation during the ablation process were captured on video tape with flash photography. The total mass removed was determined by quantifying the absorption signature

of the ablated material. Wavelengths of 506 nm and 577 nm were used to study the effects of wavelength and absorption on the bubble formation and mass removed.

The results of the parametric study in the second chapter showed that larger fibers were more efficient in tubes. It was thought that bubble dynamics were affected by the spot size and caused the difference in ablation efficiencies. In the previous chapter, gel was ablated using $300\,\mu$m and $1000\,\mu$m fibers under semi-infinite conditions. Both mass removal and bubble dynamics were similar with the two fibers; this result did not agree with those from chapter 2. In this study, flash photography was used to see if the bubble dynamics were different in the confining cylindrical geometry. Figures (5.4) and (5.5) show the evolution of the bubbles with the two fibers. The maximum sizes and lifetimes seem to be similar. However, ablation with the $1000\,\mu$m fiber appears more violent visually. Since the boundary presented by the bigger fiber is more confining in the 3 mm tubes, the bubble likely expands more into the gelatin than into the water. This may result in more gel being dislodged upon bubble collapse. This again suggests that larger diameter catheters would be better for creating wider lumens during laser thrombolysis. However, the size of the catheter would be limited by flexibility requirements and the size of the vessel. Also, larger spot sizes require higher threshold energies; any energy above that will create larger bubbles that may pose danger to the artery.

Porcine clot was ablated to see whether the process was similar to gel ablation. Significantly more clot than gel was removed with the thirty pulses delivered in both cases (figure 5.6). The higher ablation efficiency with clot is also evident in the flash photography experiment that was carried out at the same time as the mass removal experiments. This difference in ablation efficiencies is most likely due to differences in the mechanical strengths of clot and gel. Bubbles of almost equal size were created with every pulse while ablating clot. On the other hand, the bubbles in gel ablation got progressively smaller with successive pulses. After about five pulses no bubbles could be seen at $100\,\mu$s although a deepening of the crater was observed. Acoustic reports were always heard. This was most like because the bubbles formed after the first five pulses were so small that they had already collapsed by the time the image was captured at $100\,\mu$s after the laser pulse. These smaller bubbles with shorter lifetimes had less ablative energy than bigger bubbles.

Ablation efficiencies were not affected by pulse repetition rate for both clot and gel (figure 5.6). This confirms the earlier postulated theory that efficiency is independent of repetition rate because the bubble lifetimes are much shorter than the time interval between pulses. Each

laser pulse thus initiates an independent ablation event. The only influence a laser pulse has on the ablative efficiency of the next pulse is to change the target geometry due to removal of material and thus affecting bubble dynamics. Visualization of clot ablation at 1 Hz, 3 Hz, and 6 Hz seemed to indicate that more material is removed at higher repetition rates. This could be because the ablated material from the previous pulse had not yet been removed by the time the next pulse arrived. An important conclusion of this study is that thrombolysis could be performed at higher repetition rates without compromising efficiency. The total time for therapy would then be considerably shortened.

Contact between the catheter tip and the target surface did not result in a pistoning of the tip. Such a pistoning effect effect had been suspected to be the cause of arterial dissections reported in some studies of laser thrombolysis and angioplasty. A source for such a force would have come from the bubble trying to expand against the catheter tip. However, as seen in this study, the vapor bubble expands readily into the clot and gel with the majority of the bubble volume being under the surface. Therefore not much force is exerted against the catheter and there is not much recoil. The pulse energy used here was 50 mJ that is close to that used in clinical settings. Higher energies will create more energetic bubbles that may exert force against the catheter tip causing recoil. The dissections observed in the earlier studies [62] were likely caused by mechanical manipulations of the delivery device.

Finally, clot ablation at 506 nm and 577 nm was compared. Clot absorption varies from $100 \, \text{cm}^{-1}$ at 506 nm to $300 \, \text{cm}^{-1}$ at 577 nm. The earlier parametric study with gelatin had predicted that ablation efficiency was largely independent of absorption. This was confirmed by the equivalent mass removals at 506 nm and 577 nm reported in this chapter. Bubble action was also similar in the two cases. Laser thrombolysis can therefore be done at most visible wavelengths without compromising efficiency.

The main conclusions of this study are: (i) bubble formation is similar on clot and gel. (ii) ablation efficiency is independent of pulse repetition rate between 1–6 Hz. (iii) contact does not result in pistoning with a pulse energy of 50 mJ. (iv) ablation efficiency and bubble formation in clot are similar at 506 nm and 577 nm. (v) clot ablation is about an order of magnitude more efficient than gel ablation.
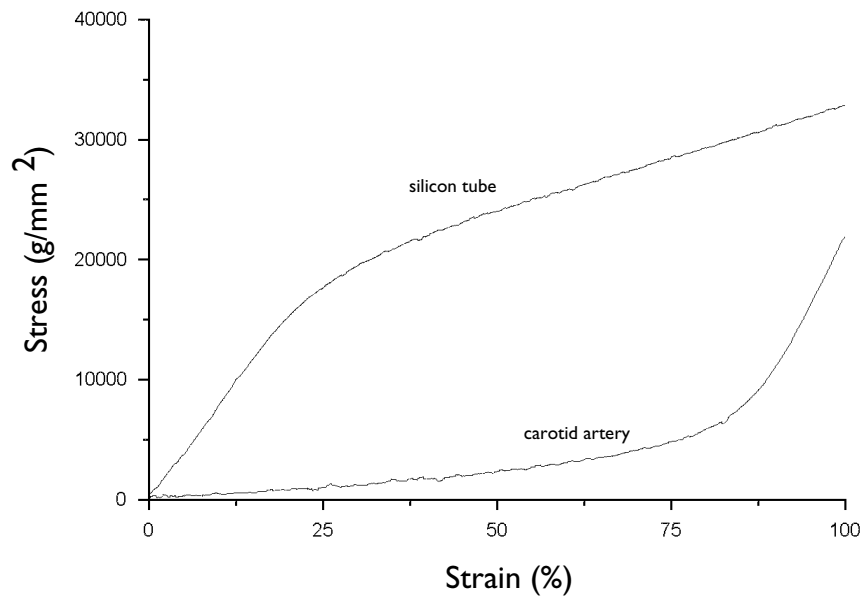
Figure 5.1: Longitudinal stress-strain curves for the silicon tube and a porcine carotid artery. The tube had an inner diameter of $3\,\mathrm{mm}$ and a wall thickness of $400\,\mu\mathrm{m}$. The carotid artery was $4\,\mathrm{mm}$ in diameter and had a thickness of about $500\,\mu\mathrm{m}$. The Young's modulus of the silicon tube is much greater than that for an artery. Coronary arteries are generally smaller and thinner than carotid arteries.
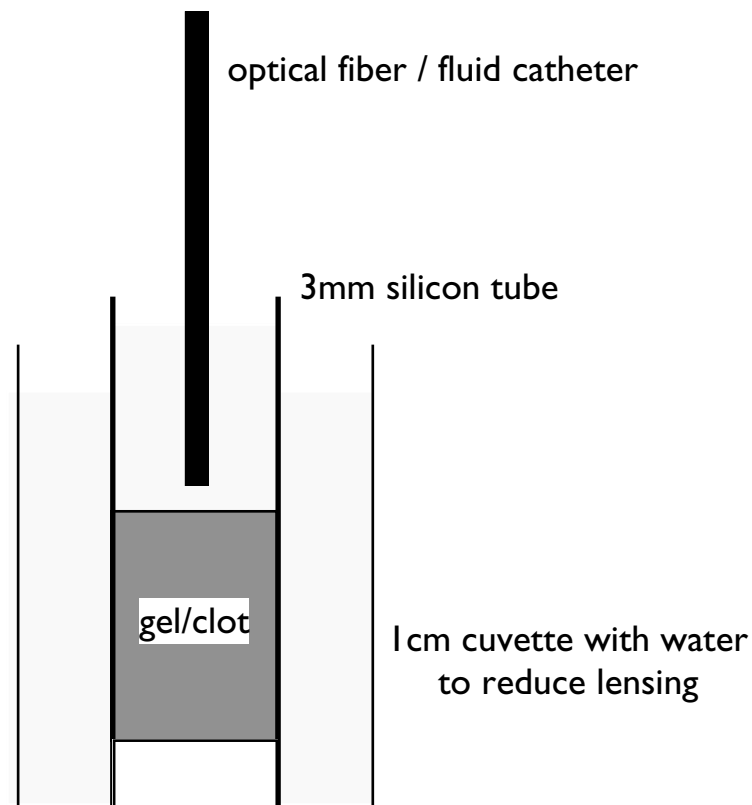
Figure 5.2: Porcine clot or gelatin is confined in a 3 mm diameter silicon tube. Laser energy is delivered in 1 μs pulses via an optical fiber or a flushing catheter to the target surface in either contact or non-contact mode. For mass removal measurement, water is flushed at 4 ml/min around the target site. The ablated material is collected in 4 ml water. For visualization using flash photography, the tube is immersed in a 1 cm cuvette filled with water. This reduces the lensing effect of the curvature of the tubes.
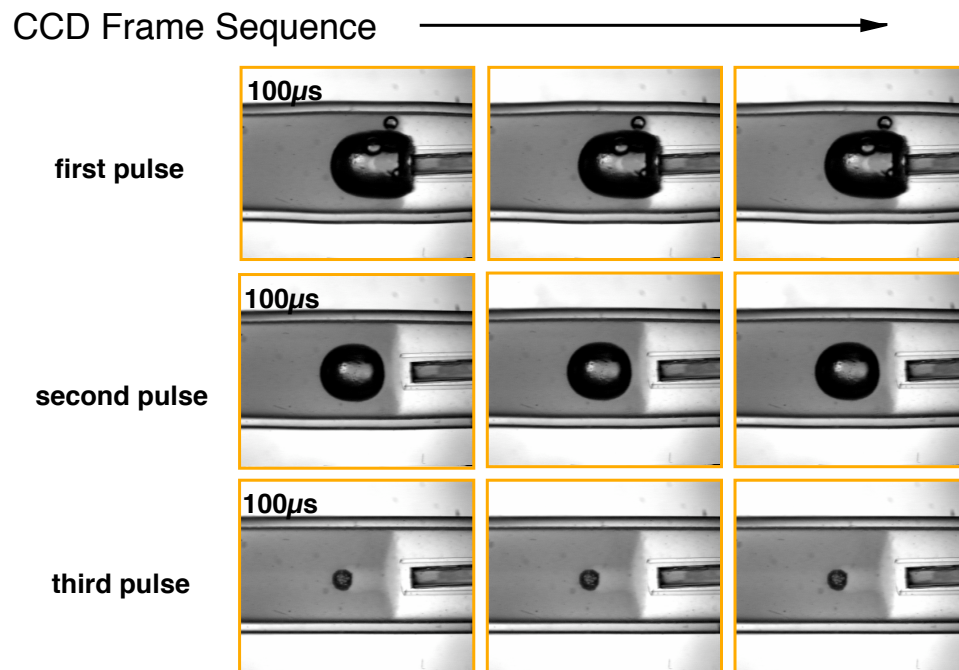
Figure 5.3: Ablation of gelatin at $1\,Hz$ and $50\,mJ$ pulse energy out of a $400\,\mu m$ fiber in a $1\,mm$ catheter. Images are captured $100\,\mu s$ after the laser pulse. Since the fiber tip is only about 0.5–$1\,mm$ from the end of the catheter, the spot size is about 400–$600\,\mu m$ in diameter. The catheter tip is in contact with the gel surface. The bubble size becomes smaller with successive laser pulses. Crater formation can be observed. No pistoning of the catheter tip is observed due to contact. This figure also shows the frame sequence of the CCD camera. The camera captures a frame and stores it in memory. It keeps feeding that frame to the video recorder until it gets another trigger and captures a fresh frame.
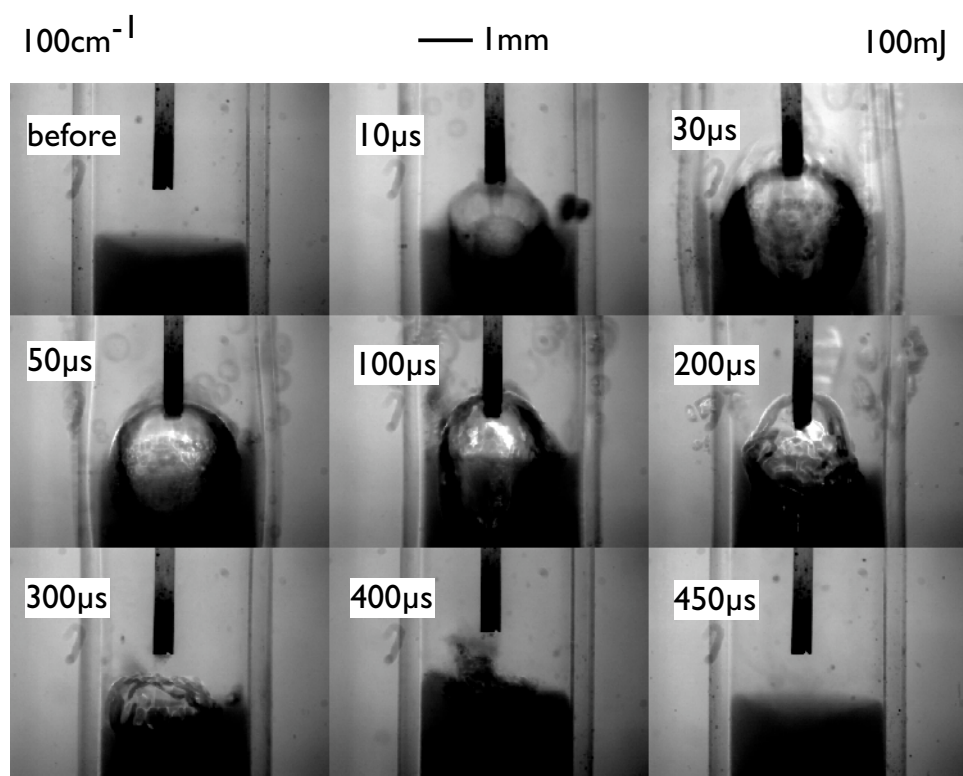
Figure 5.4: Bubble formation due to single microsecond laser pulses in a 3 mm silicon tube. Light was delivered with a $300\,\mu$m fiber. Absorption was $100\,\mathrm{cm}^{-1}$.
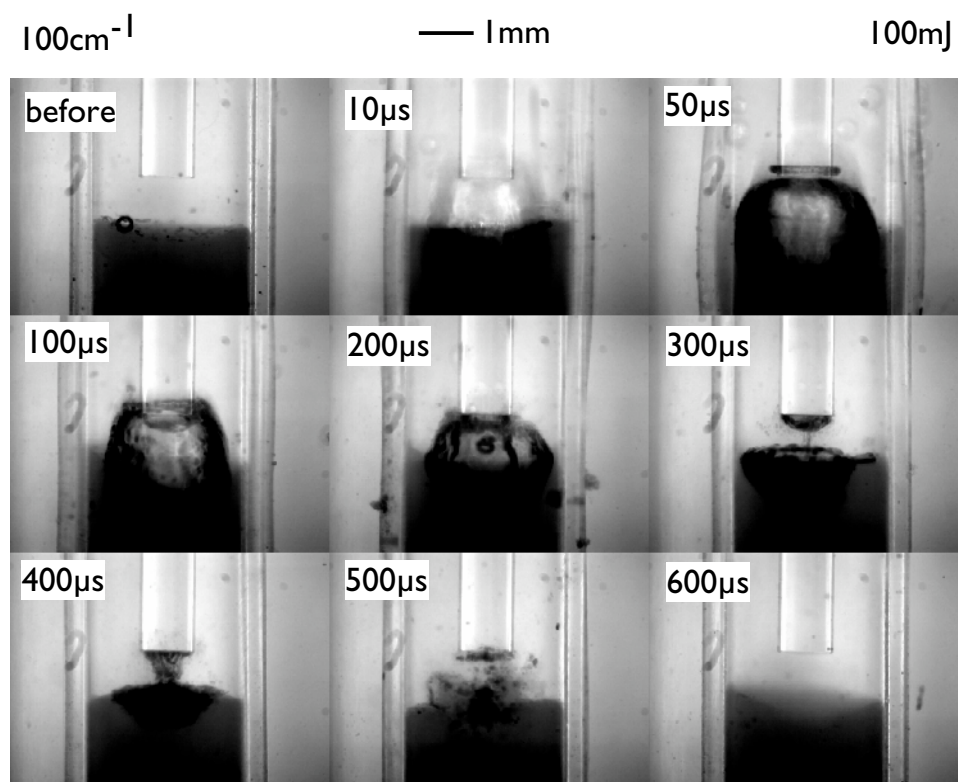
Figure 5.5: Bubble formation due to single microsecond laser pulses in a 3 mm silicon tube. Light was delivered with a 1000 μm fiber. Absorption was 100 cm^{-1}. Bubble size and lifetime seem to be similar to those in the case of delivery by a 300 μm fiber. However, the mass removal appears more violent with the 1000 μm fiber, particularly at bubble collapse. A possible reason is that the bigger fiber produces a more confining effect in the 3 mm tube, and therefore the bubble expands more into the gelatin instead of into the water.
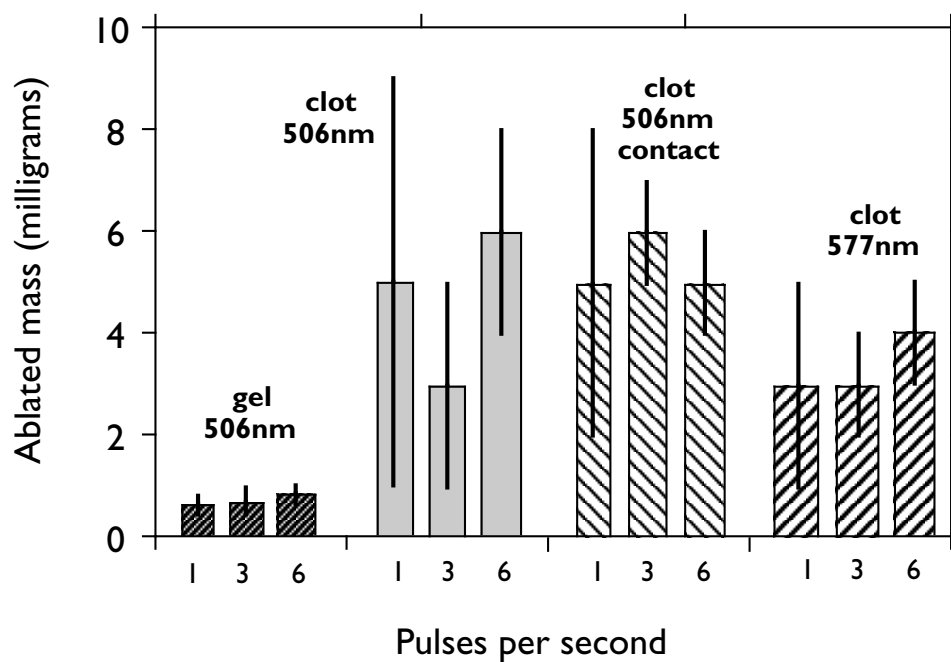
Figure 5.6: Ablation of clot and gel. More clot than gel is removed per pulse. Repetition rate has little effect on the total mass removed. The were no significant differences in ablation masses of clot between 506 nm ($\mu_a \approx 100\,\mathrm{cm}^{-1}$) and 577 nm ($\mu_a \approx 300\,\mathrm{cm}^{-1}$). Ablation was not affected by contact of the catheter with the clot.
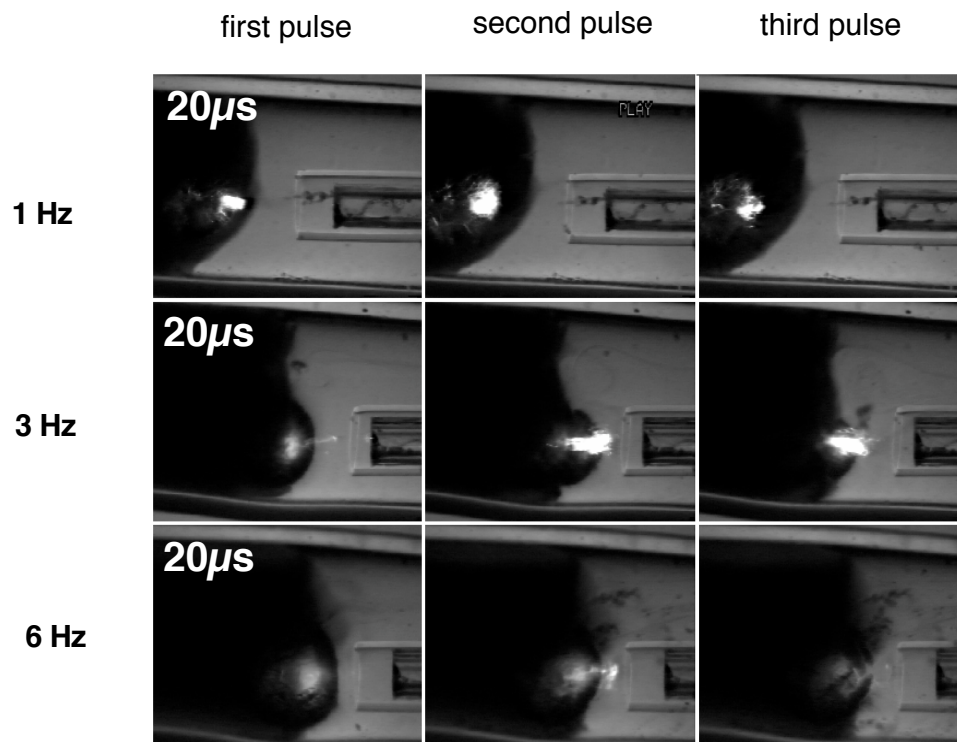
Figure 5.7: Clot ablation at 1 Hz, 3 Hz, and 6 Hz. The pulse energy was 50 mJ coming out of a 400 μm fiber in a 1 mm catheter. The catheter was not in contact with the clot surface. Wavelength was 506 nm. The white light is the back-illuminating strobe light being transmitted through the bubble. Bubble action and ablation seems more violent at higher repetition rates, but the total mass removed was similar. Bubble action was similar at 577 nm.

Chapter 6

General discussion and conclusions

The broad aim of the experimental studies described in this thesis was to investigate and quantify the ablation phenomena during laser thrombolysis. This chapter summarizes the problems addressed and the main conclusions of the thesis. The practical implications for laser thrombolysis are then discussed. The motivation behind the work was that a better understanding of the ablation process would provide data for the design of optimal laser and delivery systems.

6.1   Laser thrombolysis

The cardiovascular system is the principal conduit for the supply of nutrients and oxygen and for the removal of carbon dioxide in the body. Any compromise to this system such as blockages and hemorrhages can reduce the blood supply to vital organs and result in far-reaching consequences that are often fatal. A vast majority of heart diseases and strokes are caused by blockages of arteries by atherosclerotic plaque and clot. A number of pharmacological and mechanical treatment techniques have been developed to remove the blockages; each has its advantages and disadvantages depending on the location and nature of the blockage.

Laser thrombolysis is a minimally invasive interventional cardiovascular procedure that seeks to remove clot blocking coronary, cerebral, and peripheral arteries. Microsecond laser pulses are delivered by a fluid catheter to ablate the clot. The advantages over traditional recanalization techniques is seen in the rapidity of the procedure and in the potential to remove clot without incurring injury to the artery. The technique has shown the ability to partially restore blood flow in completely thrombosed coronary artery bypass grafts ($8\,\text{mm}\times6\,\text{cm}$) within ten minutes [113].

The fluid catheter that delivers the laser pulses is essentially an optically clear fluid stream in a plastic tubing. The fluid flows out of the open end of the catheter and washes away blood and ablation debris clearing the path for direct laser delivery to the clot. The liquid core makes

the catheter more flexible than a traditional glass optical fiber, and the softer edges pose less danger to the arterial wall. Also, the fluid used is radio-opaque allowing real time monitoring of the procedure using angiography. The size of the catheter will largely be influenced by the flexibility requirements, the size of the vessel blocked by the clot, and an optimal laser spot size.

6.2   Summary of goals and results

The process of establishing laser thrombolysis as an accepted treatment modality in cardiovascular disease required basic investigations into the ablation process and *in vivo* trials. This thesis addressed some of the questions about the basic ablation phenomena with the aim to enhance the efficiency and safety of the procedure. The three broad areas investigated are as follows:

- microsecond ablation threshold exposures for clot and artery,

- optimal laser parameters for efficient ablation,

- vapor bubble formation during pulsed laser ablation.

Throughout this study, the absorbing material of interest was clot. However, much of the experimental work was done using a gel-based clot model. This allowed precise control over the optical properties of the target so that a parametric study could be carried out. Optimization of laser parameters required quantification of the mass removal. In this study, a unique method was developed to measure mass removal following pulsed ablation of a soft target under a liquid. There was some limited validation of the experimental model: ablation thresholds for gel were similar to those reported for clot and artery, and single pulse bubble behavior also seemed similar. However, the mechanical properties of clot and gel are not similar. This was shown in chapter 5 where clot was ablated more efficiently than gel.

6.2.1   Ablation thresholds

Goal

Laser thrombolysis uses wavelengths in the visible region of the electromagnetic spectrum: clot absorbs these wavelengths much more than the artery. Since the ablation threshold is lower at higher absorption coefficients, the energy density required to ablate clot is less than that required to ablate the artery. This provides visible lasers the unique potential to selectively target clot.

The wavelength and spot size determine the threshold energy required to achieve ablation. Previous studies had measured differences in microsecond ablation thresholds for lysed blood, clot and atheroma under saline at 577 nm, 465 nm and 488 nm [50, 52, 91]. However, the relationship between the absorption and the threshold radiant exposure had not yet been established. This will enable one to predict microsecond ablation thresholds for clot at any wavelength. Also, an estimate of the threshold surface temperature will provide information about how ablation is initiated.

Results

The issue of threshold was explored in chapter 3. Microsecond ablation thresholds were measured as a function of absorption over a range of 10–2000 cm^{-1}. The measured values are within 10% of the published ablation thresholds for lysed blood, clot, and atheromas at the corresponding absorption coefficients. We can now predict microsecond ablation threshold of clot and artery at any visible wavelength. Practically, this is important for choosing the radiant exposure such that it is between the thresholds for clot and artery.

From a basic science perspective, the threshold data provides insight into the initiation of the ablation process. Ablation is initiated at a threshold radiant exposure (energy per unit area) rather than by the total delivered energy. This is because the temperatures achieved at the surface of the absorbing medium is directly proportional to the radiant exposure and the absorption coefficient (equation 2.3). A calculation of the threshold surface temperature using equation (3.5) suggests that the surface needs to be raised to just above 100°C. The radiant exposure required to raise the surface temperature to 100°C is given by

$$E_{th} = \frac{\rho c \, \Delta T_{100}}{\mu_a}. \tag{6.1}$$

A vapor bubble is formed when the radiant exposure is just above threshold (figure 3.9). While modeling ablation, it is sometimes assumed that the material up to a depth equal to the the penetration depth δ is vaporized. Let us consider a case where the target had an absorption of 50 cm^{-1} ($\delta = 200 \, \mu$m). A threshold energy of 50 mJ delivered by a 1 mm fiber was measured at this absorption. The energy required to heat 1 g of water from 27°C to 100°C and then to vaporize it at 1 atmosphere is about 2675 J. If a cylindrical volume of 1 mm diameter and 200 μm depth is to be completely vaporized, the required energy to completely vaporize it is therefore 400 mJ. This is almost an order of magnitude higher than the measured threshold energy. Obviously, a much smaller volume is vaporized. At threshold, the surface is heated to 100°C, and any extra

energy will go into the phase change of the surface layer.

6.2.2 Laser parameters for efficient ablation

Goals

The selective absorption of light by thrombus in the visible region is a main rationale for laser thrombolysis. However it was not clear which visible wavelength was most efficient for clot ablation. One of the main goals of this thesis was to identify an optimal wavelength for laser thrombolysis. Fixing the wavelength for laser thrombolysis will simplify the laser design and help replace the bulky pulsed-dye laser that is currently being used. Other laser parameters that were studied are the spot size, pulse energy, and pulse repetition rate. The spot size will influence the choice of the catheter diameter to deliver the laser energy.

Results

The experiments described in the second chapter showed that the absorption coefficient of the gel did not seriously affect the amount of material removed once the pulse energy was above threshold (figure 2.5). This suggested that almost any visible wavelength can be used for laser thrombolysis without compromising the efficiency (figure 2.9). To ensure that the results of gel ablation were extendable to clot, this conclusion was partially confirmed by the experiments in the fifth chapter where clot was ablated at $506\,\mathrm{nm}$ ($\mu_a = 100\,\mathrm{cm}^{-1}$) and $577\,\mathrm{nm}$ ($\mu_a = 300\,\mathrm{cm}^{-1}$); the ablation efficiency was similar in both cases.

Larger spot sizes removed material more efficiently in $3\,\mathrm{mm}$ tubes than smaller spot sizes at similar energies (figure 2.7). The experiments in the fifth chapter led to the hypothesis that the larger efficiency was due to the confining effects produced by a large catheter in a vessel. This result suggests that larger catheters will remove more clot and also create wider lumen in the arteries. The practical limitations are catheter flexibility and high threshold energies. Also, smaller spot sizes produced by smaller catheters would dig deeper craters into the clot, and therefore a channel could potentially be drilled through the clot in a shorter time.

The absorption and spot size experiments showed that while the radiant exposure is the critical parameter to reach threshold, it becomes less important in the mass removal once threshold is exceeded. Higher absorption coefficients result in higher surface temperatures; yet, the mass removal did not change significantly for similar energies. In fact, the ablation efficiency was not influenced by how much the delivered energy exceeded the threshold energy for that particular

spot size (figure 2.6). Also, mass removal in the 1 cm cuvettes was similar at similar pulse energies delivered by different fibers. The important parameter in determining the amount of material removed is the total pulse energy delivered, and not the radiant exposure. The other implication is that heating is not the principal factor in the ablation process.

The results of the parametric study also suggest that laser thrombolysis can be done at higher repetition rates than the currently chosen 3 Hz without compromising the ablation efficiency. This number was chosen because a higher repetition rate disrupted the streamlined fluid flow and degraded the optical transmission when the catheter tip was 1 cm from the clot. The experiments in chapters 4 and 5 showed that ablative events following delivery of a single pulse generally last for only half a millisecond. The ablation debris must be removed by the fluid stream before the next pulse can be fired. In practice, the tip of the catheter is usually 0–3 mm from the clot in a typical 3 mm coronary artery. At a flow rate of 0.3 m/s, it takes about 50 ms for the fluid stream to displace the volume between the catheter tip and the clot surface and clear the debris. This means that the next laser pulse can be fired about 100 ms after the previous pulse. Pulse repetition rates of 6 Hz and 9 Hz have been successfully tested *in vivo* in a swine model [114]. In an independent observation, no degradation in the optical transmission by the fluid was observed [114].

The choice of the wavelength should be dictated by the complexity of laser design or by the adaptability of an existing laser system. The obvious choice seems to be the doubled Nd:YAG laser emitting at 532 nm. This wavelength is well within the acceptable region for efficient laser thrombolysis. Based on the parametric experiments, efforts are underway to build a doubled Nd:YAG system for laser thrombolysis. This solid state device would be much smaller than the pulsed-dye laser making it easier to operate. It also does not require handling of potentially hazardous laser dyes. The maximum energy output is about 100 mJ in 10–100 μs pulses, a modest requirement for such a laser system. Pulse repetition rate is fixed at 10 Hz. The issue of an optimal pulse length has not been addressed in this thesis. It is believed that a pulse length of 10–100 μs would work for laser thrombolysis since that range is still within the thermal relaxation time of clot. A longer pulse duration also makes energy coupling into a small optical fiber ($\sim$100 μm) easier, an essential requirement for ablating clot in small cerebral vessels. However, the bubble dynamics may be different at longer pulse durations. Some researchers have suggested that less energetic bubbles are formed at longer pulses, and therefore they induce less mechanical damage to the collateral tissue [115]. Also, ablation thresholds may increase slightly for longer pulses.

This system has yet to be tested *in vitro* and *in vivo*.

6.2.3   Vapor bubble formation

Goals

Pulsed laser ablation of tissue under a liquid is an explosive process that is often accompanied by the formation of vapor bubbles. In laser thrombolysis, these bubbles are formed when part of the clot is vaporized following absorption of the laser pulse. The results of the parametric study in chapter 2 led to the hypothesis that the mechanical action of the bubble was actively involved in the ablation process. It had also been suspected that the bubble dynamics may interact with the delivery catheter and the vessel walls resulting in mechanical damage to the vessel. Ablation was photographically studied in the fourth and fifth chapters of this thesis to better understand the roles of heating and bubble dynamics in the mass removal process. The effect of geometry on bubble evolution was also studied in the 3 mm tubes with the catheter in contact and non-contact modes to identify any events that may cause mechanical trauma to the vessel.

Results

The visualization experiments in the fourth and fifth chapters showed that the vapor bubbles expanded and collapsed within $500\,\mu$s. As a rule of thumb, for every millimeter of maximum bubble diameter, the bubble lifetime is $100\,\mu$s. This agrees with an equation proposed by Lord Rayleigh relating the maximum bubble size and the collapse time [103]. Bigger bubbles were formed at higher energies, but the size was relatively independent of the fiber size except near threshold. The greater efficiency of large fibers in tubes was not reproduced when gel was ablated in semi-infinite conditions. It is now suspected that the 3 mm tube amplifies the confining effects of the 1 mm fiber and causes the bubble to expand more forward into the gel than into the water.

A simple model proposed by Lord Rayleigh was used to estimate the bubble energy based on its maximum size and lifetime [103]. Less than 5% of the total laser energy is coupled into the pressure-volume work of the bubble. It is not clear what happens to the rest of the energy. From the maximum volume of the bubble, we could try to arrive at an energy balance. Let us consider the case where a pulse energy of $100\,$mJ was delivered by a $300\,\mu$m fiber ($520\,\mu$m spot size) to a $300\,$cm^{-1} target. The observed maximum bubble size was $3\,$mm diameter, and the lifetime was $400\,\mu$s. Assuming that the content of the bubble at maximum size is a perfect gas at 1 atmosphere and $300\,$K, we can calculate the number of moles of ablated material in the bubble

using the equation

$$PV = nRT. \tag{6.2}$$

where R is the gas constant and n is the number of moles. For a 3 mm bubble, this works out to be 574 nanomoles or 11 μg of material (1 mole of water = 18 g). Using the enthalpy of 2675 J/g, the energy required to vaporize 11 μg is 29 mJ, well within the supplied energy of 100 mJ.

We can do the calculation from the opposite direction where we determine the amount of material vaporized based on the incident radiant exposure and the absorption of the target. The heat $H(z)$ (units of J/cm^3) produced within the 300 cm^{-1} gel is obtained by multiplying the Beer's law light distribution (equation 2.1) with the absorption coefficient μ_a,

$$H(z) = \mu_a E_0 \exp(-\mu_a z). \tag{6.3}$$

This energy is used for heating, and for vaporization if any energy is left. In this particular example, using equation (6.3) we can calculate that a heat of 2500 J/cm^3 is produced at a depth of 60 μm. The energy beyond that depth is wasted as heat. Therefore material up to a depth 55 μm or a volume of 0.012 mm^3 is completely vaporized. The energy required for that is about 31 mJ. This is quite close to the 29 mJ that we calculated based on the bubble volume. The total energy deposited into the first 60 μm is 82 mJ; of this, 31 mJ is used for vaporization, and the remaining 51 mJ may go towards expansion of the vapor and into acoustic transients.

It would now seem that we could do a straightforward energy partitioning based on heating and vaporization. However, this is not the case since bubbles have also been observed at radiant exposures that are insufficient for vaporization. Consider for example the case where a pulse energy of 100 mJ is delivered to 60 cm^{-1} gel by 1 mm fiber (1 mm spot size) resulting in a radiant exposure of 127 mJ/mm^2. From equation (6.3), the heat produced at the surface is 765 J/cm^3, and it decreases exponentially into the material. A strict application of Beer's law will therefore not account for vaporization, *but a bubble is still formed*. The size of the bubble is again about 3 mm diameter, and using the same analysis described above, the mass of material inside is about 11 μg. The energy required for this 29 mJ, and the supplied energy is 100 mJ. Therefore, in absolute terms, there is sufficient energy available for vaporization. The threshold experiments showed that enough energy had to be supplied to raise the surface to 100°C to set the stage for ablation. Apparently, any extra energy supplied will participate in some kind of thermal energy transfer between the heated sites such that there is enough latent heat available at a particular site for vaporization to be initiated. It is not clear what physical processes are behind this apparent energy transfer, and how the vaporization sites are chosen.

Once the material is vaporized, extra energy is available for expansion of the vapor and acoustic transients. The calculated pressure-volume work of the bubble was less than 5% of the total pulse energy in all cases studied. Some of the energy left after vaporization probably goes into an initial acoustic transient when the vaporized material expands. Energy that does not heat material to 100°C is wasted as heat and does not participate in the ablative event.

The bubble energies scale linearly with the pulse energy under conditions well above threshold. Mass removal also scales linearly with the pulse energy suggesting that there may be a correlation between bubble energy and mass removal above threshold. It was shown in chapter 2 that heating and vaporization accounted for a very small fraction of the ablated mass. The major part is removed either by the bubble work or by initial acoustic transients.

Does this mean that forming an energetic bubble is the way to go in laser thrombolysis? More energetic bubbles are bigger in size, and this may not be desirable. In fact, it was seen in chapter 5 that bubble expansion at clinically relevant energies dilated the 3 mm silicon tubes (figures 5.4 and 5.5). Real arteries are weaker than the tubes (figure 5.1), and the dilation is blood vessels will most likely be more pronounced. This could cause vessel wall damage such as dissections and perforations, particularly in the weak and small cerebral arteries. Further, while the interaction of the bubble with the catheter touching the target surface did not result in a pistoning effect in a straight vessel geometry, it may still happen at higher energies, in smaller vessels, or when there is a curve in the vessel. It is therefore probably wiser to use lower energies closer to threshold so that smaller bubbles are created.

6.3   Can we work at threshold?

Analysis of the mass removal data at threshold brings a new perspective to the ablation mechanism. Figure (2.6) shows the ablation thresholds incorporated into the mass removal at various absorption coefficients. It suggests that mass removal is not influenced by whether the supplied radiant exposure is just above threshold (e.g., $60\,\mathrm{mJ/mm^2}$ on $50\,\mathrm{cm^{-1}}$ gel; threshold $= 50\,\mathrm{mJ/mm^2}$) or well above threshold (e.g., $60\,\mathrm{mJ/mm^2}$ on $700\,\mathrm{cm^{-1}}$ gel; threshold $= 4\,\mathrm{mJ/mm^2}$). All that matters is that the energy is above threshold. However, bubble size and lifetime are quite different in the two cases. This is readily seen in figure (4.10) where the bubble formed with a 30 mJ pulse via a $1000\,\mu\mathrm{m}$ fiber on $100\,\mathrm{cm^{-1}}$ gel is much smaller than the one formed when the same energy is delivered by a $300\,\mu\mathrm{m}$ fiber. In the former case, the conditions are close to threshold, while in the latter the energy was well above threshold. Yet, mass removal was

almost the same in both the cases.

The question now arises: *how important is the bubble in the mass removal process?* Does it just happen to be formed, its size and energy being dependent on how much extra energy is left after the vaporization process? The actual work in the ablation process may be done by the unaccounted energy that manifests itself in an initial acoustic transient. It may then be possible to remove clot without creating a big bubble.

This question has implications important enough to warrant further studies of ablation efficiency near threshold. It is particularly critical for applications to stroke treatment where overdilation of vessels must generally be avoided (vessel dilation may beneficial in the treatment of vasospasm). Threshold conditions can be achieved by choosing the appropriate combination of pulse energy, spot size, and absorption coefficient. The easiest way is to just reduce the pulse energy for a fixed spot size and absorption. If the bubble size can be drastically reduced by operating just above threshold, any compromise in total mass removal can be accommodated by firing more pulses, using a higher repetition rate, or both. The studies required to answer this question are similar to those described in this thesis. However, the physical dimensions of the delivery device and the vessel model and the pulse energies need to be reduced to more closely represent conditions of laser thrombolysis in cerebral vessels, e. g., a 100–200 μm fiber delivering 1–10 mJ pulses in 1–3 mm tubes.

6.4 Where is laser thrombolysis now?

When this study was initiated, laser thrombolysis was seen as an alternate procedure to treat thrombosis of coronary arteries and bypass grafts that causes acute myocardial infarction. The experiments described in this thesis, particularly those using the silicon vessel models, were performed with this aim in mind. The thrombus burden encountered in bypass grafts can be quite large, maybe 3–5 mm in diameter and 10 mm in length. One of the disadvantages of current techniques of removing thrombotic occlusions had been the inability to completely remove a large thrombus burden.

Can laser thrombolysis remove large thrombus burden and clear completely thrombosed vessels? In the second chapter, it was reported that the channel drilled into the clot model had a diameter similar to the spot size, i.e., a 1 mm spot made a 1 mm wide hole. The mural gel was not removed. Most coronary arteries are about 3 mm in diameter. Complete vessel closure in

coronary arteries is generally due to a large atherosclerotic occlusion and some thrombus, generally the size of a grain of rice. Complete removal of the thrombus in such cases may therefore be possible if the thrombus burden is small. However, complete closure of bypass grafts is mostly due to a large clot burden, and several passes of the catheter through the clot would be necessary to create a larger lumen. Once the catheter has been inserted and advanced to the clot, it is difficult to control its precise position within the vessel lumen, and the catheter tends to retrace the first path. It is unlikely that the presently configured delivery system can remove all the clot. Some of the newer animal results seem to confirm this hypothesis [113]. Any mural clot left behind would act as a substrate for further clot formation, and re-occlusion cannot be ruled out. However, clinical experience has suggested that re-occlusion was not a problem [114].

Wider lumens could be formed by using a larger delivery catheter. The device will however then be less flexible making negotiating tortuous bends difficult and dangerous. Further, the threshold energy for ablation will be higher. Another way to remove more clot from the sides would be to use some kind of a side-firing device. This presents serious engineering challenges as it requires some reflective device to direct the laser beam sideways. There are some experimental prototypes that are currently being tested *in vitro*. Bubble dynamics will probably be different because the geometry has changed. A side-firing device will also encounter the situation mentioned briefly in the third chapter, where the vessel wall will lie directly under the targeted clot. If a sizeable bubble is formed, the collapse may result in damage to the artery even if the vessel wall is not irradiated directly.

On the other hand, laser thrombolysis is regarded as an attractive treatment modality for strokes that are caused by thrombosis of cerebral arteries and sometimes by emboli originating elsewhere in the body. Part of the reason for this is that there is really no other viable treatment. Thrombolytics often take too long to take effect, and ballooning techniques are avoided. The critical part in treatment of cerebral occlusions is the rapid restoration of blood flow to prevent neurological deficit. Laser thrombolysis has already proven its ability to remove clot more rapidly than any other technique. Also, the clot burden in most stroke cases is very small. Presently, animal trials are planned using a canine model. Some of the main challenges lie in the engineering of a delivery device small enough to negotiate a cerebral vessel. Threshold energies for a small spot size ($\sim$100–200 μm) are low ($\sim$0.5 mJ), and any more energy delivered may cause a bubble big enough to burst the delicate vessel.

Laser thrombolysis is still in the developmental stage. This study has investigated and quantified some basic ablation phenomena taking place during laser thrombolysis. It has not addressed *in vivo* studies and biological effects of the laser radiation and therefore cannot claim to be a complete evaluation of laser thrombolysis. However, based on some of the observations, one can make intelligent guesses about what would happen *in vivo*. This study has produced results of immediate practical interest, spawned speculation about the ablation process, and has made suggestions regarding clinical practice.

Bibliography

[1] F. Fuster, L. Badimon, J. J. Badimon, and J. H. Chesebro, "The pathogenesis of coronary artery disease and the acute coronary syndromes," *New Engl. J. Med.*, vol. 326, pp. 242–250, 1992. part 1 of 2.

[2] F. Fuster, L. Badimon, J. J. Badimon, and J. H. Chesebro, "The pathogenesis of coronary artery disease and the acute coronary syndromes," *New Engl. J. Med.*, vol. 326, pp. 310–318, 1992. part 2 of 2.

[3] J. H. Chesebro and S. Goldman, "Coronary artery bypass surgery: Antithrombotic therapy," in *Thrombosis in Cardiovasular Disorders* (V. Fuster and M. Verstraete, eds.), W. B. Saunders Company, 1992.

[4] Nat. Stroke Assoc., *Stroke facts*, 1995.

[5] M. J. Davies, "Pathology of arterial thrombosis," in *Thrombosis* (T. W. Meade, ed.), Churchill Livingstone, 1994.

[6] D. P. de Bono, M. R. Simoons, and J. Tijssen, "Early intravenous heparin enhances coronary patency after altepase thrombolysis: Results of a randomised double blind," *Br. Heart J.*, vol. 67, pp. 122–128, 1992.

[7] The GUSTO investigators, "An international randomized trial comparing four thrombolytic strategies for acute myocardial infarction," *N. Engl. J. Med.*, vol. 329, pp. 673–682, 1993.

[8] E. Goudreau, G. DiSciascio, and K. Kelly, "Coronary angioplasty of diffuse coronary artery disease," *Am. Heart J.*, vol. 121, p. 12, 1991.

[9] R. J. Ivanhoe, W. S. Weintraub, and J. S. Douglas Jr., "Percutaneous transluminal angioplasty of chronic total occlusions: Primary success, restenosis, and long-term clinical follow-up," *Circulation*, vol. 85, p. 106, 1992.

[10] J. Rosenblum, S. H. Strertzer, and R. E. Shaw, "Rotational ablation of balloon angioplasty failures," *J. Invasive Cardiol.*, vol. 4, p. 132, 1992.

[11] C. L. Grines, K. F. Browne, M. Vandormael, G. Stone, J. O'Keefe, P. Overlie, Puchrowicz, M. R. Strzelecki, and W. W. O'Neill, "Primary angioplasty in myocardial infarction (PAMI) trial," *Circulation*, vol. 86, pp. I–641, 1992.

[12] L. Badimon, J. J. Badimon, and V. Fuster, "Pathogenesis of thrombosis," in *Thrombosis in Cardiovasular Disorders* (V. Fuster and M. Verstraete, eds.), W. B. Saunders Company, 1992.

[13] D. de Bono, "Management of thrombosis in coronary heart disease," in *Thrombosis* (T. W. Meade, ed.), Churchill Livingstone, 1994.

[14] Third International Study of Infarct Survival (ISIS-3) Collaborative group, "A randomised comparison of streptokinase vs tissue plasminogen activator vs anistreplase and of aspirin plus heparin vs aspirin alone among 41,299 cases of suspected acute myocardial infarction," *Lancet*, vol. 339, pp. 753–770, 1992.

[15] J. M. Gore, C. B. Granger, M. L. Simoons, M. A. Sloan, W. D. Weaver, H. D. White, G. barbash, F. Van de Werf, P. E. Aylward, E. J. Topol, and R. M. Califf, "Stroke after thrombolysis: mortality and functional outcomes in the GUSTO-I trial," *N. Eng. J. Med.*, vol. 92, pp. 2811–2818, 1992.

[16] A. M. Linkoff, J. J. Popma, S. G. Ellis, J. A. Hacker, and E. J. Topol, "Abrupt vessel closure complicating coronary angioplasty: Clinical, angiographic, and therapeutic profile," *J. Am. Coll. Cardiol.*, vol. 19, p. 926, 1992.

[17] S. G. Ellis, W. W. O'Neill, and E. R. Bates, "Implications for patient triage from survival and left ventricular functional recovery analysis in 500 patients treated with coronary angioplasty for acute myocardial infarction," *J. Am. Coll. Cardiol.*, vol. 13, pp. 1251–1259, 1989.

[18] J. Hirshfeld Jr., J. S. Schwartz, and R. Jugo, "Restenosis after coronary angioplasty: A multivariate statistical model to relate lesion and procedure variables to restenosis," *J. Am. Coll. Cardiol.*, vol. 18, p. 647, 1991.

[19] P. Langhorne and M. S. Dennis, "Management of thrombosis in stroke," in *Thrombosis* (T. W. Meade, ed.), Churchill Livingstone, 1994.

[20] R. Verhaeghe and H. Bounameaux, "Peripheral arterial occlusion: Thromboembolism and antithrombotic therapy," in *Thrombosis in Cardiovasular Disorders* (V. Fuster and M. Verstraete, eds.), W. B. Saunders Company, 1992.

[21] M. H. Wholey and A. J. Nussbaum, "Angioplasty and interventional vascular procedures in the peripheral, renal, visceral, and extracranial circulation," in *Textbook of Interventional Cardiology* (E. J. Topol, ed.), W. B. Saunders Company, 1993.

[22] P. J. De Feyter, P. Serruys, and M. van den Brand, "Percutaneous transluminal angioplasty of a totally occluded venous bypass graft: A challenge that should be resisted," *Am. J. Cardiol.*, vol. 61, p. 189, 1988.

[23] T. P. Gavaghan, J. Copeland, and T. Moritz, "Immediate postoperative aspirin improves vein graft patency early and late after coronary artery bypass graft surgery," *Circulation*, vol. 83, pp. 1526–1533, 1991.

[24] V. V. Kakkar, "Prevention and management of venous thrombosis," in *Thrombosis* (T. W. Meade, ed.), Churchill Livingstone, 1994.

[25] P. E. McGuff, D. Bushnell, H. S. Saroff, and R. A. Deterling, "Studies of surgical applications of laser light," *Surg. Forum*, vol. 14, pp. 143–145, 1963.

[26] W. S. Grundfest, F. Litvack, J. S. Forrester, H. J. C. S. T. Goldenberg, L. Morgenstern, M. Fishbein, I. S. McDermid, D. M. Rider, T. J. Pacala, and J. B. Laudenslager, "Laser ablation of human atherosclerotic plaque without adjacent tissue injury," *J. Am. Coll. Cardiol.*, vol. 5, pp. 929–933, 1985.

[27] G. Lee, "Effects of laser irradiation on human thrombus: Demonstration of a linear dissolution-dose relation between clot length and energy density," *Am. J. Cardiol.*, vol. 52, pp. 876–877, 1983.

[28] F. Crea, A. Fenech, W. Smith, C. R. Conti, and G. S. Abela, "Laser recanalization of acutely thrombosed coronary arteries in live dogs," *J. Am. Coll. Cardiol.*, vol. 6, pp. 1052–1056, 1985.

[29] D. S. J. Choy, S. Strertzer, and H. Z. Rotterdam, "Transluminal laser catheter angioplasty," *Am. J. Cardiol.*, vol. 50, pp. 1206–1208, 1982.

[30] D. S. J. Choy, S. H. Stertzer, R. D. Myler, J. Marco, and G. Fournay, "Human coronary laser recanalization," *Clin. Cardiol.*, vol. 7, pp. 377–381, 1984.

[31] G. S. Abela, S. Normann, D. Cohen, R. L. Feldman, E. A. Geiser, and C. R. Conti, "Effects of carbon dioxide, Nd:YAG and argon laser radiation on coronary atheromatous plaques," *Am. J. Cardiol.*, vol. 50, pp. 1199–1205, 1982.

[32] G. S. Abela, S. J. Normann, D. M. Cohen, D. Franzini, R. L. Feldman, F. Crea, A. French, C. J. Pepine, and C. R. Conti, "Laser recanalization of occluded atherosclerotic arteries *in vivo* and *in vitro*," *Circulation*, vol. 71, pp. 403–411, 1985.

[33] R. Ginsberg, L. Wexler, and R. S. Mitchell, "Percutaneous transluminous laser angioplasty for peripheral vascular disease: Clinical experience with 16 patients," *Radiology*, vol. 156, pp. 619–624, 1985.

[34] P. C. Douek, R. Correa, R. Neville, E. F. Unger, M. Shou, S. Banai, V. J. Ferrans, S. E. Epstein, M. B. Leon, and R. F. Bonner, "Dose-dependent smooth muscle cell proliferation induced by thermal injury with pulsed infrared lasers," *Circulation*, vol. 86, pp. 1249–1256, 1992.

[35] H. Hussein, "A novel laser probe for treatment of occlusive vessel disease," *Opt. Tech. Med.*, vol. 605, pp. 59–66, 1986.

[36] A. J. Welch, A. B. Bradley, J. H. Torres, M. Motamedi, J. J. Ghidoni, J. A. Pearce, H. Hussein, and R. A. O'Rourke, "Laser probe ablation of normal and atherosclerotic human aorta *in vitro*: a first thermographic and histologic analysis," *Circulation*, vol. 76, pp. 1353–1363, 1987.

[37] G. L. LeCarpentier, S. Rastegar, A. J. Welch, S. A. Prahl, and H. Hussein, "Comparative analysis of laser ablation of plaque using direct laser irradiation and a metal contact probe," in *Phys. Med. Biol.*, vol. 33, pp. 17–21, 1988.

[38] J. D. Labs, P. L. Caslowitz, and G. M. Williams, "Experimental treatment of thrombotic vascular occlusion," *Lasers Surg. Med.*, vol. 11, pp. 363–371, 1991.

[39] T. Tomaru, G. S. Abela, J. Gonzales, P. Giacomino, S. E. Friedl, and G. R. Barbeau, "Laser recanalization of thrombosed arteries using thermal and/or modified optical probes; angiographic and angioscopic study," *Angiology*, vol. 43, pp. 412–420, 1992.

[40] R. Srinivasan and W. Leigh, "Ablative photo-decomposition action of far-ultra-violet (193 nm) laser radiation on poly (ethylene terophythalate) films," *J. Am. Chem. Soc.*, vol. 104, pp. 5784–5785, 1982.

[41] S. L. Jacques, "Role of tissue optics and pulse duration on tissue effects during high-power laser irradiation," *Appl. Opt.*, vol. 32, pp. 2447–2454, 1993.

[42] S. L. Jacques, "Role of tissue optics and pulse duration on tissue effects during high-power laser irradiation," *Appl. Opt.*, vol. 32, pp. 2447–2454, 1993.

[43] R. Linsker, R. Srinivasan, J. J. Wynne, and D. R. Alonso, "Far-ultraviolet laser ablation of atherosclerotic lesions," *Lasers Surg. Med.*, vol. 4, pp. 201–206, 1984.

[44] R. R. Anderson and J. A. Parrish, "Selective photothermolysis: Precise microsurgery by selective absorption of pulsed radiation," *Science*, vol. 220, pp. 524–527, 1983.

[45] W. S. Grundfest, I. F. Litvack, T. Goldenberg, T. Sherman, L. Morgenstern, R. Carroll, M. Fishbein, J. Forrester, J. Margitan, S. McDermid, T. Pacala, D. M. Rider, and J. B. Laudenslager, "Pulsed ultraviolet lasers and the potential for safe laser angioplasty," *Am. J. Surg.*, vol. 150, pp. 220–226, 1985.

[46] J. M. Isner, R. F. Donaldson, L. I. Deckelbaum, R. H. Clarke, S. M. Laliberte, D. M. Salem, and M. A. Konstam, "The excimer laser: Gross, light microscopic, and ultrastructural analysis of potential advantages for use in laser therapy of cardiovascular disease," *J. Am. Coll. Cardiol.*, vol. 6, pp. 1102–1109, 1985.

[47] G. H. Pettit, I. S. Saidi, F. K. Tittel, R. Sauerbrey, J. Cartwright, R. Farrell, and C. R. Benedict, "Thrombolysis by excimer laser photoablation," *Lasers Life Sci.*, vol. 5, pp. 185–197, 1993.

[48] L. I. Deckelbaum, J. M. Isner, R. F. Donaldson, R. H. Clarke, S. Laliberte, A. S. Aharon, and J. S. Bernstein, "Reduction of laser-induced pathologic tissue injury using pulsed energy delivery," *Am. J. Cardiol.*, vol. 56, pp. 662–667, 1985.

[49] F. Litvack, N. L. Eigler, and J. R. Margolis, "Percutaneous excimer laser coronary angioplasty," *Am. J. Cardiol.*, vol. 66, pp. 1027–1032, 1990.

[50] M. R. Prince, T. F. Deutsch, A. F. Shapiro, R. J. Margolis, A. R. Oseroff, J. T. Fallon, J. A. Parrish, and R. R. Anderson, "Selective ablation of atheromas using a flashlamp-excited dye laser at 465 nm," *Proc. Natl. Acad. Sci. USA*, vol. 83, pp. 7064–7068, 1986.

[51] M. R. Prince, T. F. Deutsch, M. M. Mathwes-Roth, R. Margolis, J. A. Parrish, and A. R. Oseroff, "Preferential light absorption in atheromas *in vitro*," *J. Clin. Invest.*, vol. 78, pp. 295–302, 1986.

[52] G. M. LaMuraglia, R. R. Anderson, J. A. Parrish, D. Zhang, and M. R. Prince, "Selective laser ablation of venous thrombus: Implications for a new approach in the treatment of pulmonary embolus," *Lasers Surg. Med.*, vol. 8, pp. 486–493, 1988.

[53] G. M. LaMuraglia, M. R. Prince, N. S. Nishioka, S. Obremski, and R. Birngruber, "Optical properties of human arterial thrombus, vascular grafts, and sutures: Implications for selective laser thrombus ablation," *IEEE J. Quantum Electron.*, vol. 26, pp. 2200–2206, 1990.

[54] K. W. Gregory, M. R. Prince, G. M. LaMuraglia, T. J. Flotte, L. Buckley, J. M. Tobin, A. A. Ziskind, J. Caplin, and R. R. Anderson, "Effect of blood upon the selective ablation of atherosclerotic plaque with a pulsed dye laser," *Lasers Surg. Med.*, vol. 10, pp. 533–543, 1990.

[55] K. Gregory, "Laser thrombolysis," in *Interventional Cardiology* (E. J. Topol, ed.), vol. 2, ch. 5, pp. 892–902, W. B. Saunders Company, 1994.

[56] G. E. Kopchok, R. A. White, M. Tabbara, V. Saadatmanesh, and S. Peng, "Holmium:YAG laser ablation of vascular tissue," *Lasers Surg. Med.*, vol. 10, pp. 405–413, 1990.

[57] H. J. Geschwind, J. L. Dubois-Rande, R. Zelinsky, J. F. Morelle, G. Boussignac, and F. Veyssiere, "Percutaneous coronary mid-infrared laser angioplasty," *Am. Heart J.*, vol. 122, pp. 552–558, 1991.

[58] W. Knopf, K. Parr, J. Moses, C. Cates, W. Groh, C. Stark, R. Johnson, E. Harlamert, A. Fiedotin, and D. Murphy-Chutorian, "Holmium laser angioplasty in coronary arteries," *J. Am. Coll. Cardiol.*, vol. 19, p. 325A, 1992.

[59] K. Rosenfield, A. Pieczek, D. W. Losordo, B. D. Kosowsky, K. Ramaswamy, J. O. Pastore, and J. M. Isner, "Excimer laser thrombolysis for rapid clot dissolution in lesions at high risk for embolization: A potentially useful new application for excimer laser," *J. Am. Coll. Cardiol.*, vol. 19 (suppl), p. 104, 1992.

[60] P. Estela, J. A. Bittl, J. M. Landzberg, and T. J. Ryan, "Intracoronary thrombus increases the risk of excimer laser coronary angioplasty," *Circulation*, vol. 86 (suppl), p. 654, 1992.

[61] O. N. Topaz, A. Eliezer, A. Rozenbaum, S. Battista, C. Peterson, and D. G. Wysham, "Laser facilitated angioplasty and thrombolysis in acute myocardial infarction complicated by prolonged or recurrent chest pain," *Cathet. Cardiovasc. Diagn.*, vol. 28, pp. 7–16, 1993.

[62] R. de la Torre and K. W. Gregory, "Cavitation bubbles and acoustic transients may produce dissections during laser angioplasty," *J. Am. Coll. Cardiol.*, vol. 19, p. 48A, 1992.

[63] S. Hassenstein, H. Hanke, and S. Hanke, "Incidence of thrombotic occlusions in experimental holmium laser angioplasty compared to excimer laser angioplasty," *Circulation*, vol. 84(suppl. II), p. 124, 1991.

[64] M. R. Prince, F. T. Deutch, R. Margolis, M. M. Mathews-Roth, J. A. Parrish, and A. R. Oseroff, "Preferential light absorption in atheromas: Implication for laser angioplasty," *J. Clin. Invest.*, 1985.

[65] M. R. Prince, *Selective Photo-Removal of Athermatous Arterial Obstructions*. PhD thesis, Harvard–M. I. T. Division of Health Sciences and Technology, 1985.

[66] G. M. LaMuraglia, S. Murray, R. R. Anderson, and M. R. Prince, "Effect of pulse duration on selective ablation of atherosclerotic plaque by 480- to 490-nanometer laser radiation," *Lasers Surg. Med.*, vol. 8, pp. 18–21, 1988.

[67] K. W. Gregory and R. R. Anderson, "Iodinated contrast fluid can replace quartz in laser catheters," *Circulation*, vol. 80, p. 107, 1989. (Supp 2).

[68] K. W. Gregory and R. R. Anderson, "Liquid core light guide for laser angioplasty," *IEEE J. Quantum Electron.*, vol. 26, pp. 2289–2296, 1990.

[69] K. W. Gregory, P. C. Block, W. A. Knopf, L. A. Buckley, and C. M. Cates, "Laser thrombolysis in acute myocardial infarction," *J. Am. Coll. Cardiol.*, (submitted).

[70] E. D. Jansen, *Pulsed Laser Ablation of Biological Tissue: Influence of Laser Parameters and Tissue Properties on Thermal and Mechanical Damage*. PhD thesis, University of Texas at Austin, 1994.

[71] T. van Leeuwen, *Bubble Formation During Pulsed Mid-Infrared and Excimer Laser Ablation: Origin and Implications for Laser Angioplasty*. PhD thesis, Rijksuniversiteit te Utrecht, 1993.

[72] S. A. Prahl, I. A. Vitkin, U. Bruggemann, B. C. Wilson, and R. R. Anderson, "Determination of optical properties of turbid media using pulsed photothermal radiometry," *Phys. Med. Biol.*, vol. 37, pp. 1203–1217, 1992.

[73] T. Asshauer, G. Delacrétaz, E. D. Jansen, A. J. Welch, and M. Frenz, "Acoustic transients in pulsed holmium laser ablation: Effects of pulse duration," *SPIE Proceedings of Laser Interaction with Hard and Soft Tissue II*, vol. 2323, pp. 117–129, 1994.

[74] M. Frenz, V. Romano, A. D. Zweig, H. P. Weber, N. I. Chapliev, and A. V. Silenok, "Instabilities in laser cutting of soft media," *J. Appl. Phys.*, vol. 66, pp. 4496–4503, 1989.

[75] S. Chandrasekhar, *Radiative Transfer*. New York: Dover, 1960.

[76] S. A. Prahl, *Light Transport in Tissue*. PhD thesis, University of Texas at Austin, 1988.

[77] M. S. Patterson, B. C. Wilson, and D. R. Wyman, "The propagation of optical radiation in tissue I. Models of radiation transport and their application," *Lasers Med. Sci.*, vol. 6, pp. 155–168, 1991.

[78] M. S. Patterson, B. C. Wilson, and D. R. Wyman, "The propagation of optical radiation in tissue II. Optical properties of tissues and resulting fluence distributions," *Lasers Med. Sci.*, vol. 6, pp. 379–390, 1991.

[79] A. J. Welch, R. Birngruber, K. P. Boergon, V. P. Gabel, and F. Hillenkamp, "The influence of scattering on the wavelength dependent light absorption in blood," in *Proceedings of the Symposium: Lasers in Medicine and Biology*, vol. 14, pp. 1–8, 1977.

[80] L. Wang and S. L. Jacques, "Hybrid model of Monte Carlo simulation and diffusion theory for light reflectance by turbid media," *J. Opt. Soc. Am. B*, vol. 10, pp. 1746–1751, 1993.

[81] L. Wang and S. L. Jacques, "Analysis of diffusion theory and similarity relations for light reflectance by turbid media," in *SPIE: Proceedings of Photon Migration and Imaging in Random Media and Tissues*, 1993.

[82] K. Rink, Delacrétaz, G. Pittomvils, R. Boving, and J. P. Lafaut, "Incidence of cavitation in the fragmentation process of extracorporeal shock lithotriptors," *Appl. Phys. Lett*, vol. 64, pp. 2596–2598, 1994.

[83] A. Vogel, P. Schweiger, A. Frieser, M. N. Asiyo, and R. Birngruber, "Intraocular Nd:YAG laser surgery: Light-tissue interaction, damage range, and reduction of collateral effects," *IEEE J. Quantum Electron.*, vol. 26, pp. 2240–2259, 1990.

[84] F. Partovi, J. A. Izatt, R. M. Cothren, C. Kittrell, J. E. Thomas, S. Strikwerda, J. R. Kramer, and M. S. Feld, "A model for thermal ablation of biological tissue using laser radiation," *Lasers Surg. Med.*, vol. 7, pp. 141–154, 1987.

[85] J. T. Walsh Jr., *Pulsed Laser Ablation of Tissue: Analysis of the Removal Process and Tissue Healing.* PhD thesis, Harvard/M. I. T. Division of Health Sciences and Technology, 1988.

[86] J. T. Walsh Jr. and T. F. Deutsch, "Pulsed CO_2 laser ablation of tissue: Effect of mechanical properties," *IEEE Trans. Biomed. Eng.*, vol. 36, pp. 1195–1201, 1989.

[87] F. Litvack, W. S. Grundfest, T. Goldenberg, J. Laudenslager, T. Pacala, J. Segalowitz, and J. Forrester, "Pulsed laser angioplasty: Wavelength power and energy dependencies relevant to clinical application," *Lasers Surg. Med.*, vol. 8, pp. 60–65, 1988.

[88] S. Strikwerda, C. Bott-Silverman, N. B. Ratliff, M. Goormastic, R. M. Cothren, B. Costello, C. Kittrell, M. S. Feld, and J. R. Kramer, "Effects of varying argon ion laser intensity and exposure time on the ablation of atherosclerotic plaque," *Lasers Surg. Med.*, vol. 8, pp. 66–71, 1988.

[89] M. R. Prince, G. M. LaMuraglia, P. Teng, T. F. Deutsch, and R. R. Anderson, "Preferential ablation of calcified arterial plaque with laser-induced plasmas," *IEEE J. Quantum Electron.*, vol. QE-23, pp. 1783–1786, 1987.

[90] S. L. Jacques, "Laser-tissue interactions. Photochemical, photothermal and photomechanical," *Lasers General Surg.*, vol. 72, pp. 531–557, 1992.

[91] R. de la Torre, *Intravascular laser induced cavitation: A study of the mechanics with possible detrimental and beneficial effects*, Master's thesis, Harvard–M. I. T. Division of Health Sciences and Technology, Cambridge, MA, 1992.

[92] S. W. Barnaby and J. Thornycroft, "Torpedo boat destroyers," *Proc. Inst. Civ. Engrs.*, vol. 122, p. 57, 1895.

[93] F. R. Young, *Cavitation*. McGraw Hill, 1989.

[94] W. Lauterborn, "Kavitation durch laserlicht," *Acustica*, vol. 31, pp. 51–78, 1974.

[95] W. Lauterborn, "Cavitation bubble dynamics - new tools for an intricate problem," *Appl. Sci. Research*, vol. 38, pp. 165–178, 1982.

[96] A. Vogel and W. Lauterborn, "Acoustic transient generation by laser-produced cavitation bubbles near solid boundaries," *J. Acoust. Soc. Am.*, vol. 84, pp. 719–731, 1988.

[97] A. Vogel, W. Lauterborn, and R. Timm, "Optical and acoustic investigations of the dynamics of laser-produced cavitation bubbles near a solid boundary," *J. Fluid Mech.*, vol. 206, pp. 299–238, 1989.

[98] C. F. Naudé and A. T. Ellis, "On the mechanism of cavitation damage by nonhemispherical cavities collapsing in contact with a solid boundary," *Trans. A. S. M. E. Series, J. Basic Eng.*, vol. 83, pp. 648–656, 1961.

[99] T. B. Benjamin and A. T. Ellis, "The collapse of cavitation bubbles and the pressures thereby produced against solid boundaries," *Phil. Trans. R. Soc. Lond.*, vol. 260. A., pp. 221–240, 1966.

[100] W. Lauterborn and H. Bolle, "Experimental investigations of cavitation-bubble collapse in the neighborhood of a solid boundary," *J. Fluid Mech.*, vol. 72, pp. 391–399, 1975.

[101] A. Vogel, W. Hentschel, J. Holzfuss, and W. Lauterborn, "Cavitation bubble dynamics and acoustic transient generation in ocular surgery with pulsed neodymium:YAG lasers," *Ophthalmology*, vol. 93, pp. 1259–1269, 1986.

[102] E. A. Neppiras, "Acoustic cavitation," *Phys. Rep.*, vol. 61, p. 160, 1980.

[103] Lord Rayleigh, "On the pressure developed in a liquid during the collapse of a spherical cavity," *Phil. Mag.*, vol. 34, pp. 94–98, 1917.

[104] A. Vogel, *Optische und akustische Untersuchungen der Dynamik lasererzeugter Kavitationsblasen nahe fester Grenzflächen*. PhD thesis, Georg-August-Universität Göttingen, 1987.

[105] A. Vogel, S. Busch, K. Jungnickel, and R. Birngruber, "Mechanisms of intraocular photodisruption with picosecond and nanosecond laser pulses," *Lasers Surg. Med.*, vol. 15, pp. 32–43, 1994.

[106] V. Venugopalan, *The Thermodynamic Response of Polymers and Biological Tissues to Pulsed Laser Irradiation*. PhD thesis, Massachusetts Institute of Technology, 1994.

[107] V. Venugopalan, A. D. Zweig, T. F. Deutsch, N. S. Nishioka, and B. B. Mikić, "Physical mechanisms controlling the generation of laser-induced stresses," in *Proceedings of Laser-Tissue Interaction V* (S. L. Jacques, ed.), vol. 1882, pp. 102–111, SPIE, 1993.

[108] V. Venugopalan, N. S. Nishioka, and B. B. Mikić, "The effect of laser parameters on the zone of thermal injury produced by laser ablation of biological tissue," *J. Biomed. Eng.*, vol. 116, pp. 62–70, 1994.

[109] K. Rink, G. Delacrétaz, and R. P. Salathé, "Fragmentation process induced by microsecond laser pulses during lithotripsy," *Appl. Phys. Lett.*, vol. 61, pp. 258–260, 1992.

[110] K. Rink, G. Delacrétaz, and R. P. Salathé, "Fragmentation process of current laser lithotriptors," *Lasers Surg. Med.*, 1994.

[111] E. J. Chapyak and R. P. Godwin, "Numerical studies of bubble dynamics in laser thrombolysis," *SPIE Proceedings of Lasers in Surgery: Advanced Characterization, Therapeutics, and Systems VI*, vol. 2671, pp. 84–87, 1996.

[112] M. Strauss, P. A. Amendt, R. A. London, D. J. Maitland, M. E. Glinsky, P. M. Celliers, D. S. Bailey, D. A. Young, and S. L. Jacques, "Computational modeling of laser thrombolysis for stroke treatment," *SPIE Proceedings of Lasers in Surgery: Advanced Characterization, Therapeutics, and Systems VI*, vol. 2671, pp. 11–21, 1996.

[113] E. A. Chasteney, P. S. Ravichandran, D. Tuke-Bahlman, A. Shearin, and K. W. Gregory, "Rapid thrombolysis in experimental coronary artery bypass grafts," *J. Am. Coll. Cardiol.*, abstracts issue, p. 348, 1995. Abstract.

[114] Alan Shearin, Oregon Medical Laser Center, Personal communication, 1996.

[115] E. D. Jansen, T. Asshauer, M. Frenz, M. Motamedi, G. Delacrétaz, and A. J. Welch, "Effect of pulse duration on bubble formation and laser-induced pressure waves during holmium laser ablation," *Lasers Surg. Med.*, vol. 18, pp. 278–293, 1996.

Biographical Note

Ujwal Setlur Sathyam was born in Stuttgart, Germany, on May 18, 1970, the son of Srimathi Sathyam and Setlur Rangaswamy Sathyam. After completing his Pre-University degree (12. grade) in 1988, he entered the Karnataka Regional Engineering College at Mangalore University, India. He received the degree of Bachelor of Engineering in Electronics and Communication from Mangalore University in June 1992. In September 1992, he enrolled in his graduate studies in Electrical Engineering at the Oregon Graduate Institute of Science and Technology, Portland, Oregon. He received the degree of Master of Science in Electrical Engineering from the Oregon Graduate Institute in July 1994. In June 1993, he entered candidacy for the degree of Doctor of Philosophy in Electrical Engineering at the Oregon Graduate Institute.

Permanent address: # 7, 11. Main, 17. 'A' Cross, Malleswaram
                    Bangalore 560055, India

This dissertation was typed by the author and typeset in L^AT_EX.